Dissertation zur Erlangung des Doktorgrades
der Fakultät für Chemie und Pharmazie
der Ludwig-Maximilians-Universität München

Optimization of the Selective Ruthenium-Catalyzed Carbon Dioxide Reduction to Dimethoxymethane

and

Mechanistic Investigation into the Acetate-Initiated Catalytic Trimerization of Aliphatic Isocyanates

Max Julian Siebert
aus
Aurich, Deutschland

2020

Erklärung

Diese Dissertation wurde im Sinne von § 7 der Promotionsordnung vom 28. November 2011 von Herrn Prof. Dr. Oliver Trapp betreut.

Eidesstattliche Versicherung

Diese Dissertation wurde eigenständig und ohne unerlaubte Hilfe erarbeitet.

München, den 26.06.2020

Max Siebert

Dissertation eingereicht am 29.06.2020
1. Gutachter: Prof. Dr. Oliver Trapp
2. Gutachter: Prof. Dr. Paul Knochel
Mündliche Prüfung am 30.07.2020

Für meine Familie.

Abstract

It is a constant endeavor of science to use the globally available resources more efficiently – either by optimization of existing processes, research and establishment of new reactions, or use of waste and by-products. In this dissertation, the pursuit of efficiency is the guiding principle of both industrially relevant projects.

In the first part of this thesis, an alternative process for the preparation of an important basic chemical of the chemical industry, formaldehyde or its synthon dimethoxymethane, was optimized, starting from the greenhouse gas carbon dioxide and hydrogen: (1) In a systematic screening, numerous catalysts were examined regarding their suitability for the catalytic conversion of carbon dioxide to dimethoxymethane. For the most promising catalyst, seven relevant process parameters were optimized in a univariate screening, which resulted in an activity increase of more than 350 % compared to previously described systems. The ligand of this catalyst was also structurally modified, and the influence of the electronic and steric changes on the catalytic activity was investigated. (2) In order to overcome the limitations of a univariate screening in such a multidimensional parameter space and also to demonstrate the efficiency of multivariate methods, the most active system was improved in an algorithmic workflow by further 350 %. Combined with the low experimental effort, this illustrates the potential of mathematical tools and algorithms, which should also be used more intensively in university research. (3) The presented fast and precise optimization of the transformation of carbon dioxide to dimethoxymethane was realized using a self-designed and -built autoclave system. With this setup, homogeneously catalyzed reactions that require reaction gases can be easily carried out under challenging combinations of temperature and pressure. The potential of this design was further demonstrated in the asymmetric hydrogenation of prochiral acrylic acid derivatives, revealing a correlation of the resulting enantiomeric excess with temperature.

In the second part of this thesis, the mechanism of the industrially used carboxylate-catalyzed trimerization of aliphatic isocyanates to isocyanurates was investigated. For the employed acetate catalyst, an unexpectedly complex catalysis mechanism was discovered, involving three different consecutive catalysis cycles. This project paradigmatically demonstrates the strength of a combined approach of computational and experimental chemistry.

Zusammenfassung

Es ist ein ständiges Bestreben der Wissenschaft, die weltweit verfügbaren Ressourcen immer effizienter zu nutzen – sei es durch die Optimierung bestehender Prozesse, die Erforschung und Etablierung neuer Reaktionswege oder den Einsatz von Abfall- und Nebenprodukten. In dieser Dissertation ist das Streben nach Effizienz das Leitprinzip beider industriell relevanten Projekte.

Im ersten Teil dieser Arbeit wurde ein alternativer Prozess für die Darstellung einer wichtigen Basischemikalie der chemischen Industrie, Formaldehyd bzw. dessen Synthon Dimethoxymethan, ausgehend vom Treibhausgas Kohlenstoffdioxid und Wasserstoff optimiert: (1) In einem systematischen Screening wurden zahlreiche Katalysatoren auf ihre Eignung für die katalytische Umwandlung von Kohlenstoffdioxid zu Dimethoxymethan untersucht. Für den vielversprechendsten Katalysator wurden sieben relevante Prozessparameter in einem univariaten Screening optimiert, was zu einer Aktivitätssteigerung von über 350 % im Vergleich zu zuvor beschriebenen Systemen führte. Der Ligand dieses Katalysators wurde zudem strukturell verändert und der Einfluss der elektronischen und sterischen Änderungen auf die katalytische Aktivität untersucht. (2) Um die Limitierung des durchgeführten univariaten Screenings in solch einem multidimensionalen Parameterraum zu überwinden und die Effizienz von multivariaten Methoden aufzuzeigen, wurde das aktivste System nun in einem algorithmischen Arbeitsablauf um weitere 350 % verbessert. Verbunden mit dem geringen experimentellen Aufwand, verdeutlicht dies das Potential mathematischer Werkzeuge und Algorithmen, das auch in der Hochschulforschung intensiver genutzt werden sollte. (3) Die hier beschriebene schnelle und präzise Optimierung der Transformation von Kohlenstoffdioxid zu Dimethoxymethan wurde durch ein selbst entworfenes und gebautes Autoklavensystem realisiert. Dieser Aufbau ermöglicht die Durchführung homogen-katalysierter Reaktionen, bei denen Reaktionsgase vorhanden sind und außergewöhnliche Kombinationen von Temperatur und Druck benötigt werden. Das Potential dieses Autoklavenaufbaus wurde darüber hinaus in der asymmetrischen Hydrie-

rung prochiraler Acrylsäurederivate gezeigt, für die eine Korrelation des resultierenden Enantiomerenüberschusses mit der Temperatur nachgewiesen werden konnte.

Im zweiten Teil dieser Arbeit wurde der Mechanismus der industriell genutzten Carboxylat-katalysierten Trimerisierung von aliphatischen Isocyanaten zu Isocyanuraten untersucht. Für den verwendeten Acetat-Katalysator wurde ein unerwartet komplexer Katalyse-Mechanismus aufgedeckt, der drei aufeinanderfolgende, unterschiedliche Katalysezyklen beinhaltet. Dieses Projekt zeigt paradigmatisch die Stärke eines kombinierten Aufklärungsansatzes von Computer- und Experimentalchemie auf.

Scientific Contributions

This dissertation has already been published in parts and presented at conferences in the form of scientific talks and poster presentations.

Publications

[1] M. Siebert, M. Seibicke, A. F. Siegle, S. Kräh, O. Trapp
J. Am. Chem. Soc. **2019**, *141*, 334–341.
Selective Ruthenium-Catalyzed Transformation of Carbon Dioxide: An Alternative Approach toward Formaldehyde

[2] M. Seibicke, M. Siebert, A. F. Siegle, S. M. Gutenthaler, O. Trapp
Organometallics **2019**, *38*, 1809–1814.
Application of Hetero-Triphos Ligands in the Selective Ruthenium-Catalyzed Transformation of Carbon Dioxide to the Formaldehyde Oxidation State

[3] M. Siebert, G. Krennrich, M. Seibicke, A. F. Siegle, O. Trapp
Chem. Sci. **2019**, *10*, 10466–10474.
Identifying High-Performance Catalytic Conditions for Carbon Dioxide Reduction to Dimethoxymethane by Multivariate Modelling

[4] M. Siebert, G. Storch, O. Trapp
Org. Process Res. Dev. **2020**, DOI: 10.1021/acs.oprd.0c00192.
A Fast and Reliable Screening Setup for Homogeneous Catalysis with Gaseous Reactants at Extreme Temperatures and Pressures

[5] M. Siebert, R. Sure, P. Deglmann, A. C. Closs, F. Lucas, O. Trapp
J. Org. Chem. **2020**, DOI: 10.1021/acs.joc.0c00944.
Mechanistic Investigation into the Acetate-Initiated Catalytic Trimerization of Aliphatic Isocyanates: A Bicyclic Ride

Scientific Talks

[1] M. Siebert, M. Seibicke, O. Trapp, *17th International Conference on Carbon Dioxide Utilization (ICCDU)*, Aachen, Germany, 25.06.2019.
An Alternative Approach towards Formaldehyde: Univariate and Multivariate Analysis in the Ruthenium-Catalyzed Transformation of Carbon Dioxide to Dimethoxymethane

[2] M. Siebert, O. Trapp, *Gordon Research Seminar Organometallic Chemistry (GRS)*, Newport (RI), USA, 07.07.2019.
An Alternative Approach towards Formaldehyde: Univariate and Multivariate Analysis in the Ruthenium-Catalyzed Transformation of Carbon Dioxide to Dimethoxymethane

[3] M. Siebert, G. Krennrich, O. Trapp, *16th DoE-Congress (University Frankfurt & IHK Kassel-Marburg)*, Kassel, Germany, 17.10.2019.
Machine Learning, Optimization and Design of Experiments – Identifying Optimal Catalytic Conditions for Carbon Dioxide Reduction to Dimethoxymethane

Poster Presentations

[1] M. Siebert, M. Seibicke, A. Siegle, I. Jevtovikj, T. Schaub, O. Trapp, *1st Status Conference CO_2Plus*, Berlin, Germany, 17./18.10.2018.
CO_2Form – Screening of Tridentate Phosphine Ligands for the Selective Transformation of Carbon Dioxide to Formaldehyde

[2] M. Siebert, O. Trapp, *12th CaRLa Winterschool (University Heidelberg & BASF)*, Heidelberg, Germany, 17.-22.02.2019.
Selective Ruthenium-Catalyzed Transformation of Carbon Dioxide – an Alternative Approach towards Formaldehyde

[3] M. Seibicke, M. Siebert, O. Trapp, *17th International Conference on Carbon Dioxide Utilization (ICCDU)*, Aachen, Germany, 23.-27.06.2019.
Hetero-Triphos Ligands in the Selective Ruthenium-Catalyzed Transformation of Carbon Dioxide to Dimethoxymethane

[4] M. Siebert, O. Trapp, *Gordon Research Conference Organometallic Chemistry (GRC)*, Newport (RI), USA, 07.-12.07.2019.
An Alternative Approach towards Formaldehyde: Univariate and Multivariate Analysis in the Ruthenium-Catalyzed Transformation of Carbon Dioxide to Dimethoxymethane

Contents

Part I

Catalytic Carbon Dioxide Reduction

1 Introduction

Carbon dioxide plays a decisive role in climate change due to its greenhouse properties and continuous accumulation in the atmosphere. Its dramatic levels are based on a constantly increasing use of the world's fossil resources, together with negative interventions in the terrestrial and oceanic biosphere.[1–3] After the atmospheric CO_2 concentration stayed nearly constant at around 280 ppm for 10000 years, it continuously increased since the middle of the 18th century, being strongly correlated with the beginning of the industrial revolution. During the early 21th century, the atmospheric concentration exceeded 400 ppm, resulting in anthropogenic global warming that is unprecedented not only in terms of absolute temperatures but also in terms of spatial consistency in the context of the last 2000 years.[4–7]

The solution to this global problem and the potentially resulting climate crisis might become one of the greatest tasks for mankind. However, it also bears an opportunity. If CO_2 is obtained as side-product in a process, its utilization would improve the overall resource efficiency along the value chains, thereby additionally providing a renewable resource for the generations to come. Further, it would allow to reduce the human influence on the carbon cycle by reducing the emission of CO_2 into the atmosphere.[8,9] Still, ecological benefits always compete with economic interests, and for these reasons there will be no shift towards a green alternative process if it is not profitable after all.

---

[1] *IPCC, 2019: IPCC Special Report on Climate Change and Land*, (Eds.: P. R. Shukla et al.), in press, **2019**.
[2] *IPCC, 2019: IPCC Special Report on the Ocean and Cryosphere in a Changing Climate*, (Eds.: H.-O. Pörtner et al.), in press, **2019**.
[3] *IPCC, 2018: Global Warming of 1.5°C*, (Eds.: V. Masson-Delmotte et al.), in press, **2018**.
[4] R. Neukom et al., *Nature* **2019**, *571*, 550–554.
[5] *IPCC, 2014: Climate Change 2014 (Synthesis Report)*, (Eds.: Core Writing Team et al.), IPCC, Geneva, Switzerland, **2014**.
[6] T. Eggleton, *A Short Introduction to Climate Change*, Cambridge University Press, New York, **2013**.
[7] P. J. Crutzen, *Nature* **2002**, *415*, 23–23.
[8] J. A. Martens et al., *ChemSusChem* **2017**, *10*, 1039–1055.
[9] P. Falkowski et al., *Science* **2000**, *290*, 291–296.

Due to the negative effects of utilizing fossil resources on the global climate as well as the global resource limitations, however, political decisions will increasingly influence this balance between ecological and economic drivers towards a more sustainable future.[10–12] In addition, the scientific community and the chemical industry have to perceive this opportunity independent of extrinsic factors by generally promoting sustainable process development, alternative energies as well as recycling of waste and pollutants. By this, the costs for more economic processes will be reduced, thereby facilitating and concurrently accelerating the transition.[13–19]

[10] T. Sterner et al., *Nat. Sustain.* **2019**, *2*, 14–21.
[11] Y. Geng et al., *Nature* **2019**, *565*, 153–155.
[12] R. Schlögl, *Angew. Chem. Int. Ed.* **2015**, *54*, 4436–4439.
[13] B. Rego de Vasconcelos, J.-M. Lavoie, *Front. Chem.* **2019**, *7*, 392.
[14] M. D. Burkart et al., *ACS Catal.* **2019**, *9*, 7937–7956.
[15] J. Artz et al., *Chem. Rev.* **2018**, *118*, 434–504.
[16] M. Aresta et al., *Chem. Rev.* **2014**, *114*, 1709–1742.
[17] P. Markewitz et al., *Energy Environ. Sci.* **2012**, *5*, 7281–7305.
[18] M. Aresta in *Carbon Dioxide as Chemical Feedstock*, (Ed.: M. Aresta), Wiley-VCH, Weinheim, **2010**.
[19] W. Keim in *Carbon Dioxide as a Source of Carbon: Biochemical and Chemical Uses*, (Eds.: M. Aresta, G. Forti), Springer, Dordrecht, **1987**.

1.1 Considering Carbon Dioxide as Resource

Global fossil CO_2 emissions are constantly increasing, exceeding 37 Gt in 2019.[20] A total amount of (2040 ± 310) Gt CO_2 was released into the atmosphere between 1750 and 2011 due to cumulative anthropogenic CO_2 emissions, half of which was released within the last 40 years of this period. Nature is able to absorb significant amounts of CO_2 in carbon cycle reservoirs, but the highly complex absorption mechanisms are limited and severe effects on natural systems, such as ocean acidification, are already observed. Still 40 % of the CO_2 emissions ((880 ± 35) Gt CO_2) have remained in the atmosphere, leading to the aforementioned increase in atmospheric CO_2 concentration.[5]

Consequently, not only the optimization of our global economy towards reduced CO_2 emissions but also the utilization of non-avoidable and already released anthropogenic CO_2 has to be realized.[1] For the latter, CO_2 has to be either separated from waste streams and purified adequately to meet the desired specifications or directly captured from air. The costs for this process vary strongly, for instance between 15 – 90 \$/t CO_2 based on the amount of gaseous pollutants for CO_2 from power stations and 80 – 130 \$/t CO_2 when it is recovered from the atmosphere.[16] At the moment, the utilization of CO_2 from industrial processes (3300 – 3500 Mt CO_2/a) seems to be the most promising approach for the near future as these provide a continuous point source with high CO_2 concentrations. Interesting sectors with high CO_2 emissions range from the iron and steel industry (about 900 Mt CO_2/a) over oil refineries (850 – 900 Mt CO_2/a) to the cement industry (about 1000 Mt CO_2/a). Already several processes utilize carbon dioxide as resource, but most of these examples use CO_2 extracted from natural sources instead of recovered CO_2, underlining the importance for innovative solutions for cheap and efficient CO_2 recovery and caption.[16] Although the process of capturing carbon dioxide is as important as its chemical utilization discussed in the following, elaboration on this topic would go beyond the scope of this work.[2]

[20] M. Muntean et al., *Fossil CO_2 emissions of all world countries - 2018 Report*, Publications Office of the European Union, Luxembourg, **2018**.

1 It has to be stressed, that the use of CO_2 does not necessarily reduce and may even lead to higher overall CO_2 emissions. Different tools, as life cycle assessments, carbon footprint and carbon utilization fraction, can evaluate and quantify the benefits. Not only the process efficiency itself but also factors like the use of renewable energies play an important role.

2 Numerous reviews provide the interested reader with the recent achievements in this field.[21–28]

Due to the urgency of the problem but also the potential for the global economy, a transition from the linear to a cyclic carbon economy will evolve over the next decades.

2 State of Knowledge

Numerous chemical transformations utilizing CO_2 have been realized, covering the incorporation of CO_2 into organic molecules, the full reduction to hydrocarbons in the sense of energy storage, or the selective reduction to an oxidation state between the fully oxidized (CO_2) and the reduced form (CH_4). Even though all these three approaches are important for a potential industrial application and each method has specific advantages and disadvantages, the following will exclusively deal with the last mentioned.[3] Several catalytic methods for CO_2 reduction are known and mostly based on electrochemical and photochemical systems.[4] This work, however, will concentrate on catalytic systems employing hydrogen gas as reductant,[5] as it is considered a highly promising approach for the translation to renewable energies.

In this field, a large part of the research is directed towards the production of industrially relevant molecules that are nowadays obtained on a large scale starting from fossil resources. The selective reduction of CO_2 into functional molecules can be classified by the oxidation state of the resulting product. The reduction towards the formic acid / CO and methanol level is already well established, while the reduction towards the formaldehyde oxidation state still remains challenging.[50,51] Since the present work tackles the latter transformation, this chapter also focuses on this field, discussing reactions that directly end at the desired formaldehyde oxidation state.[6]

[50] J. Klankermayer et al., *Angew. Chem. Int. Ed.* **2016**, *55*, 7296–7343.
[51] J. Klankermayer, W. Leitner, *Science* **2015**, *350*, 629–630.

3 A comprehensive overview of incorporation strategies[29–36] and energy storage applications[37,38] is given in the literature.

4 The recent progress of electrochemical[39–43] or photochemical[41,43–49] conversion in this field is stated in numerous reviews.

5 For other intensively studied reducing agents, reference to the literature is made at the appropriate place.

6 Several comprehensive reviews highlight the recent achievements for the reduction towards the formic acid[50,52–55] and methanol[43,50,52,53,55,56] oxidation state.

Reducing CO_2 to formaldehyde would not only result in an important industrial chemical but also deliver a promising method for hydrogen storage.[57,58] [7]

[57] T. Schaub, *Phys. Sci. Rev.* **2018**, *3*, 20170015.
[58] T. Schaub in *Hydrogen Storage*, (Eds.: T. Zell, R. Langer), De Gruyter, Berlin, **2018**.

[7] An introduction in the use of formaldehyde as hydrogen storage is found in the literature.[59–61]

2.1 Industrial Synthesis of Formaldehyde

Formaldehyde is an important basic chemical for numerous industrial sectors with a strongly increasing demand over the last decades, with the majority being used for the synthesis of resins. In 2011, the global consumption was around 13×10^6 t/a with a manufacturing capacity of around 18×10^6 t/a based on 100 wt% (Figure 2.1).[62]

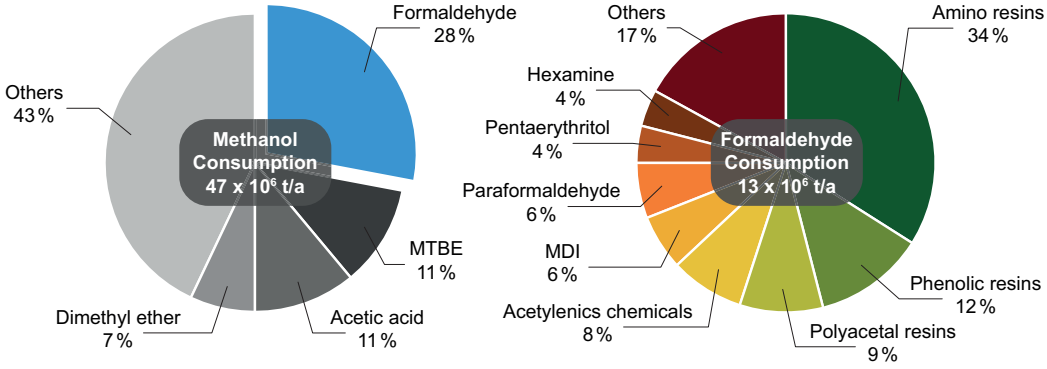

Figure 2.1: Global consumption of methanol (left) and formaldehyde (right) classified by use and with values based on 100 wt%.

Nowadays, formaldehyde is industrially produced from methanol by three different processes, either based on silver catalysts or metal oxide catalysts: (i) partial oxidation and dehydrogenation of methanol using air in the presence of silver crystals, steam, and excess methanol at 680 – 720 °C (BASF process); (ii) similar to the first process but utilization of either crystalline silver or silver gauze and a lower temperature of 600 – 650 °C; (iii) oxidation of methanol using only excess air in the presence of a modified iron-molybdenum-vanadium oxide catalyst at 250 – 400 °C (Formox process). The first and third process have high methanol conversions of 97 – 98 % and 98 – 99 %, respectively. The low primary conversion of only 77 – 87 % for the second process is increased to completeness by distillation of the product and recycling of methanol. For the two silver-catalyzed processes, the dehydrogenation reaction is highly temperature-dependent. High temperatures are required to increase conversion, with the exact temperature depending on the excess of methanol (Figure 2.2A). For the Formox process (Figure 2.2B), conversion is complete already at lower temperatures. Above 470 °C, the further reversible oxidation to carbon monoxide as side reaction increases significantly. All three processes have advantages as well as disadvantages and are selected

[62] A. W. Franz et al. in *Ullmann's Encyclopedia of Industrial Chemistry*, Wiley-VCH, **2016**.

after considering several factors, such as the plant size or whether the steam generated during the process can be utilized for other applications. Alternative catalytic syntheses, which convert alkanes, alkenes, and ethers to formaldehyde, are not of industrial relevance due to economic reasons. The oxidation of methane and the partial hydrogenation of CO do not compete with the mentioned processes due to lower formaldehyde yields.[62]

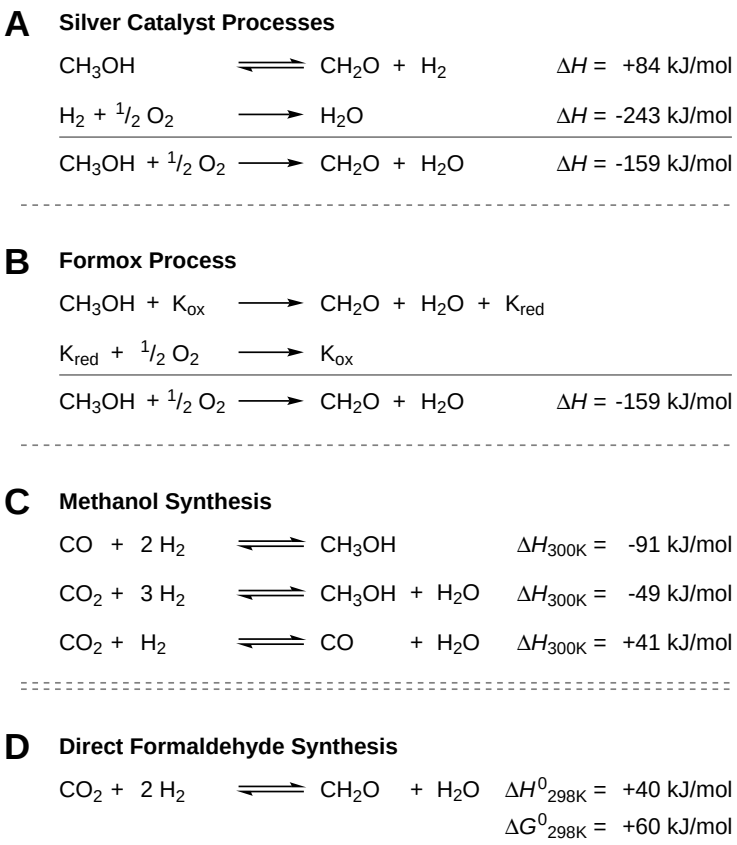

Figure 2.2: Overview of the (industrial) catalytic processes for formaldehyde production. In some cases, no temperature could be specified for the respective reaction enthalpy. **A**: Silver catalyst processes. **B**: Formox process. The two-step oxidation reaction involves an oxidized (K_{ox}) and a reduced (K_{red}) form of the catalyst. **C**: Methanol synthesis. The reverse water-gas shift reaction connects both reductive conversions and has to be taken into account. **D**: Direct formaldehyde synthesis starting from CO_2.

Therefore, the industrial production of formaldehyde is exclusively based on methanol. The methanol in turn is produced from synthesis gas containing both CO and CO_2. The CO_2 is necessary for the transformation as the H_2 content of the synthesis gas obtained from fossil resources is normally too high. In principle, all carbonaceous resources can be used for the production of synthesis gas, and the choice often depends on local economic

and ecological factors. Overall, natural gas is the most used resource for the production of methanol worldwide. Nowadays, methanol is produced on an industrial scale exclusively utilizing a low-pressure process (5 – 10 MPa), instead of using high and medium pressures or oxidizing hydrocarbons. Even though the catalytic system with Cu, ZnO, and Al_2O_3 seems rather simple, the mechanism of the process is still discussed in literature. Since the influence of the CO_2 content on the reaction kinetics has not been clarified yet, the question whether catalysis proceeds via CO or CO_2 hydrogenation cannot be answered conclusively (Figure 2.2C). In 2011, almost 47×10^6 t/a of pure methanol were consumed, with the largest part going into formaldehyde production (28 % of the methanol produced worldwide; Figure 2.1).[63] [8]

Considering the overall two-stage formaldehyde production, it becomes obvious that an alternative process which solely uses CO_2 and avoids the additional reaction step – the necessary oxidation after a chemically unnecessary overreduction – would be highly desirable. The challenge from a chemical perspective and consequently one reason that such a process is not established yet is to selectively stop at the formaldehyde oxidation state. The transformation of CO_2 to formaldehyde with hydrogen gas is highly endergonic and endothermic (Figure 2.2D), resulting in further reduction of the carbonyl function under the required reaction conditions.[57,58,64] Beside improvements in the selective formaldehyde synthesis, another important driver for such an innovative process is the availability of cheap hydrogen gas based on renewable energy sources as an industrially viable reducing agent.

[63] J. Ott et al. in *Ullmann's Encyclopedia of Industrial Chemistry*, Wiley-VCH, **2012**.
[64] S. Dabral, T. Schaub, *Adv. Synth. Catal.* **2019**, *361*, 223–246.

[8] Alternative routes to methanol starting from CO_2 have been discussed for decades and would also provide an ecological solution for the formaldehyde production. This route would still be based on two processes but could at least use the infrastructure from the existing formaldehyde production. The key of success for such an alternative methanol synthesis is the production of renewable hydrogen gas.

2.2 Hydrogen Gas based on Renewable Energy Sources

Hydrogen gas has been important for the chemical industry for decades, but it is mostly produced from non-renewable primary energy sources (*i.e.* oil, coal, natural gas, or nuclear).[65,66] In 2013, 96 % of the total hydrogen production was based on these resources, with about 48 % coming from methane (steam reforming), 30 % from petroleum fractions in refineries (steam reforming or partial oxidation), and 18 % from coal (gasification). The remaining 4 % represent the share of water electrolysis, but only 20 % of this contribution was based on renewable energy sources.[65,67–70]

The broad application of hydrogen gas based on renewable energy sources and a shift towards a sustainable hydrogen economy is limited by the costs.[68,71] While cheap hydrogen gas is obtained from coal (1.05 – 1.83 $/kg) and natural gas (2.48 – 3.17 $/kg), the costs are much higher in case of hydrogen gas from wind power and water electrolysis (5.55 – 6.77 $/kg) or photovoltaic energy and water electrolysis (about 23 $/kg).[69,72] However, costs for electrolyzers and renewable energies are decreasing, which leads to lower production costs for the resulting hydrogen gas. Within the next decade, it is expected that the price will fall below 2 – 3 $/kg for the best production sites.[67]

Hydrogen gas has become an attractive candidate as energy carrier and for energy storage, if it is produced via ecological methods.[65,67,68,73] The renewable primary energy sources have different advantages and disadvantages. The use of biomass opens up economically viable scenarios for the renewable hydrogen gas production (1.44 – 2.83 $/kg) in the near future, but such routes are not in alignment with the ecological aspects discussed before due to the connected formation of CO_2.[70,72] Solar energy is a versatile primary energy source as it can be used in electricity-driven water electrolysis as well as thermal or photocatalytic

[65] N. Armaroli, V. Balzani, *ChemSusChem* **2011**, *4*, 21–36.
[66] S. Dunn in *Concise Encyclopedia of the History of Energy*, (Ed.: C. J. Cleveland), Elsevier, Boston, **2009**.
[67] *IRENA, 2020: Global Renewables Outlook: Energy transformation 2050*, International Renewable Energy Agency, Abu Dhabi, **2020**.
[68] *REN21: Renewables 2019 Global Status Report*, REN21 Secretariat, Paris, **2019**.
[69] *Renewable Hydrogen Technologies*, (Eds.: L. M. Gandía et al.), Elsevier, Amsterdam, **2013**.
[70] M. Ball et al. in *The Hydrogen Economy: Opportunities and Challenges*, (Eds.: M. Ball, M. Wietschel), Cambridge University Press, New York, **2009**.
[71] W. McDowall, M. Eames, *Energy Policy* **2006**, *34*, 1236–1250.
[72] J. R. Bartels et al., *Int. J. Hydrog. Energy* **2010**, *35*, 8371–8384.
[73] *IRENA, 2018: Hydrogen from renewable power: Technology outlook for the energy transition*, International Renewable Energy Agency, Abu Dhabi, **2018**.

water splitting. For electricity-driven water electrolysis, also wind, hydroelectric, geothermal, or marine energy can be used.[69]

An important factor to consider is the need for and availability of highly pure and unpolluted water. This represents another hurdle for the on-site production of hydrogen gas based on renewable energies in several arid regions where solar energy would otherwise be highly beneficial to establish cost efficient production processes.[69] This underlines the need for a global solution to achieve a more sustainable economy based partly on hydrogen gas in the near future.

2.3 Catalytic Reduction of CO_2 towards the Formaldehyde Oxidation State

Several approaches utilize sophisticated reducing agents for the conversion of CO_2 to the formaldehyde oxidation state, mostly including hydroboration,[9] hydrosilylation,[10] or the use of metal hydrides.[11] These approaches are of high academic value, but as the reductants used are either not efficient (as they are costly), not atom-efficient (as they lead to a large amount of waste), or both, the respective approaches are not relevant for industrial application and thus will not be discussed any further. Instead, catalytic processes utilizing solely carbon dioxide and hydrogen gas will be presented in the following.

Heterogeneous Systems

The first heterogeneous system for the transformation of CO_2 to formaldehyde employed a Pt–Cu/SiO_2 catalyst (Figure 2.3A). The presence of platinum was crucial for formaldehyde formation as otherwise only methanol was observed. The highest formation rate of 0.87×10^{-4} mol/min per gram of catalyst as well as the best selectivity of 80 % for formaldehyde was obtained at a Pt/Cu ratio of 3:100 at 150 °C and 6 bar with a H_2/CO_2 ratio of 20:1.[126]

Formaldehyde was also obtained when bimetallic Ni–Co nanoparticle catalysts with residual phosphorous species were studied in the reduction of CO_2 by H_2. For the catalytic transformation, the nanoparticles were supported by mesoporous silica (Figure 2.3B). A gas ratio H_2/CO_2/He of 20.7:6.6:14.7 at 6 bar was used at two different reaction temperatures of 200 °C and 350 °C. Compared to nickel or cobalt nanoparticles, the catalytic system showed an unexpected selectivity. At 200 °C, over 30 % of formaldehyde was produced along with

[126] D.-K. Lee et al., *Appl. Organomet. Chem.* **2001**, *15*, 148–150.

9 Several examples in the literature describe the formation of bis(boryl)acetal species as one of many products,[74–86] but only few optimized the system with regard to its formation or application as formaldehyde synthon.[87–93]

10 Even though the formation of bis(silyl)acetal species is already known for a long time as an intermediate in hydrosilylation of CO_2 to the methanol or methane level,[94–105] only few examples that describe the selective formation of the acetal or its application as formaldehyde synthon have been published.[106–112] One of the first examples of hydrosilylation even led to the formation of formaldehyde.[113]

11 The conversion of CO_2 to the formaldehyde oxidation state was first realized using the organozirconium Schwartz reagent.[114–118] Similar reductive procedures were reported for further transition metals.[119,120] Structural studies reported complexes with analog $\mu_{2/4}$-$CH_2O_2^{2-}$ bridges, representing the formaldehyde oxidation state, but did not start from molecular CO_2.[121–125]

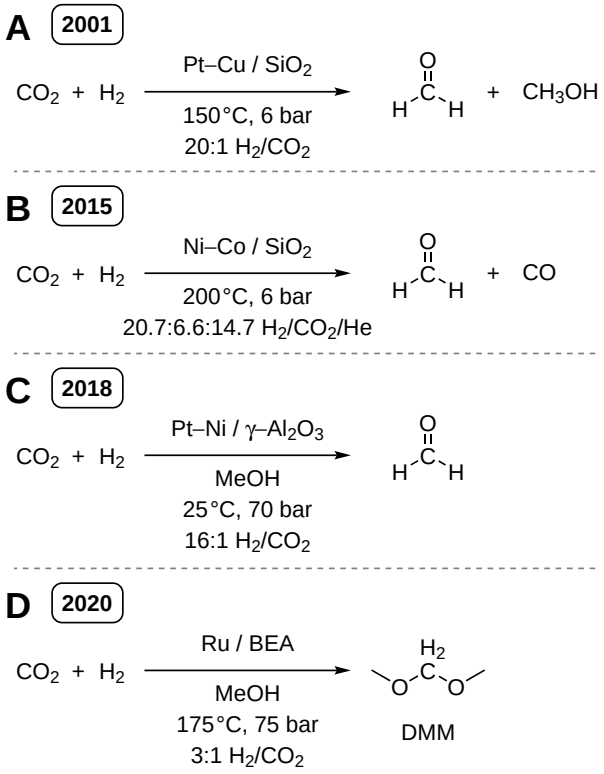

Figure 2.3: Overview of heterogeneous catalytic systems which reduce CO_2 to the formaldehyde oxidation state using H_2 as reductant. **A**: Catalytic system based on platinum and copper. Formation of formaldehyde together with methanol as the only side-product. **B**: Catalytic system based on bimetallic nanoparticles consisting of nickel and cobalt. Formation of formaldehyde together with CO as the main product. **C**: Catalytic system based on platinum and nickel. The catalysis was performed in methanol, and no side-products were detected. **D**: Catalytic system based on ruthenium and an acidic zeolite (BEA). The catalysis was performed in methanol, and dimethoxymethane (DMM) was obtained as final catalysis product.

70 % of CO and small amounts of CH_4 with a CO_2 conversion of 0.24 %. In contrast, only little formaldehyde was formed at 350 °C, at which methanol was the main side-product beside over 80 % of CO with a CO_2 conversion of 0.92 %.[127]

In 2018, a further heterogeneous system overcame the unfavorable thermodynamics by performing the catalysis in liquid media using methanol as solvent, resulting in an overall slightly exothermic process (Figure 2.3C). In total, four catalytic systems based on platinum or ruthenium with copper or nickel supported by γ–alumina were studied for the catalytic conversion. Two different pathways via CO or formic acid as intermediate were considered. As no intermediates were observed, both routes are possible. In case of the former, CO_2 is

[127]S. Carenco et al., *Small* **2015**, *11*, 3045–3053.

converted into CO via reverse water-gas shift reaction followed by direct hydrogenation of CO to formaldehyde. For formic acid as intermediate, CO_2 is hydrogenated to formic acid followed by dehydration-hydrogenation. It was shown that conversion of formic acid to formaldehyde in methanol is feasible, even though the rate of formation for formaldehyde was significantly lower than the rate of consumption for formic acid, indicating a competing decomposition pathway. The catalysts based on platinum (Pt–Cu/Al_2O_3 and Pt–Ni/Al_2O_3) proved to be superior compared to the ruthenium-based catalysts (Ru–Cu/Al_2O_3 and Ru–Ni/Al_2O_3). The molar yield of formaldehyde increases with increasing H_2/CO_2 ratio, and the highest equilibrium yield of 1.80 mmol/L per gram of catalyst was obtained with Pt–Ni at a H_2/CO_2 ratio of 16:1 at 70 bar and 25 °C.[128]

In a fourth heterogeneous system, CO_2 was reductively transformed to the formaldehyde oxidation state, yielding oxymethylene ethers (OMEs). OMEs correspond to oligomers of formaldehyde with the recurring structural unit (CH_2O) and two capping groups, typically a methyl and a methoxy group. Usually, an index indicates the number of the (CH_2O) units. A catalytic system based on ruthenium together with H–type zeolite beta (BEA) and hydrogen gas as reductant was used, for which different ruthenium contents were studied (Figure 2.3D). Methanol was used as solvent, which is necessary for the formation of dimethoxymethane (DMM), representing OME_1, and higher oxymethylene dimethyl ethers. Its dehydration by the catalyst led to dimethyl ether as side product. Even though the exothermic formation of DMM under the conditions used should be favored at lower temperatures, the yield of DMM increased with increasing temperature, indicating kinetic limitations for this transformation. At 175 °C and a H_2/CO_2 ratio of 3:1 with a total pressure of 75 bar, the yield was 9.04 mmol/L per gram of Ru/BEA catalyst after 40 min. Additionally, OME_2 was produced at these conditions. The DMM yield decreased already after short reaction times, indicating degradation pathways for the product. In this context, the influence of water was investigated. Addition of water led to formation of only traces of DMM, whereas addition of 3 Å molecular sieve led either to a higher yield of DMM at a low loading or to lower yields but stabilization of DMM at higher loading. For this system, no CO was observed in the gas phase, and a direct hydrogenation of CO_2 to formic acid was proposed. The catalysis proceeds via further reduction to formaldehyde, followed by addition of two molecules of methanol to yield DMM.[129]

[128] F. L. Chan et al., *Catal. Today* **2018**, *309*, 242–247.
[129] W. Ahmad et al., *Appl. Catal. B* **2020**, *269*, 118765.

Homogeneous Systems

The first homogeneous system utilizing hydrogen gas as reductant was based on a ruthenium complex chelated by EDTA (Figure 2.4A). The reduction of CO_2 gave formic acid and formaldehyde, with the respective rates of formation exhibiting first-order dependence on the catalyst as well as CO_2 and H_2 concentrations. The rates of decomposition to yield CO and H_2O showed the same dependence. For formaldehyde, the rate of decomposition was found to be faster than the rate of formation at the investigated conditions of 40 °C and 34 bar, limiting the system in its application for formaldehyde synthesis.[130]

In 2016, the first homogeneous system capable of selectively converting CO_2 to the formaldehyde oxidation state using hydrogen gas was described, yielding the desired product in high purity.[131] The idea was to trap formaldehyde at its oxidation state by using alcohols to form acetals, with dimethoxymethane (DMM) being the product obtained with methanol (Figure 2.4B).[12] This approach is also favored in terms of thermodynamics compared to the direct synthesis of formaldehyde from CO_2 as the free reaction enthalpy is only slightly endergonic and becomes even exergonic at higher pressures.[64] A highly versatile ruthenium catalyst with a tripodal triphosphine ligand [Ru(triphos)(tmm)] was employed in the catalysis.[13] First attempts without using any additive did not give any hydrogenation products. The use of the Brønsted acid $HNTf_2$ at 120 °C as well as 20 bar CO_2 and 60 bar H_2 resulted in a small turnover number (TON) of 4. In addition, methyl formate (MF) was obtained in similar amounts, which was considered to be an intermediate in the reaction pathway towards DMM. Changing the additive to the Lewis acid $Al(OTf)_3$ and reducing the temperature to 80 °C increased the TON for DMM to 98. It was found that increasing and decreasing the catalyst loading led to decreasing and increasing catalytic performance, respectively, which was additionally influenced by the additive to catalyst

[130] M. M. T. Khan et al., *J. Mol. Catal.* **1989**, *57*, 47–60.
[131] K. Thenert et al., *Angew. Chem. Int. Ed.* **2016**, *55*, 12266–12269.

12 DMM is an important chemical as it can be used as formaldehyde synthon or hydrolyzed to formaldehyde and methanol.[64] Further it can also be employed as almost carbon-neutral blending component for diesel fuels directly or after transformation into higher oxymethylene ethers (OME).[132,133] The importance of the last mentioned application for the transportation and energy sectors is discussed in literature.[12,134]

13 The [Ru(triphos)(tmm)] complex had been previously used for several catalytic hydrogenation reactions with CO_2.[50]

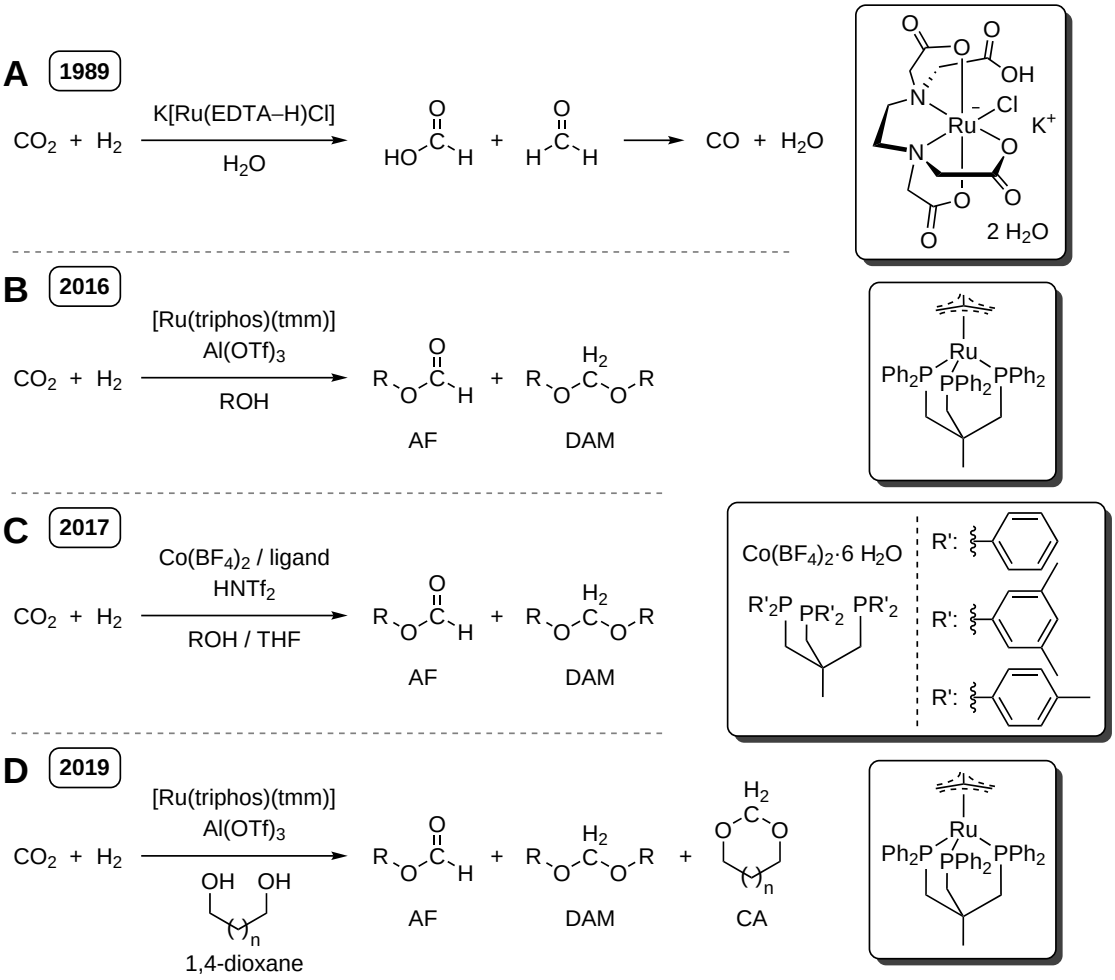

Figure 2.4: Overview of homogeneous catalytic systems which reduce CO_2 to the formaldehyde oxidation state using H_2 as reductant. **A**: Catalytic system using a Ru–EDTA complex. Formaldehyde and formic acid were obtained as transient intermediates, being finally transformed into CO and H_2O. **B–D**: Overview of homogeneous catalytic systems which selectively reduce CO_2 to the formaldehyde oxidation state using H_2 as reductant and alcohols for esterification and acetalization. In all cases, alkyl formates (AF) and dialkoxymethanes (DAM) were obtained. **B**: Catalytic system using a ruthenium complex. The best results were obtained using the Lewis acid $Al(OTf)_3$ as co-catalyst. **C**: Catalytic system using cobalt salts and triphos ligands. The best results were obtained using the Brønsted acid $HNTf_2$ as co-catalyst and THF as co-solvent. **D**: Catalytic system using a ruthenium complex. The best results were obtained using the Lewis acid $Al(OTf)_3$ as co-catalyst and 1,4-dioxane as co-solvent. In addtion to AF and DAM, cyclic acetals (CA) were obtained.

ratio.[131] The former effect was attributed to catalyst deactivation by dimerization.[135–137] At finally optimized conditions (catalyst loading of 6 μmol, 80 °C, 20 bar CO_2, and 60 bar H_2), TONs for DMM and MF of 214 and 104 were reached, respectively. By labeling experiments using fully deuterated methanol together with nonlabelled CO_2 and H_2, the origin of the central methylene group could be assigned to CO_2 as the C1 source. Additionally, different alcohols were investigated for the suitability in esterification and acetalization, but all showed a reduced performance in the catalytic investigation compared to methanol. The observation of methoxymethanol (MM) in the experiments indicated a step-wise reaction mechanism via reduction of CO_2 and simultaneous esterification to MF, further reduction to MM, and finally acetalization to DMM.[131]

Shortly after this achievement, a non-precious transition-metal catalyst system based on cobalt salts and the same triphos ligand was used together with a solvent mixture of THF and MeOH (Figure 2.4C). In a first proof-of-concept study, MF was transformed to DMM applying 80 bar H_2 at room temperature with a low TON and yield of 15 and 2 %, respectively. Screening of cobalt salts and adding the Brønsted acid $HNTf_2$ gave 373 as highest TON for DMM with a yield of 56 %. Starting from CO_2 (20 bar CO_2 and 60 bar H_2), a higher temperature of 100 °C was necessary, yielding DMM and MF with TONs of 92 and 32, respectively. Even higher catalytic activity was observed when changing the alcohol to ethanol, yielding diethoxymethane and ethyl formate with TONs of 109 and 14, respectively. Interestingly, the formation of methanol due to over-reduction was stated for this catalytic system when using ethanol. While this reduces the overall efficiency with regard to the reduction towards the formaldehyde level, it could still open a pathway to DMM using solely CO_2 and H_2. Further variation of the alcohol did not lead to any improvements but resulted in the selective transformation of CO_2 to methanol for certain alcohols.[138] Additionally, sterically more demanding and more electron-rich structural analogs of the ligand[139] were investigated, yielding an even higher TON for DMM of 157 together with a TON for MF of 37.[138]

In an additional study, the catalytic system based on ruthenium was applied for the synthesis of cyclic and linear acetals, starting from CO_2, H_2, and biomass derived diols (Figure

[135]S. Wesselbaum et al., *Chem. Sci.* **2015**, *6*, 693–704.
[136]T. vom Stein et al., *J. Am. Chem. Soc.* **2014**, *136*, 13217–13225.
[137]J. Coetzee et al., *Chem. Eur. J.* **2013**, *19*, 11039–11050.
[138]B. G. Schieweck, J. Klankermayer, *Angew. Chem. Int. Ed.* **2017**, *56*, 10854–10857.
[139]M. Meuresch et al., *Angew. Chem. Int. Ed.* **2016**, *55*, 1392–1395.

2.4D). In a large substrate scope, the effect of structurally different diols on the product distribution between the cyclic and the linear product was investigated. Due to increased selectivity for the cyclic acetal at longer reaction times, it was proposed that – in contrast to the acetalization of the alkoxymethanols to dialkoxymethanes in case of alcohols – the diol enables a competition between inter- and intramolecular acetalization. The alkoxymethanols derived from diols can either react with a further diol to give the linear acetal or undergo cyclization to yield the cyclic acetal. Overall, ethane- and propanediols preferentially formed cyclic acetals, whereas longer aliphatic chains between the two hydroxyl groups led to reversed selectivity, favoring the linear acetals.[140]

[140]K. Beydoun, J. Klankermayer, *Chem. Eur. J.* **2019**, *25*, 11412–11415.

3 Objectives

The shift from fossil to renewable resources, especially carbon dioxide, for the synthesis of industrial bulk chemicals is in alignment with the drive for more sustainable processes. Although the results presented in chapter 2 are already promising, the catalytic activities are still far too low to consider industrial realization. The fact that only few studies on CO_2 reduction observe intermediates in the formaldehyde oxidation state, not to mention isolating formaldehyde or a derived synthon, demonstrates how challenging this transformation is. As the carbonyl function is susceptible to further reduction, a catalytic system enabling the desired transformation needs to be perfectly designed and optimized. Homogeneous catalysis is considered promising to conquer this task, since steric and electronic properties of the catalyst can be well adjusted by changing the ligands or the metal center, and spectroscopic and spectrometric methods allow mechanistic investigations with comparatively little effort. Even though industry always prefers heterogeneous catalysis, *inter alia* due to the ease of product separation and catalyst recovery, an homogeneous catalytic system providing high activity, selectivity, and the ability to be recovered will definitely be considered for a potential application.

The superior objective of this part of the dissertation is the design and optimization of a highly active and selective homogeneous catalytic system for the transformation of CO_2 to the formaldehyde oxidation state (Figure 3.1). The main product of the catalytic system shall be formaldehyde or a corresponding synthon, which shall be stable and isolable. In case of a synthon, a conversion to formaldehyde should be plausible and efficient from an atom-economic point of view. In support of this objective, the four following points shall be addressed.

1. An initial screening of different catalysts shall provide better understanding of structural prerequisites to identify a lead structure. A comprehensive optimization of the process parameters shall increase the catalytic performance and improve the overall process efficiency.
2. The most active catalyst shall be further structurally varied, with the resulting catalysts being investigated for their catalytic activity. The catalytic systems shall be optimized starting from the conditions obtained in the previous screening.
3. More efficient optimization strategies utilizing an algorithmic workflow shall be established and used for the complex optimization in the multidimensional parameter space. The data already obtained in previous screenings shall be used as starting point for the algorithmic workflow.
4. A setup for fast and reliable screening of the investigated transformation shall be designed and built. The autoclave setup should deliver precise results over a wide temperature range at high pressures, and the coupling of analytical equipment should be considered.

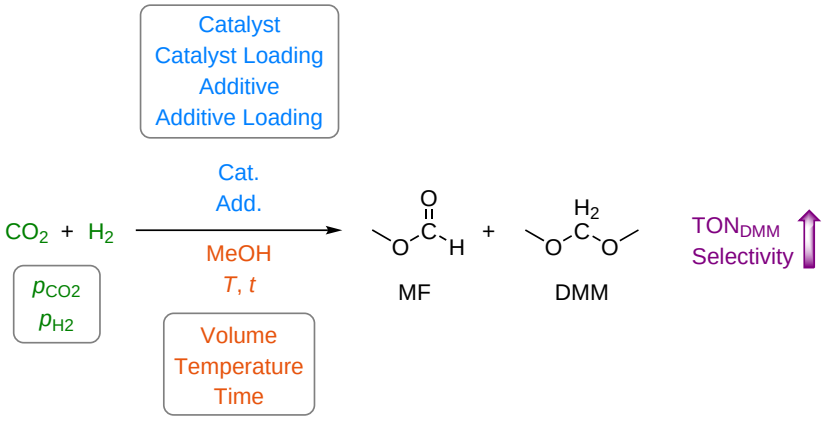

Figure 3.1: Optimization of the selective synthesis of dimethoxymethane (DMM) starting from CO_2 and H_2 with the intermediate methyl formate (MF) as only side-product. The parameters to be optimized are shown in boxes, and the optimization goal is written in purple.

4 Published Work

4.1 Selective Ruthenium-Catalyzed Transformation of Carbon Dioxide: An Alternative Approach toward Formaldehyde

Max Siebert, Max Seibicke, Alexander F. Siegle, Sabrina Kräh, and Oliver Trapp

Prologue

An industrially relevant alternative synthesis of formaldehyde – in the form of dimethoxymethane – starting solely from carbon dioxide and hydrogen gas is presented. The homogeneous catalytic system consisting of a ruthenium complex and a Lewis acid was optimized by screening catalysts as well as catalytic conditions. By this, the catalytic activity was increased by more than 350 % compared to prior work.

Author Contributions

M. Siebert designed and performed the catalytic experiments. M. Siebert, M. Seibicke, and S. K. performed the syntheses. All authors contributed to the interpretation of the data. The manuscript was written by M. Siebert, and all authors contributed to the manuscript. O. T. supervised the project.

License

Supporting Information

The supporting information is available at https://doi.org/10.1021/jacs.8b10233.

JACS
JOURNAL OF THE AMERICAN CHEMICAL SOCIETY
Cite This: J. Am. Chem. Soc. 2019, 141, 334−341
Article
pubs.acs.org/JACS

Selective Ruthenium-Catalyzed Transformation of Carbon Dioxide: An Alternative Approach toward Formaldehyde

Max Siebert, Max Seibicke, Alexander F. Siegle, Sabrina Kräh, and Oliver Trapp*

Department Chemie, Ludwig-Maximilians-Universität München, Butenandtstraße 5-13, 81377 München, Germany

Supporting Information

ABSTRACT: Formaldehyde is an important precursor to numerous industrial processes and is produced in multimillion ton scale every year by catalytic oxidation of methanol in an energetically unfavorable and atom-inefficient industrial process. In this work, we present a highly selective one-step synthesis of a formaldehyde derivative starting from carbon dioxide and hydrogen gas utilizing a homogeneous ruthenium catalyst. Here, formaldehyde is obtained as dimethoxymethane, its dimethyl acetal, by selective reduction of carbon dioxide at moderate temperatures (90 °C) and partial pressures (90 bar H_2/20 bar CO_2) in the presence of methanol. Besides the desired product, only methyl formate is formed, which can be transformed to dimethoxymethane in a consecutive catalytic step. By comprehensive screening of the catalytic system, maximum turnover numbers of 786 for dimethoxymethane and 1290 for methyl formate were achieved with remarkable selectivities of over 90% for dimethoxymethane.

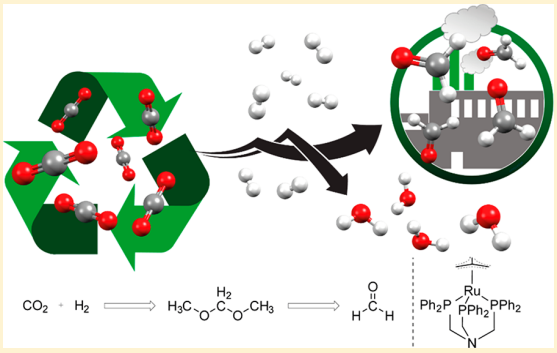

INTRODUCTION

Carbon dioxide is considered to play an important role in climate change due to its greenhouse properties and continuous accumulation in the atmosphere. Since 1750, the atmospheric concentration of CO_2 has dramatically risen from 278 ppm to 390 ppm in 2011.[1] In the following five years, the atmospheric concentration even exceeded 400 ppm, strengthening the assumption that the emission of CO_2 will further increase within the next decades, thus strongly impacting the world's climate.[2,1b] Utilization of CO_2 as an alternative feedstock for the chemical industry is an opportunity to rebalance the carbon cycle and to reduce CO_2 emissions, thereby providing a renewable resource for the anthropogenic value chains of generations to come.[3]

In the last decades, impressive progress has been made in the catalytic transformation of CO_2 toward chemically relevant products.[4] The challenge of such transformations is the high kinetic barrier resulting from the low energy level of molecular CO_2.[5] There are many examples for the synthesis of functional molecules starting from carbon dioxide and hydrogen gas, such as formic acid or formate salts,[6] alkyl formates,[7] formamides,[7a,b,8] or methanol.[9] The catalytic transformation toward the formaldehyde oxidation level remains challenging since the resulting aldehyde group is susceptible to further reduction.[4f]

Only a few reports describe the homogeneously catalyzed synthesis of formaldehyde or derivatives thereof. In 2012, Bontemps and Sabo-Etienne used pinacolborane as reducing agent in a ruthenium-catalyzed reduction of CO_2 to trap formaldehyde as bis(boryl)methylene acetal.[10] Free formaldehyde was observed via NMR analysis in the borane-mediated reduction of CO_2 using a slightly modified polyhydride ruthenium complex. In the presence of a primary amine, the corresponding imine was formed, which could be hydrolyzed, yielding formalin solution.[11] A similar hydroboration of CO_2 was achieved using iron, cobalt, and copper complexes.[12] In 2015, Oestreich and Metsänen reported a ruthenium-catalyzed hydrosilylation of CO_2 to bis(silyl)-methylene acetal using triethylsilane.[13] Likewise, López-Serrano and Rodríguez obtained the same acetal using a nickel catalyst under similar conditions.[14] The groups of Berke and Piers utilized frustrated Lewis pairs derived from rhenium and scandium complexes in combination with $B(C_6F_5)_3$ for the selective hydrosilylation of CO_2.[15] These reports are of high academic value but do not meet industrial needs due to the stoichiometric use of reducing reagents. The first catalytic conversion of CO_2 to the formaldehyde oxidation level using molecular hydrogen and a homogeneous catalyst was described by Klankermayer et al. in 2016. In the presence of alcohols, CO_2 was transformed into dialkoxymethane ethers using a ruthenium complex and acidic cocatalysts (Scheme 1). The best result was obtained using a molecular ruthenium-triphos catalyst and aluminum triflate, yielding dimethoxymethane (DMM) with a turnover number (TON) of 214. Besides the product, methyl formate (MF) was formed with a TON of 104.[16]

In 2017, Klankermayer and Schieweck used the triphos ligand and derivatives thereof in combination with cobalt salts

Received: September 21, 2018
Published: December 9, 2018

DOI: 10.1021/jacs.8b10233
J. Am. Chem. Soc. 2019, 141, 334−341

Scheme 1. Acetalization Approach toward the Formaldehyde Oxidation Level[16]

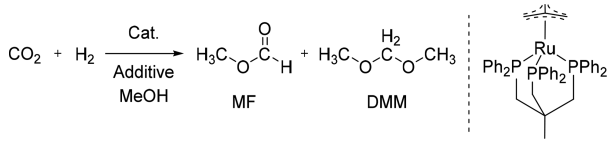

and an acidic cocatalyst for the same catalytic transformation. The selectivity for DMM was improved compared to the previously reported ruthenium system with TONs for DMM and MF reaching 157 and 37, respectively.[17]

We envisaged that variation of the electronic and steric properties of the triphos ligand as well as of the coordinating units would lead to a significant increase in stability and activity of the catalytic systems, thus yielding higher TONs for DMM and MF. Herein, we report a highly optimized ruthenium-catalyzed transformation of carbon dioxide to DMM and MF, thereby providing an attractive approach for the synthesis of formaldehyde in an energetically favorable and atom-efficient industrial process.

RESULTS AND DISCUSSION

For the comprehensive screening of potential catalysts for the transformation of CO_2 to formaldehyde derivatives, we synthesized structurally flexible ruthenium catalysts to tune steric and electronic properties (Scheme 2). All catalysts were

Scheme 2. Ruthenium Complexes for the Catalytic Transformation of CO_2 to DMM

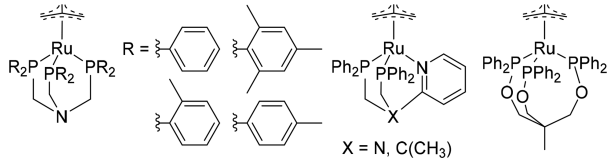

based on tripodal ligands and the doubly charged trimethylenemethane anion as counterion. First, we varied the electronic and steric properties of the ligand by changing the backbone of the widely used triphos ligand in combination with increasing sterical demand in the coordinating phosphine units. We chose the *N*-triphos ligand as basic ligand motif due to its versatile application and the simplicity of synthesis.[18] Second, we exchanged one of the phosphine units with a hemilabile pyridyl ligand to increase activity of the resulting catalysts. Last, we changed the linker from methylene to oxymethylene groups to vary the coordinating properties of the ligands.

The synthesis of tripodal *N*-triphos ligands bearing a nitrogen atom in the backbone was achieved according to a modular two-step procedure published by Gade et al.[19] The respective phosphines were transformed into the air- and moisture-stable phosphonium salts **1a−c** by reaction with formaldehyde in the presence of acid with 54−95% yield (Scheme 3A).[20] The ligands *N*-triphos^{Ph} (**2a**), *N*-triphos$^{o\text{-}Tol}$ (**2b**), and *N*-triphos$^{p\text{-}Tol}$ (**2c**) were prepared by reaction of **1a−c** with triethylamine and ammonium chloride with good to excellent yields (74−90%, Scheme 3A). The ligand *N*-triphos^{Mes} (**2d**) could not be synthesized according to this procedure, as the addition of triethylamine in the second step favored the elimination of formaldehyde, yielding the initial reactant dimesitylphosphine. Ligand **2d** was synthesized by

Scheme 3. Synthetic Procedures toward the Tripodal Ligands

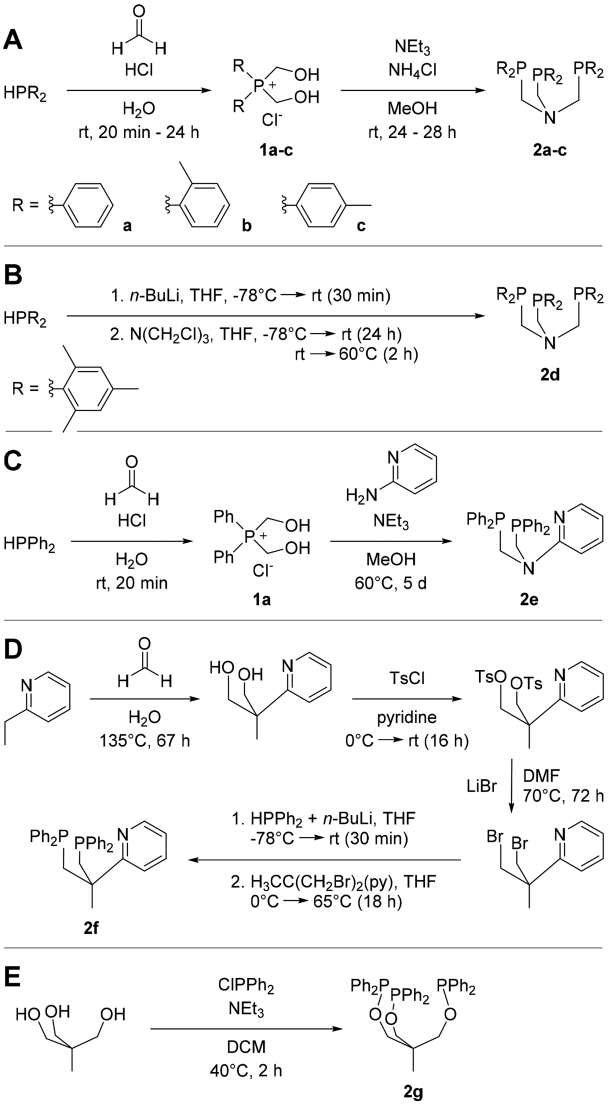

reaction of the lithiated phosphine with tris(chloromethyl)-amine with 38% yield (Scheme 3B). Using the phosphonium salt **1a**, the ligand *N*-py-diphos^{Ph} (**2e**) was prepared by changing the amine of the previously used protocol to 2-aminopyridine (50% yield, Scheme 3C). The analogue py-diphos^{Ph} (**2f**) was synthesized in an optimized procedure, derived from the work by Doherty et al., starting with 2-ethylpyridine.[21] The ligand was isolated with 7% yield after the four-step synthesis (Scheme 3D). The tridentate phosphinite ligand triphos^{OPPh2} (**2g**) was obtained according to a procedure by Marchand-Brynaert et al.[22] Reaction of 1,1,1-tris(hydroxymethyl)ethane with chlorodiphenylphosphine in the presence of triethylamine yielded **2g** with 34% yield (Scheme 3E).

Subsequently, the ruthenium complexes were synthesized according to the protocol of Klankermayer and Leitner.[9c,23] The ligands were heated with the ruthenium precursor [Ru(2-methylallyl)$_2$(COD)] (COD = cyclooctadiene) in toluene to 110 °C (Scheme 4). The ruthenium complexes **3a,c** were isolated after 3−4 days with 44% and 21% yield, whereas the

DOI: 10.1021/jacs.8b10233
J. Am. Chem. Soc. 2019, 141, 334−341

Scheme 4. Complexation of the Synthesized Ligands

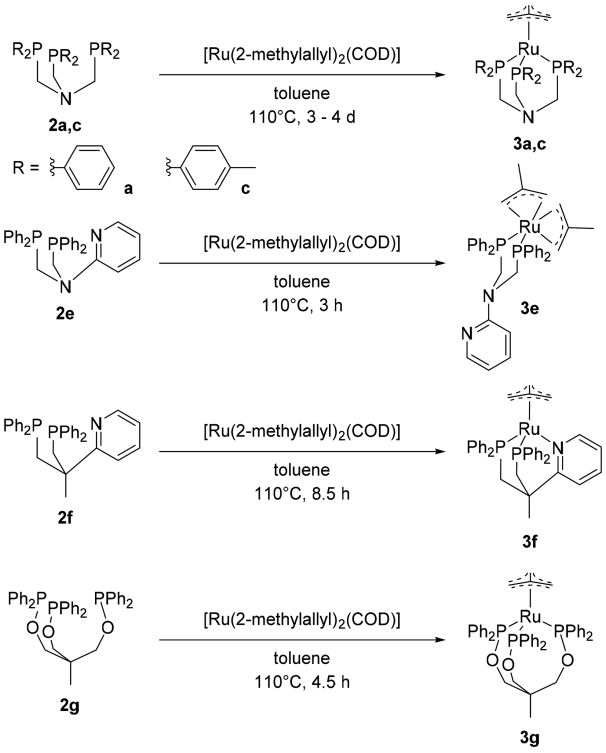

respective complexes **3b** and **3d** of the ligands **2b** and **2d** could not be isolated purely. Therefore, the complexes were formed *in situ* in later catalytic investigations. Complexes **3e–g** were isolated after heating the respective ligand with the ruthenium precursor in toluene to 110 °C for 3–8.5 h with 33–64% yield. Astonishingly, complex **3e** did not eliminate isobutene at all after heating for 3 h. The two phosphine groups of ligand **2e** coordinated to the ruthenium center, while the pyridyl ligand was unable to do so.

The X-ray crystallographic structure of **3c** confirmed the expected distorted octahedral molecular geometry (Figure 1).

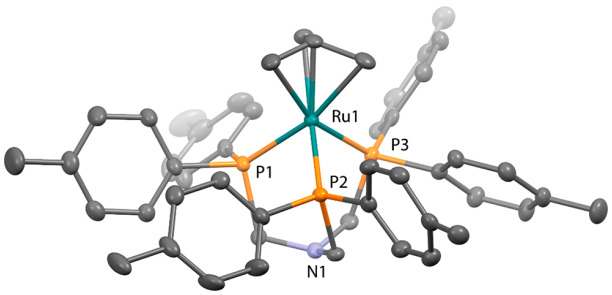

Figure 1. Molecular structure of complex **3c**. Ellipsoids are shown at the 50% probability level. Hydrogen atoms and the solvent molecule are omitted for clarity.

The obtained structure explains the difficulties in accessing complexes **3b** and **3d**. Due to the spatial proximity of the *o*-methyl groups to the phosphine, steric and repulsive forces become too strong for effective complexation (see the SI for molecular structure of ligand **2d**).

Next, all catalysts were investigated in the catalytic transformation of CO_2 to DMM and MF (Scheme 1, Table 1). Initial screening conditions were chosen according to the system described by Klankermayer et al.[16] The catalyses were performed over 18 h at 80 °C with $Al(OTf)_3$ as Lewis acid utilizing 60 bar of H_2 and 20 bar of CO_2.

Table 1. Initial Screening Results of Catalysts in the Selective Synthesis of DMM Starting from CO_2 and H_2[a,b,c]

entry	cat.	TON_{DMM}	TON_{MF}
1	[Ru][16]	214	104
2	[Co][17]	157	37
3	**3a**	292 ± 25	112 ± 4
4	**3b**[d]	2 ± 0	23 ± 0
5	**3c**	221 ± 40	90 ± 25
6	**3d**[d]	3 ± 2	6 ± 1
7	**3e**	7 ± 4	39 ± 4
8	**3f**	5 ± 0	105 ± 6
9	**3g**	32 ± 10	83 ± 7

[a]Catalysis conditions: 1.50 μmol of catalyst, 6.25 μmol of $Al(OTf)_3$, 0.5 mL of MeOH, 80 °C, 60 bar of H_2, 20 bar of CO_2, 18 h. [b]TONs were determined by ^1H NMR spectroscopy using mesitylene as internal standard. [c]All data are the average of two runs, and the standard deviation is indicated. [d]The catalyst was formed *in situ*: 1.50 μmol of [Ru(2-methylallyl)$_2$(COD)], 1.50 μmol of ligand **2b** or **2d**, respectively.

Already at the initial screening conditions, the catalysts **3a** and **3c** yielded higher TONs for DMM and MF compared to the [Ru(triphos)(tmm)] (tmm = trimethylenemethane dianion) system (Table 1, entries 1–3 and 5).[16] The complex [Ru(*N*-triphos^{Ph})(tmm)] (**3a**) showed the best results with a TON for DMM of 292 and a TON for MF of 112 (Table 1, entry 3). The modification of the aryl groups of the phosphines in the complex [Ru(*N*-triphos$^{p\text{-}Tol}$)(tmm)] (**3c**) resulted in slightly decreased activity compared to **3a** (Table 1, entry 5). The low TONs obtained with [Ru(*N*-triphos$^{o\text{-}Tol}$)(tmm)] (**3b**) and [Ru(*N*-triphos^{Mes})(tmm)] (**3d**) can be explained by the *in situ* strategy for the formation of the complexes (Table 1, entries 4 and 6). Apparently, the complexation of the ligands is not feasible under these catalytic conditions.

The complexes [Ru(*N*-py-diphos^{Ph})(2-methylallyl)$_2$] (**3e**) and [Ru(py-diphos^{Ph})(tmm)] (**3f**) showed low activity in the formation of DMM, whereas the TON of MF was moderate (Table 1, entries 7 and 8). Especially for **3f**, the TON of MF with 105 was noteworthily high (Table 1, entry 8). Interestingly, complex **3e** showed activity even though ligand **2e** coordinated only in a bidentate manner. The complex [Ru(triphos^{OPPh2})(tmm)] (**3g**) showed reasonable activity for both products (Table 1, entry 9).

On the basis of the highly promising results obtained with complex **3a**, we optimized the catalysis conditions with regard to temperature, partial pressure of H_2 and CO_2, reaction time, and additive as well as catalyst and Lewis acid concentration.

We started with investigating the influence of the temperature in a range between 20 and 120 °C (Table 2, entries 1–9, Figure 2A). The TON for both DMM and MF is strongly temperature-dependent with the highest TON for DMM between 85 and 90 °C (Table 2, entries 4 and 5) and the highest TON for MF at 70 °C or probably lower (Table 2, entry 2). The TON for DMM even exceeded 300 for 85 and 90 °C. Remarkably, the catalyst showed activity even at 20 °C (Table 2, entry 1). We chose 90 °C as the best result for

DOI: 10.1021/jacs.8b10233
J. Am. Chem. Soc. 2019, 141, 334–341

Table 2. Optimization of Catalysis Conditions with Regard to Temperature as Well as Partial Pressure of H_2 and CO_2[a,b,c]

entry	T (°C)	p_{H2} (bar)	p_{CO2} (bar)	TON_{DMM}	TON_{MF}
1	20	60	20	8 ± 5	51 ± 7
2	70	60	20	164 ± 15	161 ± 5
3	80	60	20	292 ± 25	112 ± 4
4	85	60	20	324 ± 9	93 ± 3
5	90	60	20	310 ± 12	85 ± 5
6	95	60	20	271 ± 8	73 ± 4
7	100	60	20	208 ± 9	66 ± 6
8	110	60	20	119 ± 9	52 ± 5
9	120	60	20	56 ± 8	42 ± 1
10	90	40	20	250 ± 14	69 ± 2
11	90	50	20	279 ± 21	76 ± 4
12	90	70	20	319 ± 24	82 ± 4
13	90	80	20	326 ± 31	83 ± 5
14	90	90	20	363 ± 18	92 ± 9
15	90	100	20	332 ± 27	86 ± 6
16	90	90	5	97 ± 18	8 ± 1
17	90	90	10	213 ± 10	35 ± 2
18	90	90	15	313 ± 38	68 ± 3
19	90	90	25	361 ± 21	101 ± 7
20	90	90	30	329 ± 18	108 ± 7
21	90	90	40	275 ± 14	118 ± 2

[a]Catalysis conditions: 1.50 μmol of catalyst, 6.25 μmol of $Al(OTf)_3$, 0.5 mL of MeOH, 18 h. [b]TONs were determined by ^1H NMR spectroscopy using mesitylene as internal standard. [c]All data are the average of three runs, and the standard deviation is indicated.

further optimization, thereby balancing activity and selectivity (TON_{DMM} 310 and TON_{MF} 85).

Next, the partial pressure of H_2 was varied between 40 and 100 bar, while all other parameters were kept constant (Table 2, entries 10−15, Figure 2B). The TON of DMM was highest at 90 bar of H_2 (Table 2, entry 14), whereas the TON of MF barely changed at pressures higher than 50 bar, prompting us to use 90 bar of H_2 for all further experiments (TON_{DMM} 363 and TON_{MF} 92).

Hereafter, the influence of the partial pressure of CO_2 was analyzed by changing the CO_2 pressure between 5 and 40 bar (Table 2, entries 16−21, Figure 2C). The results indicate a strong dependency of the catalyst activity on the CO_2 pressure. The TON of both DMM and MF increased with increasing CO_2 pressure. Whereas the TON for DMM reached its maximum at 20 bar of CO_2 (Table 2, entry 14), the TON for MF increased until 40 bar of CO_2 was applied (Table 2, entry 21). Due to the very low MF formation at low CO_2 pressures, the selectivity at 5 bar of CO_2 even exceeded 90% for DMM (Table 2, entry 16).

At this point, we were intrigued by the high selectivities that were achieved using low CO_2 pressures. In published work, it was stated that the catalytic hydrogenation of CO_2 terminates selectively at the formaldehyde level using the [Ru(triphos)(tmm)] system.[16] Consequently, we investigated the influence of time on the product distribution at 5 bar of CO_2. We envisioned achieving high TONs with high selectivities by increasing the reaction time to several days (Table 3, entries 1−8, Figure 2D). Surprisingly, the TONs did not increase continuously. For DMM, the TON reached a maximum after 12 h (Table 3, entry 3), whereas in the case of MF the TON decreased continuously. After 168 h, nearly no product but also no degradation products could be detected in the ^1H NMR spectra (Table 3, entry 8, see SI). Most likely, the catalyst decomposes in the course of the reaction and the resulting degraded catalyst is still able to deplete the formed DMM and MF.

Therefore, we examined the dependency of the product distribution on the time of catalysis at 20 bar of CO_2 (Table 3, entries 9−16, Figure 2E). Here, the maximum for both TON of DMM and MF was reached after 18 h (Table 3, entry 12), which is why this reaction time was chosen for further optimization.

Subsequently, the influence of the Lewis acid was investigated (Table S3.1 in the SI, Figure 2F). In general, the employed metal triflates led to higher activity of the catalytic system than the boron-based Lewis acids. $Al(OTf)_3$ gave the best results for the former (Table S3.1 in the SI, entry 1), whereas $BF_3(OEt_2)$ yielded the highest TONs for the latter (Table S3.1 in the SI, entry 8).

An immense increase in activity could be achieved by varying the concentration of the catalyst while the catalyst to Lewis acid ratio remained unchanged (Table 4, entries 1−6, Figure 2G). The maximum TON for DMM was reached at a catalyst loading of 0.38 μmol (Table 4, entry 2), whereas the TON of MF increased continuously with decreasing catalyst loading. At a catalyst loading of 0.19 μmol, the TON for MF even exceeded 1000 (Table 4, entry 1). For further experiments, we chose 0.38 μmol of catalyst loading.

Last, we investigated the influence of changing the catalyst to Lewis acid ratio while the catalyst loading was kept constant (Table 4, entries 7−11, Figure 2H). The best results were still achieved using 1.56 μmol of Lewis acid with TONs for DMM and MF of 786 and 533, respectively (Table 4, entry 2). By increasing the amount of Lewis acid beyond this, the TON of DMM did not change significantly, whereas the TON of MF decreased slightly compared to the best result (Table 4, entries 9−11). Reducing the amount of Lewis acid below 1.56 μmol led to a strong decrease in the TON of DMM and an increase in the TON of MF (Table 4, entries 7 and 8).

In further experiments, we investigated the transformation of MF to DMM by using MF instead of CO_2 as starting material for the hydrogenation reaction. After 18 h, MF was selectively transformed to DMM. Following the separation of DMM, the formed MF can thus be returned to the catalytic process, leading to higher TONs for DMM in the next reaction cycle.

After catalysis, DMM can be easily hydrolyzed to formaldehyde and methanol, yielding the desired product by distillation.[24] For an industrial application, complex **3a** has the additional advantage that it is air-stable for over two months and stable in solution under inert conditions for over 2 weeks. Further, the synthesis of the ligand can easily be scaled up (see the SI). Based on these results, an industrial process for the energetically favorable and atom-efficient conversion of CO_2 to formaldehyde using the presented catalytic system in a batch process can be envisioned. Also, the immediate product, DMM, exhibits the potential for direct application. It can be used as a fuel additive in biofuels due to its ability to reduce soot formation during the combustion in diesel engines and its origin in a renewable feedstock. Further, DMM is a building block for the synthesis of higher order oxymethylene ethers, which can be implemented as synthetic fuels providing an alternative for diesel.[4g,25]

DOI: 10.1021/jacs.8b10233
J. Am. Chem. Soc. 2019, 141, 334−341

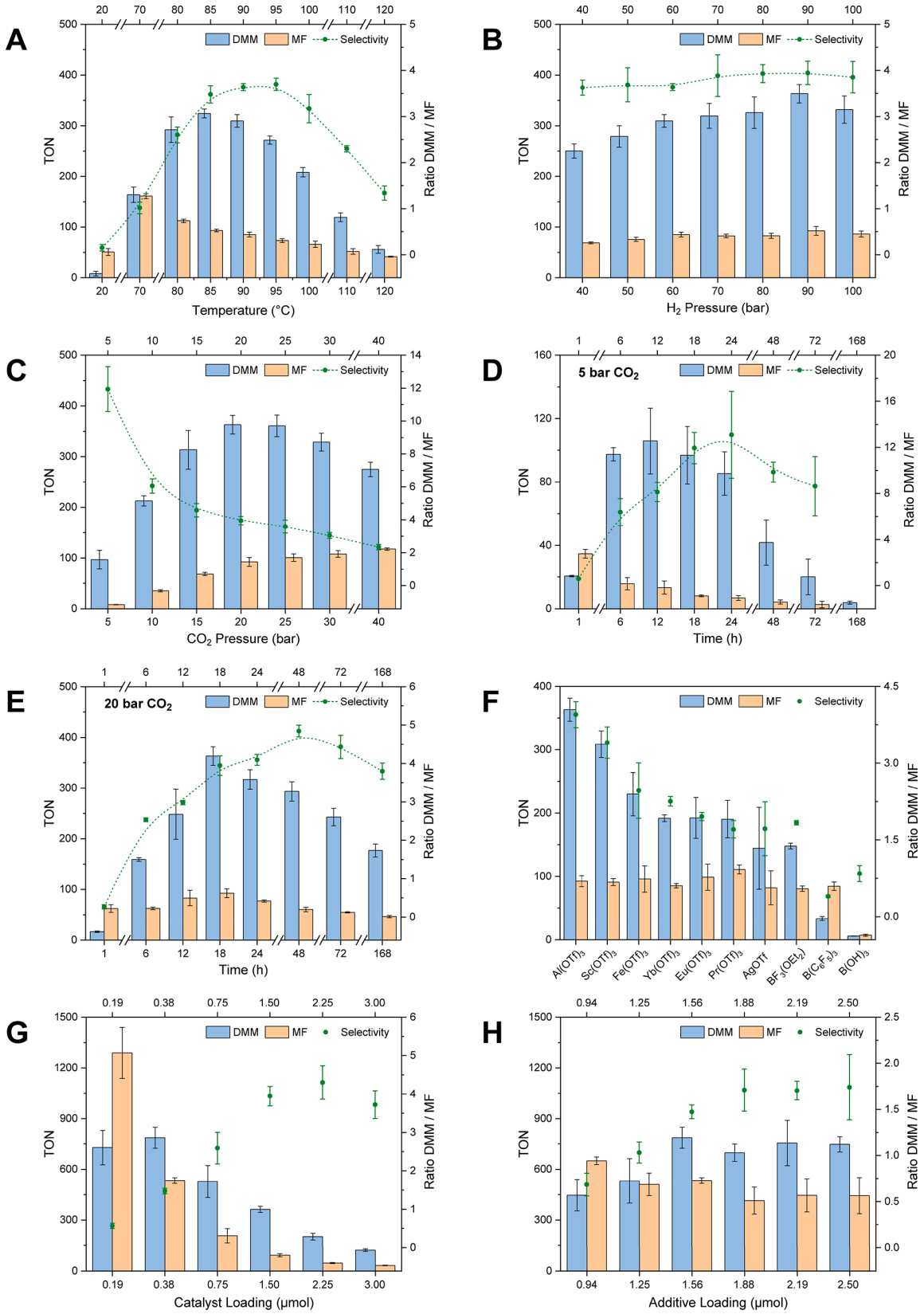

Figure 2. Summarized bar plots of the TONs in the catalytic transformation of CO_2 to DMM and MF in dependence on the investigated reaction parameters.

DOI: 10.1021/jacs.8b10233
J. Am. Chem. Soc. 2019, 141, 334−341

Table 3. Optimization of Catalysis Conditions with Regard to Time of Catalysis at 5 and 20 bar of CO_2[a,b,c]

entry	p_{CO2} (bar)	t (h)	TON_{DMM}	TON_{MF}
1	5	1	21 ± 0	35 ± 3
2	5	6	97 ± 4	16 ± 4
3	5	12	106 ± 21	13 ± 4
4	5	18	97 ± 18	8 ± 1
5	5	24	85 ± 14	7 ± 1
6	5	48	42 ± 14	4 ± 1
7	5	72	20 ± 11	3 ± 2
8	5	168	4 ± 1	0 ± 0
9	20	1	17 ± 2	63 ± 8
10	20	6	159 ± 4	63 ± 3
11	20	12	248 ± 49	83 ± 15
12	20	18	363 ± 18	92 ± 9
13	20	24	317 ± 19	77 ± 2
14	20	48	293 ± 19	61 ± 4
15	20	72	243 ± 17	55 ± 1
16	20	168	177 ± 13	47 ± 2

[a]Catalysis conditions: 1.50 μmol of catalyst, 6.25 μmol of $Al(OTf)_3$, 0.5 mL of MeOH, 90 °C, 90 bar H_2. [b]TONs were determined by ^1H NMR spectroscopy using mesitylene as internal standard. [c]All data are the average of three runs, and the standard deviation is indicated.

Table 4. Optimization of Catalysis Conditions with Regard to the Amount of the Lewis Acid[a,b,c]

entry	n_{cat} (μmol)	n_{add} (μmol)	TON_{DMM}	TON_{MF}
1	0.19	0.78	728 ± 102	1290 ± 151
2	0.38	1.56	786 ± 62	533 ± 17
3	0.75	3.13	528 ± 94	206 ± 42
4	1.50	6.25	363 ± 18	92 ± 9
5	2.25	9.38	201 ± 20	47 ± 3
6	3.00	12.50	122 ± 7	33 ± 2
7	0.38	0.94	447 ± 93	650 ± 22
8	0.38	1.25	532 ± 131	511 ± 67
9	0.38	1.88	698 ± 51	415 ± 80
10	0.38	2.19	756 ± 134	446 ± 98
11	0.38	2.50	748 ± 45	444 ± 107

[a]Catalysis conditions: $Al(OTf)_3$, 0.5 mL of MeOH, 90 °C, 90 bar of H_2, 20 bar of CO_2, 18 h. [b]TONs were determined by ^1H NMR spectroscopy using mesitylene as internal standard. [c]All data are the average of three runs, and the standard deviation is indicated.

CONCLUSION

We present optimized catalysis conditions for the homogeneously catalyzed transformation of CO_2 to DMM and MF using the ruthenium-triphos complex **3a** with regard to temperature, partial pressure of H_2 and CO_2, reaction time, and additive as well as catalyst and Lewis acid concentration. Compared to the results using the initial parameters (TON_{DMM} 292 and TON_{MF} 112), the catalytic system was significantly improved, leading to a nearly 3-fold increase of the TON of DMM to 786 (with it: TON_{MF} 533). The activity could also be optimized in favor of MF, yielding a TON of 1290 with only a slight decrease in DMM formation (TON_{DMM} 728). Further, the selectivity for DMM shows a strong dependency on the catalysis parameters and can be increased to above 90% (TON_{DMM} 97 and TON_{MF} 8). Thus, the catalytic conditions can be adjusted depending on the desired product distribution. Using molecular hydrogen and a homogeneous catalyst, this catalytic system is unique in its activity and ease of adjustment, converting CO_2 to the formaldehyde oxidation level. The present results exceed by far literature data and showcase the possibility for an atom-efficient, alternative pathway toward formaldehyde in the near future.

EXPERIMENTAL SECTION

The complete detailed description of all experiments, the spectroscopic data of compounds, and the NMR spectra of compounds and catalysis samples can be found in the Supporting Information. In order to improve comprehensibility, simplified names were used in some cases rather than using exact IUPAC names.

All novel ligand precursors (**1b** and **1c**), ligands (**2b**, **2c**, and **2d**), and complexes (**3c**, **3e**, and **3f**) were completely characterized by NMR spectroscopy, HR-MS, IR spectroscopy, and elemental analysis. The novel complex **3g** exhibited too broad signals in the NMR spectra and thus was characterized by HR-MS, IR spectroscopy, and elemental analysis. Furthermore, X-ray diffraction analysis from a single crystal was obtained for compounds **1b**, **2c** (in its phosphine oxide form), **2d**, and **3c** (see the SI).

The catalyses were performed in stainless steel high-pressure autoclaves using an NMR tube as inset and a small stirring bar for mixing. The catalyst and the additive were suspended in a Schlenk tube in MeOH, and the mixture was stirred for 1 h. The autoclave was evacuated and flushed with nitrogen three times before a 0.5 mL reaction mixture was transferred into the NMR tube inset. The carbon dioxide gas line was purged with CO_2, and the hydrogen gas line was purged with H_2 at least seven times. After the autoclave was pressurized with CO_2, the CO_2 was deposited by cooling the autoclave to −78 °C for 5 min. Then, the autoclave was further pressurized with H_2. The closed autoclave was allowed to warm to room temperature for 10 min. The reaction mixture was stirred at the mentioned temperature for the defined time. The autoclave was cooled to 0 °C for 15 min before the gas was discharged. The TONs of the catalyses were determined by ^1H NMR spectroscopy. A sample of 50 μL of the reaction mixture and 35 μL of mesitylene as internal standard were dissolved in 450 μL of dichloromethane-d_2.

The catalysis was also performed in the absence of a catalyst, a cocatalyst, or both to demonstrate the need of the catalytic system for the formation of both of these compounds. In these experiments, no significant TONs for DMM and MF were observed (see the SI). All catalyses with catalyst **3a** were performed three times. The error bars shown in Figure 2 display the standard deviation of the experiments (see the SI).

ASSOCIATED CONTENT

Supporting Information

The Supporting Information is available free of charge on the ACS Publications website at DOI: 10.1021/jacs.8b10233.

Experimental details (PDF)

Crystallographic data for **1b**, **2c**^{ox}, **2d**, and **3c** (CIF)

AUTHOR INFORMATION

Corresponding Author

*oliver.trapp@cup.uni-muenchen.de

ORCID

Oliver Trapp: 0000-0002-3594-5181

Funding

This research was funded by the German Federal Ministry of Education and Research (BMBF) within the funding initiative "CO2Plus - Stoffliche Nutzung von CO_2 zur Verbreiterung der Rohstoffbasis".

Notes

The authors declare no competing financial interest.

DOI: 10.1021/jacs.8b10233
J. Am. Chem. Soc. 2019, 141, 334−341

■ ACKNOWLEDGMENTS

Generous financial support by the German Federal Ministry of Education and Research (BMBF) within the funding initiative "CO2Plus - Stoffliche Nutzung von CO_2 zur Verbreiterung der Rohstoffbasis" is gratefully acknowledged.

■ REFERENCES

(1) (a) Eggleton, T. *A Short Introduction to Climate Change*; Cambridge University Press: New York, 2013. (b) IPCC. *Climate Change 2013: The Physical Science Basis. Contribution of Working Group I to the Fifth Assessment Report of the Intergovernmental Panel on Climate Change*; Cambridge University Press: Cambridge, UK, 2013.

(2) Dlugokencky, E.; Tans, P. *NOAA/ESRL*. www.esrl.noaa.gov/gmd/ccgg/trends/ (accessed 10.07.2018).

(3) Aresta, M. Carbon Dioxide: Utilization Options to Reduce its Accumulation in the Atmosphere. In *Carbon Dioxide as Chemical Feedstock*; Aresta, M., Ed.; Wiley-VCH: Weinheim, 2010.

(4) (a) Jessop, P. G.; Joó, F.; Tai, C.-C. Recent advances in the homogeneous hydrogenation of carbon dioxide. *Coord. Chem. Rev.* **2004**, *248*, 2425−2442. (b) Wang, W.; Wang, S.; Ma, X.; Gong, J. Recent advances in catalytic hydrogenation of carbon dioxide. *Chem. Soc. Rev.* **2011**, *40*, 3703−3727. (c) Liu, Q.; Wu, L.; Jackstell, R.; Beller, M. Using carbon dioxide as a building block in organic synthesis. *Nat. Commun.* **2015**, *6*, 5933. (d) Wang, W.-H.; Himeda, Y.; Muckerman, J. T.; Manbeck, G. F.; Fujita, E. CO_2 Hydrogenation to Formate and Methanol as an Alternative to Photo- and Electrochemical CO_2 Reduction. *Chem. Rev.* **2015**, *115*, 12936−12973. (e) Klankermayer, J.; Wesselbaum, S.; Beydoun, K.; Leitner, W. Selective Catalytic Synthesis Using the Combination of Carbon Dioxide and Hydrogen: Catalytic Chess at the Interface of Energy and Chemistry. *Angew. Chem., Int. Ed.* **2016**, *55*, 7296−7343. (f) Heim, L. E.; Konnerth, H.; Prechtl, M. H. G. Future perspectives for formaldehyde: pathways for reductive synthesis and energy storage. *Green Chem.* **2017**, *19*, 2347−2355. (g) Artz, J.; Müller, T. E.; Thenert, K.; Kleinekorte, J.; Meys, R.; Sternberg, A.; Bardow, A.; Leitner, W. Sustainable Conversion of Carbon Dioxide: An Integrated Review of Catalysis and Life Cycle Assessment. *Chem. Rev.* **2018**, *118*, 434−504.

(5) Keim, W. Industrial Uses of Carbon Dioxide. In *Carbon Dioxide as a Source of Carbon: Biochemical and Chemical Uses*, 1st ed.; Aresta, M.; Forti, G., Eds.; Springer: Dordrecht, 1987.

(6) (a) Munshi, P.; Main, A. D.; Linehan, J. C.; Tai, C.-C.; Jessop, P. G. Hydrogenation of Carbon Dioxide Catalyzed by Ruthenium Trimethylphosphine Complexes: The Accelerating Effect of Certain Alcohols and Amines. *J. Am. Chem. Soc.* **2002**, *124*, 7963−7971. (b) Himeda, Y.; Onozawa-Komatsuzaki, N.; Sugihara, H.; Kasuga, K. Simultaneous Tuning of Activity and Water Solubility of Complex Catalysts by Acid−Base Equilibrium of Ligands for Conversion of Carbon Dioxide. *Organometallics* **2007**, *26*, 702−712. (c) Tanaka, R.; Yamashita, M.; Nozaki, K. Catalytic Hydrogenation of Carbon Dioxide Using Ir(III)−Pincer Complexes. *J. Am. Chem. Soc.* **2009**, *131*, 14168−14169. (d) Schaub, T.; Paciello, R.; Mohl, K.-D.; Schneider, D.; Schaefer, M.; Rittinger, S. *Method for producing formic acid*. BASF SE, Germany, WO2010149507A2, 2010. (e) Azua, A.; Sanz, S.; Peris, E. Water-Soluble Ir^{III} N-Heterocyclic Carbene Based Catalysts for the Reduction of CO_2 to Formate by Transfer Hydrogenation and the Deuteration of Aryl Amines in Water. *Chem. - Eur. J.* **2011**, *17*, 3963−3967. (f) Schaub, T.; Paciello, R. A. A Process for the Synthesis of Formic Acid by CO_2 Hydrogenation: Thermodynamic Aspects and the Role of CO. *Angew. Chem., Int. Ed.* **2011**, *50*, 7278−7282. (g) Schmeier, T. J.; Dobereiner, G. E.; Crabtree, R. H.; Hazari, N. Secondary Coordination Sphere Interactions Facilitate the Insertion Step in an Iridium(III) CO_2 Reduction Catalyst. *J. Am. Chem. Soc.* **2011**, *133*, 9274−9277. (h) Hull, J. F.; Himeda, Y.; Wang, W.-H.; Hashiguchi, B.; Periana, R.; Szalda, D. J.; Muckerman, J. T.; Fujita, E. Reversible hydrogen storage using CO_2 and a proton-switchable iridium catalyst in aqueous media under mild temperatures and pressures. *Nat. Chem.* **2012**, *4*, 383−388. (i) Wesselbaum, S.; Hintermair, U.; Leitner, W. Continuous-Flow Hydrogenation of Carbon Dioxide to Pure Formic Acid using an Integrated $scCO_2$ Process with Immobilized Catalyst and Base. *Angew. Chem., Int. Ed.* **2012**, *51*, 8585−8588. (j) Jeletic, M. S.; Mock, M. T.; Appel, A. M.; Linehan, J. C. A Cobalt-Based Catalyst for the Hydrogenation of CO_2 under Ambient Conditions. *J. Am. Chem. Soc.* **2013**, *135*, 11533−11536. (k) Schaub, T.; Bey, O.; Meier, A.; Fries, D. M.; Hugo, R. *Method for producing formic acid by reacting carbon dioxide with hydrogen*. BASF SE, Germany, WO2013050367A2, 2013. (l) Filonenko, G. A.; Hensen, E. J. M.; Pidko, E. A. Mechanism of CO_2 hydrogenation to formates by homogeneous Ru-PNP pincer catalyst: from a theoretical description to performance optimization. *Catal. Sci. Technol.* **2014**, *4*, 3474−3485. (m) Jeletic, M. S.; Helm, M. L.; Hulley, E. B.; Mock, M. T.; Appel, A. M.; Linehan, J. C. A Cobalt Hydride Catalyst for the Hydrogenation of CO_2: Pathways for Catalysis and Deactivation. *ACS Catal.* **2014**, *4*, 3755−3762. (n) Moret, S.; Dyson, P. J.; Laurenczy, G. Direct synthesis of formic acid from carbon dioxide by hydrogenation in acidic media. *Nat. Commun.* **2014**, *5*, 4017.

(7) (a) Kröcher, O.; Köppel, R. A.; Baiker, A. Highly active ruthenium complexes with bidentate phosphine ligands for the solvent-free catalytic synthesis of *N,N*-dimethylformamide and methyl formate. *Chem. Commun.* **1997**, 453−454. (b) Ziebart, C.; Federsel, C.; Anbarasan, P.; Jackstell, R.; Baumann, W.; Spannenberg, A.; Beller, M. Well-Defined Iron Catalyst for Improved Hydrogenation of Carbon Dioxide and Bicarbonate. *J. Am. Chem. Soc.* **2012**, *134*, 20701−20704. (c) Pazicky, M.; Schaub, T.; Paciello, R.; Altenhoff, A. G.; Fries, D. M. *Verfahren zur Herstellung von Methylformiat*. BASF SE, Germany, DE102012014159A1, 2013.

(8) (a) Pazicky, M.; Schaub, T.; Paciello, R.; Lissner, A. *Verfahren zur Herstellung von Formamidverbindungen*. BASF SE, Germany, DE102012019441A1, 2013. (b) Zhang, L.; Han, Z.; Zhao, X.; Wang, Z.; Ding, K. Highly Efficient Ruthenium-Catalyzed N-Formylation of Amines with H_2 and CO_2. *Angew. Chem., Int. Ed.* **2015**, *54*, 6186−6189.

(9) (a) Huff, C. A.; Sanford, M. S. Cascade Catalysis for the Homogeneous Hydrogenation of CO_2 to Methanol. *J. Am. Chem. Soc.* **2011**, *133*, 18122−18125. (b) Han, Z.; Rong, L.; Wu, J.; Zhang, L.; Wang, Z.; Ding, K. Catalytic Hydrogenation of Cyclic Carbonates: A Practical Approach from CO_2 and Epoxides to Methanol and Diols. *Angew. Chem., Int. Ed.* **2012**, *51*, 13041−13045. (c) Wesselbaum, S.; vom Stein, T.; Klankermayer, J.; Leitner, W. Hydrogenation of Carbon Dioxide to Methanol by Using a Homogeneous Ruthenium−Phosphine Catalyst. *Angew. Chem., Int. Ed.* **2012**, *51*, 7499−7502. (d) Klankermayer, J.; Leitner, W.; vom Stein, T.; Wesselbaum, S. *Reduction method for the reduction of carbon dioxide and carbon dioxide derivatives*. RWTH Aachen University, Germany, WO2013156496A1, 2013. (e) Khusnutdinova, J. R.; Garg, J. A.; Milstein, D. Combining Low-Pressure CO_2 Capture and Hydrogenation To Form Methanol. *ACS Catal.* **2015**, *5*, 2416−2422. (f) Rezayee, N. M.; Huff, C. A.; Sanford, M. S. Tandem Amine and Ruthenium-Catalyzed Hydrogenation of CO_2 to Methanol. *J. Am. Chem. Soc.* **2015**, *137*, 1028−1031. (g) Wesselbaum, S.; Moha, V.; Meuresch, M.; Brosinski, S.; Thenert, K. M.; Kothe, J.; vom Stein, T.; Englert, U.; Hölscher, M.; Klankermayer, J.; Leitner, W. Hydrogenation of carbon dioxide to methanol using a homogeneous ruthenium−Triphos catalyst: from mechanistic investigations to multiphase catalysis. *Chem. Sci.* **2015**, *6*, 693−704. (h) Kothandaraman, J.; Goeppert, A.; Czaun, M.; Olah, G. A.; Prakash, G. K. S. Conversion of CO_2 from Air into Methanol Using a Polyamine and a Homogeneous Ruthenium Catalyst. *J. Am. Chem. Soc.* **2016**, *138*, 778−781. (i) Schneidewind, J.; Adam, R.; Baumann, W.; Jackstell, R.; Beller, M. Low-Temperature Hydrogenation of Carbon Dioxide to Methanol with a Homogeneous Cobalt Catalyst. *Angew. Chem., Int. Ed.* **2017**, *56*, 1890−1893.

(10) Bontemps, S.; Vendier, L.; Sabo-Etienne, S. Borane-Mediated Carbon Dioxide Reduction at Ruthenium: Formation of C_1 and C_2 Compounds. *Angew. Chem., Int. Ed.* **2012**, *51*, 1671−1674.

DOI: 10.1021/jacs.8b10233
J. Am. Chem. Soc. 2019, 141, 334−341

(11) Bontemps, S.; Vendier, L.; Sabo-Etienne, S. Ruthenium-Catalyzed Reduction of Carbon Dioxide to Formaldehyde. *J. Am. Chem. Soc.* **2014**, *136*, 4419−4425.
(12) (a) Jin, G.; Werncke, C. G.; Escudié, Y.; Sabo-Etienne, S.; Bontemps, S. Iron-Catalyzed Reduction of CO_2 into Methylene: Formation of C−N, C−O, and C−C Bonds. *J. Am. Chem. Soc.* **2015**, *137*, 9563−9566. (b) Aloisi, A.; Berthet, J.-C.; Genre, C.; Thuéry, P.; Cantat, T. Complexes of the tripodal phosphine ligands $PhSi(XPPh_2)_3$ (X = CH_2, O): synthesis, structure and catalytic activity in the hydroboration of CO_2. *Dalton Trans* **2016**, *45*, 14774−14788.
(13) Metsänen, T. T.; Oestreich, M. Temperature-Dependent Chemoselective Hydrosilylation of Carbon Dioxide to Formaldehyde or Methanol Oxidation State. *Organometallics* **2015**, *34*, 543−546.
(14) Ríos, P.; Curado, N.; López-Serrano, J.; Rodríguez, A. Selective reduction of carbon dioxide to bis(silyl)acetal catalyzed by a PBP-supported nickel complex. *Chem. Commun.* **2016**, *52*, 2114−2117.
(15) (a) Jiang, Y.; Blacque, O.; Fox, T.; Berke, H. Catalytic CO_2 Activation Assisted by Rhenium Hydride/$B(C_6F_5)_3$ Frustrated Lewis Pairs—Metal Hydrides Functioning as FLP Bases. *J. Am. Chem. Soc.* **2013**, *135*, 7751−7760. (b) LeBlanc, F. A.; Piers, W. E.; Parvez, M. Selective Hydrosilation of CO_2 to a Bis(silylacetal) Using an Anilido Bipyridyl-Ligated Organoscandium Catalyst. *Angew. Chem., Int. Ed.* **2014**, *53*, 789−792.
(16) Thenert, K.; Beydoun, K.; Wiesenthal, J.; Leitner, W.; Klankermayer, J. Ruthenium-Catalyzed Synthesis of Dialkoxymethane Ethers Utilizing Carbon Dioxide and Molecular Hydrogen. *Angew. Chem., Int. Ed.* **2016**, *55*, 12266−12269.
(17) Schieweck, B. G.; Klankermayer, J. Tailor-made Molecular Cobalt Catalyst System for the Selective Transformation of Carbon Dioxide to Dialkoxymethane Ethers. *Angew. Chem., Int. Ed.* **2017**, *56*, 10854−10857.
(18) (a) Phanopoulos, A.; Brown, N. J.; White, A. J. P.; Long, N. J.; Miller, P. W. Synthesis, Characterization, and Reactivity of Ruthenium Hydride Complexes of N-Centered Triphosphine Ligands. *Inorg. Chem.* **2014**, *53*, 3742−3752. (b) Phanopoulos, A.; Miller, P. W.; Long, N. J. Beyond Triphos − New hinges for a classical chelating ligand. *Coord. Chem. Rev.* **2015**, *299*, 39−60. (c) Phanopoulos, A.; White, A. J. P.; Long, N. J.; Miller, P. W. Catalytic Transformation of Levulinic Acid to 2-Methyltetrahydrofuran Using Ruthenium−*N*-Triphos Complexes. *ACS Catal.* **2015**, *5*, 2500−2512.
(19) Lloret Fillol, J.; Kruckenberg, A.; Scherl, P.; Wadepohl, H.; Gade, L. H. Stitching Phospholanes Together Piece by Piece: New Modular Di- and Tridentate Stereodirecting Ligands. *Chem. - Eur. J.* **2011**, *17*, 14047−14062.
(20) (a) Epstein, M.; Buckler, S. A. A Novel Phosphorus Heterocyclic System from the Reactions of Phosphine and Primary Phosphines with 2,4-Pentanedione. *J. Am. Chem. Soc.* **1961**, *83*, 3279−3282. (b) Fawcett, J.; Hoye, P. A. T.; Kemmitt, R. D. W.; Law, D. J.; Russell, D. R. Synthesis of bis(phosphinomethyl)amines via bis(hydroxymethyl)phosphonium salts. Isolation of 9,9-bis-(hydroxymethyl)-9-phosphoniabicyclo[3.3.1]nonane hydrogensulfate and chloride salts, and the crystal structures of $[PPh_2(CH_2OH)_2]^+Cl^-$ and $[(C_6H_{11})_2PCH_2]_2NCHMePh$. *J. Chem. Soc., Dalton Trans.* **1993**, 2563−2568.
(21) Doherty, S.; Robins, E. G.; Nieuwenhuyzen, M.; Champkin, P. A.; Clegg, W. Palladium Complexes of 2-Pyridin-2-yl Substituted 1,3-Bis(diphenylphosphino)propane: Highly Active Catalysts for the Room-Temperature Copolymerization of Carbon Monoxide with Ethene. *Organometallics* **2002**, *21*, 4147−4158.
(22) Dulière, E.; Devillers, M.; Marchand-Brynaert, J. Novel Phosphinite−Ruthenium(II) Complexes Covalently Bound on Silica: Synthesis, Characterization, and Catalytic Behavior versus Oxidation Reactions of Alcohols into Aldehydes. *Organometallics* **2003**, *22*, 804−811.
(23) vom Stein, T.; Weigand, T.; Merkens, C.; Klankermayer, J.; Leitner, W. Trimethylenemethane-Ruthenium(II)-Triphos Complexes as Highly Active Catalysts for Catalytic C−O Bond Cleavage Reactions of Lignin Model Compounds. *ChemCatChem* **2013**, *5*, 439−441.
(24) (a) Long, F. A.; McIntyre, D. Acid-catalyzed Hydrolysis of Methylal. II. Kinetic and Equilibrium Salt Effects and Correlation with H_0. *J. Am. Chem. Soc.* **1954**, *76*, 3243−3247. (b) McIntyre, D.; Long, F. A. Acid-catalyzed Hydrolysis of Methylal. I. Influence of Strong Acids and Correlation with Hammett Acidity Function. *J. Am. Chem. Soc.* **1954**, *76*, 3240−3242.
(25) Deutz, S.; Bongartz, D.; Heuser, B.; Kätelhön, A.; Schulze Langenhorst, L.; Omari, A.; Walters, M.; Klankermayer, J.; Leitner, W.; Mitsos, A.; Pischinger, S.; Bardow, A. Cleaner production of cleaner fuels: wind-to-wheel − environmental assessment of CO_2-based oxymethylene ether as a drop-in fuel. *Energy Environ. Sci.* **2018**, *11*, 331−343.

DOI: 10.1021/jacs.8b10233
J. Am. Chem. Soc. 2019, 141, 334−341

4.2 Application of Hetero-Triphos Ligands in the Selective Ruthenium-Catalyzed Transformation of Carbon Dioxide to the Formaldehyde Oxidation State

Max Seibicke, Max Siebert, Alexander F. Siegle, Sophie M. Gutenthaler, and Oliver Trapp

Prologue

The triphos ligand and its structural analogs with different apical atoms were compared regarding the activity of the resulting ruthenium complexes in the homogeneously catalyzed transformation of carbon dioxide to dimethoxymethane. The systematic variation of the apical atom together with the comprehensive screening of the catalysts allowed for determining structural prerequisites of the ligand to yield high catalytic activity in the presented catalysis.

Author Contributions

M. Seibicke designed and performed the catalytic experiments. M. Seibicke, M. Siebert, and S. M. G. performed the syntheses. All authors contributed to the interpretation of the data. The manuscript was written by M. Seibicke, and all authors contributed to the manuscript. O. T. supervised the project.

License

Supporting Information

The supporting information is available at https://doi.org/10.1021/acs.organomet.9b00107.

ORGANOMETALLICS
Article
Cite This: Organometallics 2019, 38, 1809−1814
pubs.acs.org/Organometallics

Application of Hetero-Triphos Ligands in the Selective Ruthenium-Catalyzed Transformation of Carbon Dioxide to the Formaldehyde Oxidation State

Max Seibicke, Max Siebert, Alexander F. Siegle, Sophie M. Gutenthaler, and Oliver Trapp*

Department Chemie, Ludwig-Maximilians-Universität München, Butenandtstr. 5-13, 81377 München, Germany

Supporting Information

ABSTRACT: Due to the increasing demand for formaldehyde as a building block in the chemical industry as well as its emerging potential as feedstock for biofuels in the form of dimethoxymethane and the oxymethylene ethers produced therefrom, the catalytic transformation of carbon dioxide to the formaldehyde oxidation state has become a focus of interest. In this work, we present novel ruthenium complexes with hetero-triphos ligands, which show high activity in the selective transformation of carbon dioxide to dimethoxymethane. We substituted the apical carbon atom in the backbone of the triphos ligand platform with silicon or phosphorus and optimized the reaction conditions to achieve turnover numbers as high as 685 for dimethoxymethane. The catalytic systems could also be tuned to preferably yield methyl formate with turnover numbers of up to 1370, which in turn can be converted into dimethoxymethane under moderate conditions.

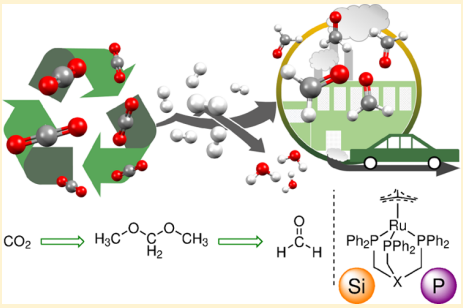

INTRODUCTION

In recent years, the utilization of carbon dioxide as renewable feedstock has become a major focus in academia and the chemical industry.[1] Driven by the postulated and already emerging dramatic global climate change due to the higher concentration of atmospheric greenhouse gases, such as CO_2, the necessity for sustainable and atom-efficient processes in industry is as high as never before.[2]

CO_2 has been utilized as the starting material for the synthesis of a variety of important organic molecules. A number of these showed the potential for process development, considering economic as well as ecologic factors.[1b,3] Yet, conversion of CO_2 to the formaldehyde oxidation level remains challenging, and only little progress was made on the road to an industrially feasible process.[3e,4]

Besides the academic approaches toward formaldehyde and its derivatives based on hydroboration,[5] hydrosilylation,[6] and frustrated Lewis pairs,[7] only a few attempts meeting the industrial requirements have been published until now. In 2016, Klankermayer and Leitner showed that the catalytic transformation of carbon dioxide to dimethoxymethane (DMM), the dimethyl acetal of formaldehyde, is viable. By employing a ruthenium-based triphos^{Ph} complex and $Al(OTf)_3$ as an additive, they achieved a turnover number (TON) of 214 for DMM (Scheme 1), and methyl formate (MF) was observed as the only side product.[8] This pathway to DMM is more atom-efficient than the common approaches, including acid-catalyzed acetalization of formaldehyde or methanol oxidation utilizing heterogeneous catalysts.[4] Furthermore, Schieweck and Klankermayer reported the use of modified triphos ligands and cobalt salts for the same reaction, achieving

Scheme 1. Overview of Different Ruthenium Catalysts for the Synthesis of DMM from CO_2

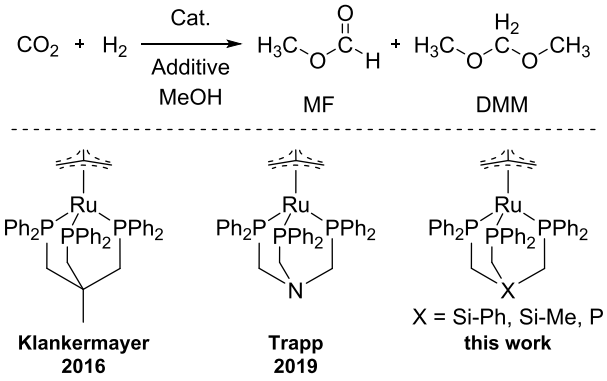

a TON of 157 for DMM with increased selectivity.[9] Recently, our group was able to raise TONs for DMM to 786 using a ruthenium catalyst with an N-triphos^{Ph} ligand and approaching the multivariate catalytic system in a stepwise optimization process (Scheme 1). This way, maxima in activity for temperature, partial pressure of hydrogen and carbon dioxide, time as well as catalyst and additive loading were determined.[10]

These excellent results, achieved by tuning the established ruthenium triphos system, encouraged us to investigate further steric and electronic modifications of the triphos ligand structure. The backbone of these tripodal ligands can be

Received: February 15, 2019
Published: April 4, 2019

DOI: 10.1021/acs.organomet.9b00107
Organometallics 2019, 38, 1809−1814

varied in a modular way, following established synthetic procedures.[11] We envisioned substitution of the apical atom in the backbone with heteroatoms, such as silicon and phosphorus (Scheme 1), to significantly alter the reactivity of the catalytic system, as has been demonstrated in other reports.[12]

RESULTS AND DISCUSSION

We started our studies by preparing triphos ligands with silicon and phosphorus in the backbone. To ensure comparability with previously reported systems and to gain insights into the effects of these structural variations, all synthesized ligands were kept tripodal and tridentate. In addition, the investigated complexes were prepared with the doubly charged trimethylenemethane anion as the counterion.

The synthesis of tripodal Si-triphos^{Ph} (**1a,b**) and P-triphos^{Ph} (**1c**) ligands was achieved in a modular two-step procedure based on publications by the groups of Tilley,[13] LaBelle,[14] Gramlich,[15] and Álvarez.[16] Deprotonation of the methyl group of $MePPh_2$, using *n*-BuLi and *N,N,N′,N′*-tetramethylethylenediamine (TMEDA), resulted in the formation of the Ph_2PMeLi–TMEDA complex, which was directly used in a nucleophilic substitution. Si-triphos^{Ph} ligands (**1a,b**) were obtained by reaction with phenyl- and methyltrichlorosilane in 71–90% yield (Scheme 2A). P-triphos^{Ph} (**1c**) was prepared in 66% yield using triphenyl phosphite (Scheme 2B).

Scheme 2. Synthetic Procedure towards the Tripodal Ligands and Their Ruthenium Complexes

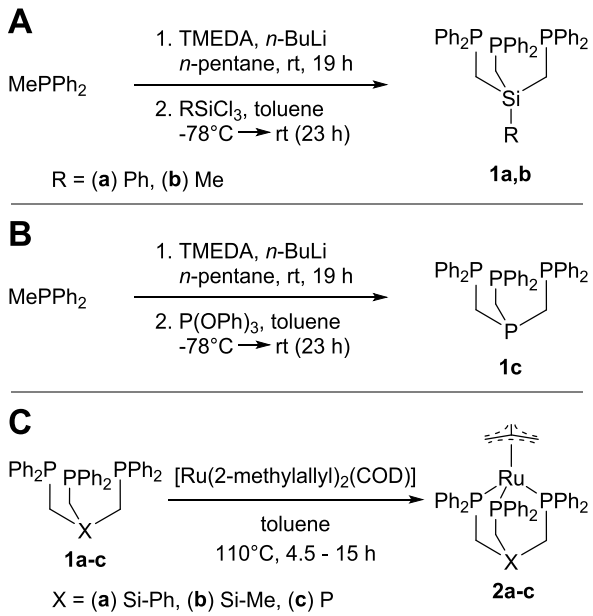

The ruthenium complexes were synthesized according to a method by Klankermayer and Leitner.[17] A mixture of [Ru(2-methylallyl)$_2$(COD)] and the respective ligand was heated in toluene to 110 °C (Scheme 2C) for 5 h (**2a**, yield: 60%), 15 h (**2b**, yield: 56%), or 4.5 h (**2c**, yield: 16%). Crystal structures of complexes **2a** and **2b**, containing the silicon-based ligands ^{Ph}Si-triphos^{Ph} (**1a**) and ^{Me}Si-triphos^{Ph} (**1b**), showed the expected distorted octahedral geometry (Figure 1A,B).

When compared to the ruthenium complex with the carbon-based triphos^{Ph} ligand, **2a** and **2b** exhibit a higher spatial distance (**2a**: 3.63 Å, **2b**: 3.64 Å) between the apical atom and the metal center. This trend results partly from the larger atomic radius of silicon, which is indicated by the longer X–C bonds of 1.88 and 1.89 Å (Table 1, entries 1–3). Furthermore, smaller X–C–P bond angles of 110° for both compounds as well as significantly higher X–C–P–Ru torsion angles of 35.0 and 37.1° have been found (Table 1, entries 1–3), whereas the tetrahedral C–X–C bond angles of the apical atoms are similar to the triphos complex. Interestingly, substitution of methyl to phenyl on the apical silicon has no significant effect on the complex geometry.

In the reported crystal structures of N-triphos ligands, the X–C–P bond angle is 114° and thus in between those of Si-triphos^{Ph} and triphos^{Ph} (Table 1, entries 1–5). The distance from nitrogen to ruthenium is the shortest at 3.46 Å, which correlates with the largest tetrahedral C–X–C bond angle of 115° and the shortest X–C bond lengths of 1.47 and 1.46 Å for all compared complexes (Table 1, entries 1–5). The X–C–P–Ru dihedral angles of N-triphos ligands are smaller (27.3 and 25.6°) than that of carbon-based triphos^{Ph} (Table 1, entries 3–5). With this information in hand, we were curious about the catalytic performance of the novel complexes.

We started screening the complexes **2a–c**, employing the previously optimized reaction conditions found for the N-triphos^{Ph} system (V = 0.5 mL, T = 90 °C, p_{H_2} = 90 bar, p_{CO_2} = 20 bar, t = 18 h, n_{cat} = 0.38 μmol, n_{add} = 1.56 μmol Al(OTf)$_3$).[10] Varying the reaction temperature, we observed maxima for TONs of DMM at 90 °C for the silicon-based complexes **2a,b** and at 100 °C for the phosphorus-based complex **2c**. Already for the first set of applied conditions, the TON for DMM exceeded 500, using catalyst **2b**. Interestingly, with higher temperatures, the selectivity (ratio of DMM/MF) increased for **2b** and **2c** but decreased for **2a** (Figure 2A). In the screening of the applied H_2 pressure, only small effects on the catalysis were observed (Figure 2B), whereas for different CO_2 pressures, the behavior of catalysts **2a–c** was found to be similar to that of the N-triphos^{Ph} system. Here, lower CO_2 pressures led to enhanced selectivity, while MF formation declined. For all three catalysts, the best performance in terms of DMM formation was found at 20 bar CO_2 pressure (Figure 2C). Next, we varied the catalyst and additive loading. As expected, both parameters influence the catalytic system significantly (Figure 2D,E). In all three cases, the TON for MF shows a reciprocal correlation with the catalyst amount, i.e., doubling the catalyst loading leads to reduction of the TON for MF by half. With increasing catalyst loading, the TON for DMM decreases for **2a**, whereas complex **2b** shows a maximum at 0.38 μmol. For **2c**, DMM formation is barely influenced. As a consequence, the selectivity increases strongly upon increasing the amount of catalyst. At a catalyst loading of 0.19 μmol, the TON for MF exceeds 1250 for all three complexes (Table 2, entries 7–9) and has a maximum of 1370 for catalyst **2b**, which, to the best of our knowledge, is currently the highest reported value in this transformation setup. Using 0.75 μmol of **2b**, the selectivity improves to the highest value of 67% (ratio of DMM/MF is 2:1). With higher additive loading, while keeping the amount of the investigated catalysts **2a–c** constant, the TON for MF declines, whereas the TON for DMM and the selectivity improve. By using 3.13 μmol additive, the TONs for DMM of the silicon-based triphos complexes **2a,b** were 678 and 685, respectively, thus reaching the highest activity herein (Table 2, entries 2 and 3).

DOI: 10.1021/acs.organomet.9b00107
Organometallics 2019, 38, 1809–1814

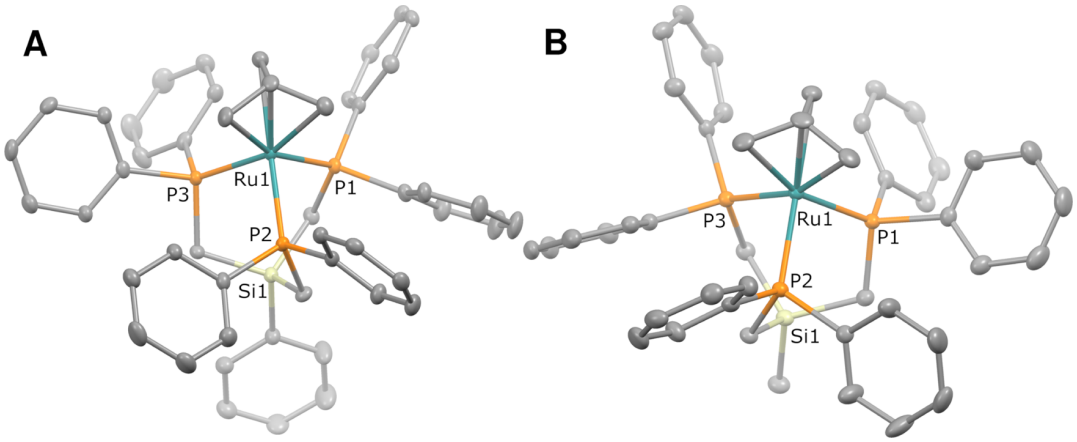

Figure 1. Molecular structure of complexes **2a** (A) and **2b** (B) with ellipsoids drawn at the 50% probability level (hydrogen atoms are omitted for clarity; carbon: gray; phosphorus: orange; ruthenium: turquoise; silicon: beige).

Table 1. Selected Structural Parameters for Triphos and Hetero-Triphos Ligands in Ruthenium Complexes with tmm as the Counterion

entry	ligand[a]	space group	X–Ru dist. (Å)	X–C bond length[b] (Å)	X–C–P bond angle[b] (deg)	C–X–C bond angle[b] (deg)	torsion angle[b,c] (deg)
1	(^{Ph}Si-triphos^{Ph})	$P\bar{1}$	3.63	1.88 ± 0.00	110 ± 0	109 ± 0	−35.0 ± 1.2
2	(^{Me}Si-triphos^{Ph})	$Pna2_1$	3.64	1.89 ± 0.00	110 ± 1	110 ± 1	37.1 ± 3.1
3	(triphos^{Ph})[18]	$P2_1/c$	3.56	1.55 ± 0.00	116 ± 0	111 ± 0	−30.8 ± 2.2
4	(N-triphos^{Ph})[19]	$R3$	3.46	1.47 ± 0.00	114 ± 0	115 ± 0	27.3 ± 0.0
5	(N-triphos^{pTol})[10]	$P\bar{1}$	3.46	1.46 ± 0.00	114 ± 1	115 ± 1	−25.6 ± 3.5

[a]In [Ru(ligand)(tmm)] complex. [b]Average of all three observables in the compound; the standard deviation is indicated. [c]X–C–P–Ru torsion angle.

Interested in the performance of the investigated catalysts compared to the established [Ru(triphos^{Ph})(tmm)] complex, we conducted an additional set of experiments with the latter, using the conditions optimized for **2a** and **2b**. Reaching TONs of 658 for DMM and 343 for MF (Table 2, entry 5), the carbon-based triphos system exhibits a similar activity in regard of the DMM formation, within the margin of error. In contrast, the TON for MF is notably increased for the silicon-based complexes **2a** and **2b**, resulting in an overall improved catalytic performance (Table 2, entries 2,3,7,8). P-triphos complex **2c**, however, showed considerably lower TONs for DMM, only exceeding the triphos reference system in MF formation (Table 2, entries 4,5,9). In general, the influence of the apex atom on the investigated conversion is much more pronounced in group 15, with N-triphos significantly outperforming its phosphorus analog (Table 2, entries 1,4,6,9).

Intrigued by the high catalytic activity of catalysts **2a–c** regarding MF (Table 2, entries 7–9), we investigated its reusability in the catalytic process. For all three catalysts, MF was selectively converted to DMM at 90 °C and 90 bar H_2 (see the Supporting Information). These results would encourage an industrial process for the synthesis of DMM in which the side product MF is transformed into DMM after workup of the catalysis products by distillation.

The exchange from carbon to silicon in the ligand backbone has improved overall activity for **2a** and **2b** (Table 2, entries 2,3,5,7,8). It seems that the larger atomic radius of silicon and the accompanying longer X–C bonds are compensated by the higher X–C–P–Ru torsion angles (Table 1, entries 1–3). We assume that this reduces steric effects at the catalytically active ruthenium center. The observed difference in product formation can thus potentially be attributed to electronic effects, as silicon is known for strongly influencing the electron density in neighboring groups.[20] This is further supported by the partly differing responses of the two silicon complexes **2a** and **2b** to variation of the catalytic parameters in the screening (Figure 2A,C,D, and Table 1, entries 1 and 2).

When exchanging nitrogen for phosphorus, the effects on activity are much more pronounced. Taking the smallest X–C–P–Ru torsion angles into account (Table 1, entries 4 and 5), the nitrogen-based ligands seem to fit ruthenium the best among the compared complexes, coinciding with the highest observed TON for DMM (Table 2, entry 1). Besides the optimum sterical prerequisite, electronic effects become more dominant by the proximity between the nitrogen and ruthenium as well as the phosphine groups. With phosphorus in the apex position, the larger atomic radius and the more diffused X–C bonds are more likely to result in weaker fixation in the ligand backbone, whereby the lower activity of **2c** in catalysis toward DMM can be rationalized (Table 2, entry 4).

■ CONCLUSIONS

We report the application of novel ruthenium hetero-triphos complexes in the homogeneous catalysis of carbon dioxide to dimethoxymethane and methyl formate with very high activity. For this purpose, we prepared complexes bearing a silicon (**2a** and **2b**) or phosphorus atom (**2c**) in the apical position of the ligand. Optimizing temperature, H_2 and CO_2 pressure as well as catalyst and additive loading, maximum turnover numbers of 685 for DMM and 1370 for MF could be achieved using complex **2b**. These results are in the same range as the TONs reported for the benchmark N-triphos^{Ph} system (DMM: 786;

DOI: 10.1021/acs.organomet.9b00107
Organometallics 2019, 38, 1809–1814

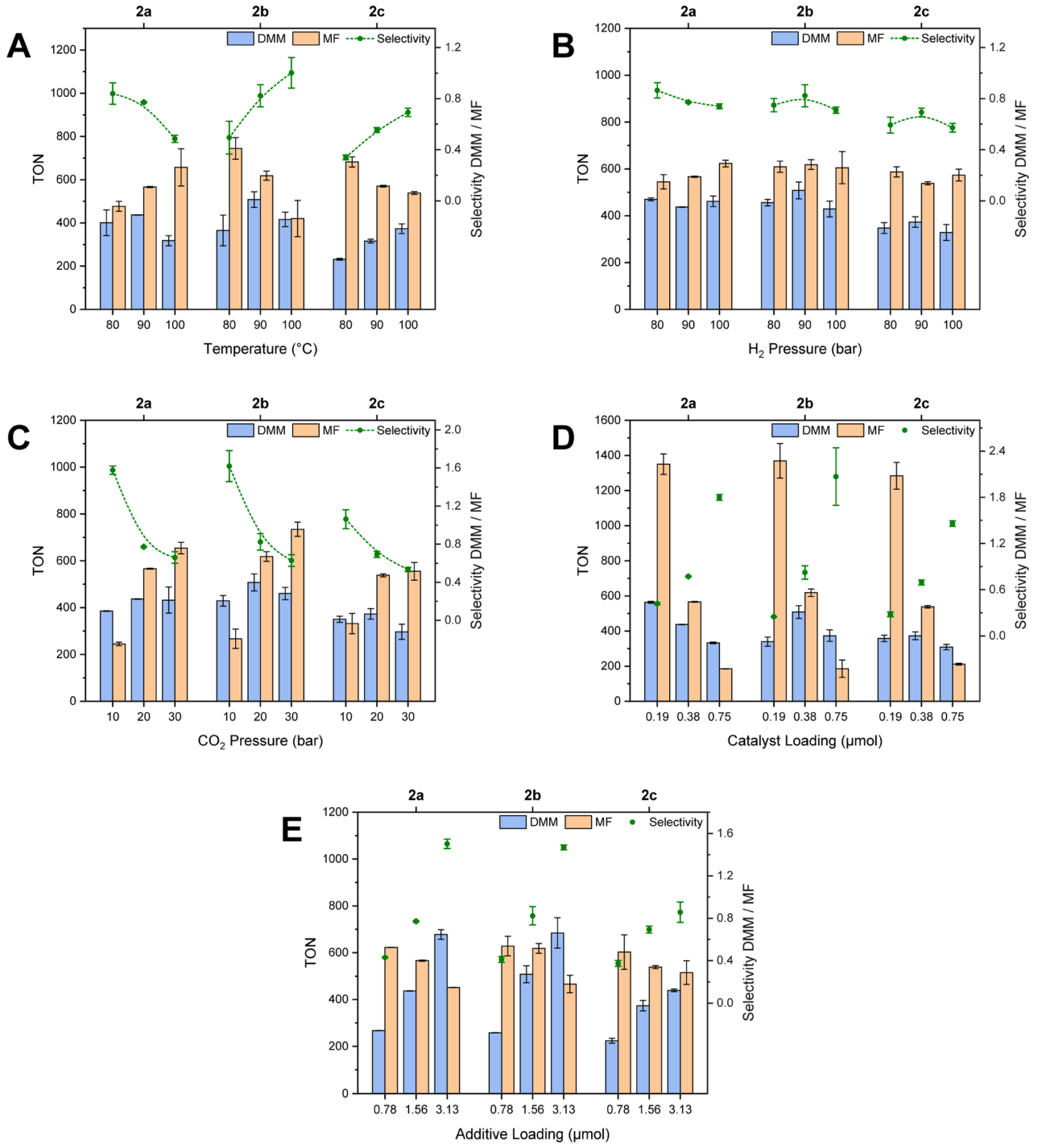

Figure 2. Bar plots of TONs in the catalytic investigation of the reductive transformation of CO_2 to DMM and MF for the screening of reaction parameters, such as temperature (A), H_2 (B) and CO_2 pressure (C) as well as catalyst (D) and additive loading (E).

MF: 1290), which represent the highest activity to date. The catalytic system can be tuned to either form DMM (in a ratio of 2:1) or MF (in a ratio of 4:1) as the main product. Utilizing the same catalyst and additive, MF can be reductively transformed into DMM under moderate conditions. Changing the apical atom from carbon to silicon notably enhances MF formation without affecting TONs for DMM and thus reduces selectivity under the given conditions. The phosphorus-based system requires higher temperatures and catalytic activity regarding DMM is attenuated in general. Using H_2 and CO_2, ^{Ph}Si-triphos^{Ph} and ^{Me}Si-triphos^{Ph} can be considered as good alternatives to N-triphos^{Ph} as ligands for the ruthenium-catalyzed synthesis of DMM, due to their high activity and facile preparation.

EXPERIMENTAL SECTION

Detailed documentation of all experiments performed and synthetic procedures as well as spectroscopic characterization of compounds

DOI: 10.1021/acs.organomet.9b00107
Organometallics 2019, 38, 1809−1814

Table 2. Overview of Catalyses with Best Results Regarding DMM and MF Using Ruthenium Triphos Catalysts.[a,b,c]

entry	cat.	T (°C)	n_{cat} (μmol)	n_{add} (μmol)	TON_{DMM}	TON_{MF}
1	[Ru(N-triphos^{Ph})(tmm)][10]	90	0.38	1.56	786 ± 62[d]	533 ± 17[d]
2	[Ru(^{Ph}Si-triphos^{Ph})(tmm)] **2a**	90	0.38	3.13	678 ± 21	452 ± 1
3	[Ru(^{Me}Si-triphos^{Ph})(tmm)] **2b**	90	0.38	3.13	685 ± 65	466 ±37
4	[Ru(P-triphos^{Ph})(tmm)] **2c**	100	0.38	3.13	439 ± 6	515 ± 51
5	[Ru(triphos^{Ph})(tmm)]	90	0.38	3.13	658 ± 54	343 ± 49
6	[Ru(N-triphos^{Ph})(tmm)][10]	90	0.19	0.78	728 ± 102[d]	1290 ± 151[d]
7	[Ru(^{Ph}Si-triphos^{Ph})(tmm)] **2a**	90	0.19	0.78	564 ± 6	1350 ± 58
8	[Ru(^{Me}Si-triphos^{Ph})(tmm)] **2b**	90	0.19	0.78	339 ± 27	1370 ± 99
9	[Ru(P-triphos^{Ph})(tmm)] **2c**	100	0.19	0.78	358 ± 18	1280 ± 76

[a]Catalytic conditions: Additive $Al(OTf)_3$, 0.5 mL MeOH, 90 bar H_2, 20 bar CO_2, 18 h. [b]TONs were determined by ^1H NMR spectroscopy using mesitylene as the internal standard. [c]All values are the average of two runs unless stated otherwise, and the standard deviation is indicated. [d]This value is the average of three runs, and the standard deviation is indicated.

used can be found in the Supporting Information. For better readability, simplified nomenclature instead of IUPAC names is used for ligands **1a–c**.

Novel complexes **2a–c** were characterized by NMR spectroscopy, high-resolution mass spectrometry (HR-MS), IR spectroscopy, and elemental analysis. X-ray diffraction analysis from a single crystal was obtained for compounds **2a** and **2b** (see the Supporting Information).

All catalyses and the corresponding analyses were performed two times following a procedure previously reported by our group.[10]

The catalysis was also performed in the absence of a catalyst, a co-catalyst, or both to demonstrate the need for the catalytic system for the formation of DMM and MF. In these experiments, no significant TONs for both of these compounds were obtained (see the Supporting Information). Error bars shown in Figure 2 display the standard deviation of the experiments (see the Supporting Information).

■ ASSOCIATED CONTENT

Supporting Information

The Supporting Information is available free of charge on the ACS Publications website at DOI: 10.1021/acs.organomet.9b00107.

Experimental details, screening of reaction conditions, and characterization data for all new compounds; CCDC 1890032 [for **2a**]; CCDC 1890031 [for **2b**] (PDF)

Accession Codes

CCDC 1890031–1890032 contain the supplementary crystallographic data for this paper. These data can be obtained free of charge via www.ccdc.cam.ac.uk/data_request/cif, or by emailing data_request@ccdc.cam.ac.uk, or by contacting The Cambridge Crystallographic Data Centre, 12 Union Road, Cambridge CB2 1EZ, UK; fax: +44 1223 336033.

■ AUTHOR INFORMATION

Corresponding Author

*E-mail: oliver.trapp@cup.uni-muenchen.de.

ORCID

Oliver Trapp: 0000-0002-3594-5181

Notes

The authors declare no competing financial interest.

■ ACKNOWLEDGMENTS

Generous financial support from the German Federal Ministry of Education and Research (BMBF) within the funding initiative "CO2Plus-Stoffliche Nutzung von CO_2 zur Verbreiterung der Rohstoffbasis" is gratefully acknowledged.

■ ABBREVIATIONS

COD, cyclooctadiene; DMM, dimethoxymethane; HR-MS, high-resolution mass spectrometry; IR, infrared radiation; MF, methyl formate; NMR, nuclear magnetic resonance; tmm, trimethylenemethane dianion; TON, turnover number

■ REFERENCES

(1) (a) Aresta, M. Carbon Dioxide: Utilization Options to Reduce its Accumulation in the Atmosphere. In *Carbon Dioxide as Chemical Feedstock*; Aresta, M., Ed.; Wiley-VCH: Weinheim, 2010. (b) Aresta, M.; Dibenedetto, A.; Angelini, A. Catalysis for the Valorization of Exhaust Carbon: from CO_2 to Chemicals, Materials, and Fuels. Technological Use of CO_2. *Chem. Rev.* **2014**, *114*, 1709–1742.

(2) IPCC. *Climate Change 2013: The Physical Science Basis. Contribution of Working Group I to the Fifth Assessment Report of the Intergovernmental Panel on Climate Change*; Cambridge University Press: Cambridge, U.K., 2013.

(3) (a) Jessop, P. G.; Joó, F.; Tai, C. C. Recent advances in the homogeneous hydrogenation of carbon dioxide. *Coord. Chem. Rev.* **2004**, *248*, 2425–2442. (b) Wang, W.; Wang, S.; Ma, X.; Gong, J. Recent advances in catalytic hydrogenation of carbon dioxide. *Chem. Soc. Rev.* **2011**, *40*, 3703–3727. (c) Liu, Q.; Wu, L.; Jackstell, R.; Beller, M. Using carbon dioxide as a building block in organic synthesis. *Nat. Commun.* **2015**, *6*, No. 5933. (d) Wang, W. H.; Himeda, Y.; Muckerman, J. T.; Manbeck, G. F.; Fujita, E. CO_2 Hydrogenation to Formate and Methanol as an Alternative to Photo- and Electrochemical CO_2 Reduction. *Chem. Rev.* **2015**, *115*, 12936–12973. (e) Klankermayer, J.; Wesselbaum, S.; Beydoun, K.; Leitner, W. Selective Catalytic Synthesis Using the Combination of Carbon Dioxide and Hydrogen: Catalytic Chess at the Interface of Energy and Chemistry. *Angew. Chem., Int. Ed.* **2016**, *55*, 7296–7343. (f) Heim, L. E.; Konnerth, H.; Prechtl, M. H. G. Future perspectives for formaldehyde: pathways for reductive synthesis and energy storage. *Green Chem.* **2017**, *19*, 2347–2355. (g) Artz, J.; Müller, T. E.; Thenert, K.; Kleinekorte, J.; Meys, R.; Sternberg, A.; Bardow, A.; Leitner, W. Sustainable Conversion of Carbon Dioxide: An Integrated Review of Catalysis and Life Cycle Assessment. *Chem. Rev.* **2018**, *118*, 434–504.

(4) Sun, R.; Delidovich, I.; Palkovits, R. Dimethoxymethane as a Cleaner Synthetic Fuel: Synthetic Methods, Catalysts, and Reaction Mechanism. *ACS Catal.* **2019**, *9*, 1298–1318.

(5) (a) Bontemps, S.; Vendier, L.; Sabo-Etienne, S. Borane-Mediated Carbon Dioxide Reduction at Ruthenium: Formation of C_1 and C_2 Compounds. *Angew. Chem., Int. Ed.* **2012**, *51*, 1671–1674. (b) Bontemps, S.; Vendier, L.; Sabo-Etienne, S. Ruthenium-Catalyzed Reduction of Carbon Dioxide to Formaldehyde. *J. Am. Chem. Soc.* **2014**, *136*, 4419–4425. (c) Jin, G.; Werncke, C. G.; Escudié, Y.; Sabo-Etienne, S.; Bontemps, S. Iron-Catalyzed Reduction of CO_2 into Methylene: Formation of C–N, C–O, and C–C Bonds. *J. Am. Chem. Soc.* **2015**, *137*, 9563–9566. (d) Aloisi, A.; Berthet, J. C.; Genre, C.; Thuéry, P.; Cantat, T. Complexes of the tripodal phosphine ligands

$PhSi(XPPh_2)_3$ (X = CH_2, O): synthesis, structure and catalytic activity in the hydroboration of CO_2. *Dalton Trans.* **2016**, *45*, 14774−14788. (e) Espinosa, M. R.; Charboneau, D. J.; Garcia de Oliveira, A.; Hazari, N. Controlling Selectivity in the Hydroboration of Carbon Dioxide to the Formic Acid, Formaldehyde, and Methanol Oxidation Levels. *ACS Catal.* **2019**, *9*, 301−314.

(6) (a) Metsänen, T. T.; Oestreich, M. Temperature-Dependent Chemoselective Hydrosilylation of Carbon Dioxide to Formaldehyde or Methanol Oxidation State. *Organometallics* **2015**, *34*, 543−546. (b) Ríos, P.; Curado, N.; López-Serrano, J.; Rodríguez, A. Selective reduction of carbon dioxide to bis(silyl)acetal catalyzed by a PBP-supported nickel complex. *Chem. Commun.* **2016**, *52*, 2114−2117.

(7) (a) Jiang, Y.; Blacque, O.; Fox, T.; Berke, H. Catalytic CO_2 Activation Assisted by Rhenium Hydride/$B(C_6F_5)_3$ Frustrated Lewis Pairs—Metal Hydrides Functioning as FLP Bases. *J. Am. Chem. Soc.* **2013**, *135*, 7751−7760. (b) LeBlanc, F. A.; Piers, W. E.; Parvez, M. Selective Hydrosilation of CO_2 to a Bis(silylacetal) Using an Anilido Bipyridyl-Ligated Organoscandium Catalyst. *Angew. Chem., Int. Ed.* **2014**, *53*, 789−792.

(8) Thenert, K.; Beydoun, K.; Wiesenthal, J.; Leitner, W.; Klankermayer, J. Ruthenium-Catalyzed Synthesis of Dialkoxymethane Ethers Utilizing Carbon Dioxide and Molecular Hydrogen. *Angew. Chem., Int. Ed.* **2016**, *55*, 12266−12269.

(9) Schieweck, B. G.; Klankermayer, J. Tailor-made Molecular Cobalt Catalyst System for the Selective Transformation of Carbon Dioxide to Dialkoxymethane Ethers. *Angew. Chem., Int. Ed.* **2017**, *56*, 10854−10857.

(10) Siebert, M.; Seibicke, M.; Siegle, A. F.; Kräh, S.; Trapp, O. Selective Ruthenium-Catalyzed Transformation of Carbon Dioxide: An Alternative Approach toward Formaldehyde. *J. Am. Chem. Soc.* **2019**, *141*, 334−341.

(11) Phanopoulos, A.; Miller, P. W.; Long, N. J. Beyond Triphos—New hinges for a classical chelating ligand. *Coord. Chem. Rev.* **2015**, *299*, 39−60.

(12) (a) Petuker, A.; Reback, M. L.; Apfel, U.-P. Carbon/Silicon Exchange at the Apex of Diphos- and Triphos-Derived Ligands—More Than Just a Substitute? *Eur. J. Inorg. Chem.* **2017**, *2017*, 3295−3301. (b) Petuker, A.; Mebs, S.; Schuth, N.; Gerschel, P.; Reback, M. L.; Mallick, B.; van Gastel, M.; Haumann, M.; Apfel, U.-P. Spontaneous Si−C bond cleavage in ($Triphos^{Si}$)-nickel complexes. *Dalton Trans.* **2017**, *46*, 907−917. (c) Petuker, A.; Merz, K.; Merten, C.; Apfel, U.-P. Controlled Flexible Coordination in Tripodal Iron(II) Phosphane Complexes: Effects on Reactivity. *Inorg. Chem.* **2016**, *55*, 1183−1191.

(13) Neumeyer, F.; Lipschutz, M. I.; Tilley, T. D. Group 8 Transition Metal Complexes of the Tripodal Triphosphino Ligands $PhSi(CH_2PR_2)_3$ (R = Ph, *i*Pr). *Eur. J. Inorg. Chem.* **2013**, *2013*, 6075−6078.

(14) Schore, N. E.; Benner, L. S.; LaBelle, B. E. Indirect metal-metal linkage: cyclic ferrocene complexes with a second metal linked via remote phosphine functionality. *Inorg. Chem.* **1981**, *20*, 3200−3208.

(15) Herold, S.; Mezzetti, A.; Venanzi, L. M.; Albinati, A.; Lianza, F.; Gerfin, T.; Gramlich, V. Synthetic methodologies for tripodal phosphines. The preparation of $MeSi(CH_2PPh_2)_3$ and n-BuSn-$(CH_2PPh_2)_3$ and a comparison of their rhodium(I) and ruthenium-(II) coordination chemistry. The X-ray crystal structures of [Rh(NBD){n-BuSn$(CH_2PPh_2)_3$}](OTf) and [Rh(NBD){MeSi-$(CH_2PPh_2)_3$}](OTf). *Inorg. Chim. Acta* **1995**, *235*, 215−231.

(16) Cámpora, J.; Maya, C. M.; Matas, I.; Claasen, B.; Palma, P.; Álvarez, E. A convenient synthesis of bis(phosphino)methanes: Formation of a nickel(II) bis(phosphino)methane monoxide complex. *Inorg. Chim. Acta* **2006**, *359*, 3191−3196.

(17) (a) Wesselbaum, S.; vom Stein, T.; Klankermayer, J.; Leitner, W. Hydrogenation of Carbon Dioxide to Methanol by Using a Homogeneous Ruthenium−Phosphine Catalyst. *Angew. Chem., Int. Ed.* **2012**, *51*, 7499−7502. (b) vom Stein, T.; Weigand, T.; Merkens, C.; Klankermayer, J.; Leitner, W. Trimethylenemethane-Ruthenium-(II)-Triphos Complexes as Highly Active Catalysts for Catalytic C−O Bond Cleavage Reactions of Lignin Model Compounds. *ChemCatChem* **2013**, *5*, 439−441.

(18) vom Stein, T.; Meuresch, M.; Limper, D.; Schmitz, M.; Hölscher, M.; Coetzee, J.; Cole-Hamilton, D. J.; Klankermayer, J.; Leitner, W. Highly Versatile Catalytic Hydrogenation of Carboxylic and Carbonic Acid Derivatives using a Ru-Triphos Complex: Molecular Control over Selectivity and Substrate Scope. *J. Am. Chem. Soc.* **2014**, *136*, 13217−13225.

(19) Phanopoulos, A.; Brown, N. J.; White, A. J. P.; Long, N. J.; Miller, P. W. Synthesis, Characterization, and Reactivity of Ruthenium Hydride Complexes of N-Centered Triphosphine Ligands. *Inorg. Chem.* **2014**, *53*, 3742−3752.

(20) Wierschke, S. G.; Chandrasekhar, J.; Jorgensen, W. L. Magnitude and Origin of the β-Silicon Effect on Carbenium Ions. *J. Am. Chem. Soc.* **1985**, *107*, 1496−1500.

DOI: 10.1021/acs.organomet.9b00107
Organometallics 2019, 38, 1809−1814

4.3 Identifying High-Performance Catalytic Conditions for Carbon Dioxide Reduction to Dimethoxymethane by Multivariate Modelling

Max Siebert, Gerhard Krennrich, Max Seibicke, Alexander F. Siegle, and Oliver Trapp

Prologue

The optimization of chemical processes is often based on intuition and is strongly limited in terms of efficiency by the variation of single variables and the manual interpretation of data. Starting from the experimental data obtained in the univariate screening, the catalytic system for the transformation of carbon dioxide to dimethoxymethane was optimized using an algorithmic workflow. The previous results were analyzed using a machine learning algorithm, and all further experiments were designed using design of experiments. With little experimental effort, the catalytic activity was further increased by more than 350 % compared to the results of the univariate screening.

Author Contributions

M. Siebert and G. K. designed the experiments. M. Siebert performed the experiments. G. K. performed computer modeling and analysis of the data. All authors contributed to the interpretation of the data. The manuscript was co-written by M. Siebert and G. K., and all authors contributed to the manuscript. O. T. supervised the project.

License

Reprinted with permission from M. Siebert, G. Krennrich, M. Seibicke, A. F. Siegle, O. Trapp, *Chem. Sci.* **2019**, *10*, 10466–10474. Published by The Royal Society of Chemistry.

Supporting Information

The supporting information is available at https://doi.org/10.1039/C9SC04591K.

Volume 10 | Number 45 | 7 December 2019 | Pages 10449–10656

Chemical Science

rsc.li/chemical-science

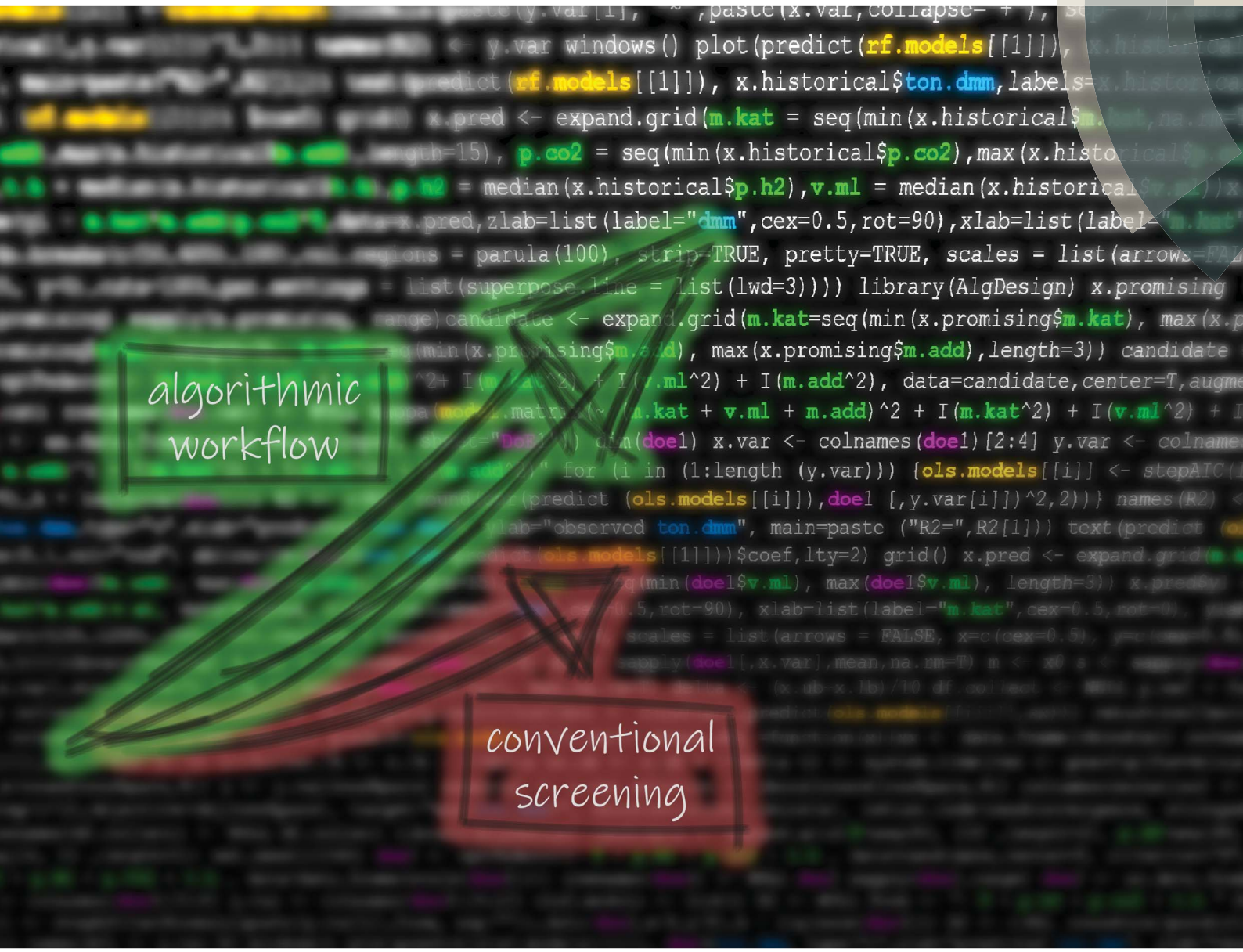

ISSN 2041-6539

ROYAL SOCIETY OF CHEMISTRY | Celebrating IYPT 2019

EDGE ARTICLE
Oliver Trapp *et al.*
Identifying high-performance catalytic conditions for carbon dioxide reduction to dimethoxymethane by multivariate modelling

Chemical Science

EDGE ARTICLE

View Article Online
View Journal | View Issue

Cite this: *Chem. Sci.*, 2019, **10**, 10466

All publication charges for this article have been paid for by the Royal Society of Chemistry

Identifying high-performance catalytic conditions for carbon dioxide reduction to dimethoxymethane by multivariate modelling†

Max Siebert, Gerhard Krennrich, Max Seibicke, Alexander F. Siegle and Oliver Trapp *

Received 11th September 2019
Accepted 23rd October 2019

DOI: 10.1039/c9sc04591k

rsc.li/chemical-science

In times of a warming climate due to excessive carbon dioxide production, catalytic conversion of carbon dioxide to formaldehyde is not only a process of great industrial interest, but it could also serve as a means for meeting our climate goals. Currently, formaldehyde is produced in an energetically unfavourable and atom-inefficient process. A much needed solution remains academically challenging. Here we present an algorithmic workflow to improve the ruthenium-catalysed transformation of carbon dioxide to the formaldehyde derivative dimethoxymethane. Catalytic processes are typically optimised by comprehensive screening of catalysts, substrates, reaction parameters and additives to enhance activity and selectivity. The common problem of the multidimensionality of the parameter space, leading to only incremental improvement in laborious physical investigations, was overcome by combining elements from machine learning, optimisation and experimental design, tripling the turnover number of 786 to 2761. The optimised conditions were then used in a new reaction setup tailored to the process parameters leading to a turnover number of 3874, exceeding by far those of known processes.

Introduction

In this century, our ecosystem faces severe problems such as global warming, environmental pollution and resource depletion. The negative impact of humankind as well as its responsibility in solving these problems can no longer be ignored.[1,2] Besides the necessity for future-oriented global politics,[3,4] both the scientific community and the chemical industry must provide answers to crucial questions regarding sustainable process development, alternative energies as well as recycling of waste and pollutants.[5–9] In this context, more efficient techniques must be developed and applied in research to reduce time, cost and resources.[10–12]

In catalytic investigations, system optimisation is typically approached by one-factor-at-a-time (OFAT) methods, successively screening along one parameter axis. Once optimised, a parameter is kept constant for the subsequent experiments. In this univariate analysis, variables are treated as being independent of each other. Beside the vast number of experiments that must be performed, local maxima with higher performances might be missed. Consequently, algorithm-based screening and optimisation techniques have been among the fastest growing research areas in recent years.[13–24] Considering the interactions of parameters, optimised results can be achieved with minimal experimental effort.[25,26]

Recently, we applied a univariate optimisation approach including several hundred catalytic reactions to improve the selective ruthenium-catalysed transformation of carbon dioxide to dimethoxymethane (DMM) reaching a turnover number (TON) of 786 (Scheme 1).[27,28] The product DMM itself is a high value feedstock for biofuels, but can also be hydrolysed yielding formaldehyde and methanol or directly employed as a formaldehyde synthon.[29,30] Beside the desired product, only methyl formate (MF) was formed with TONs of up to 1290 (Scheme 1).[27] Previously, two studies on the selective hydrogenation of CO_2 by the group of Klankermayer showed the formation of DMM and MF by using a homogeneous ruthenium catalyst[31] with TONs of 214 and 104 or a cobalt catalyst[32] with TONs of 157 and 37, respectively. Further selective reductions toward the formaldehyde oxidation state were reported utilising hydroboration,[33–37] hydrosilylation,[38,39] and frustrated Lewis pairs,[40,41] however, being mainly of academic interest due to the stoichiometric use of reducing reagents.

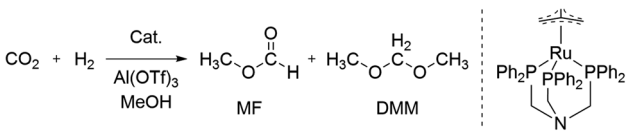

Scheme 1 Reductive transformation of CO_2 towards the formaldehyde oxidation level yielding methyl formate (MF) and dimethoxymethane (DMM).

Department Chemie, Ludwig-Maximilians-Universität München, Butenandtstr. 5-13, 81377 München, Germany. E-mail: oliver.trapp@cup.uni-muenchen.de

† Electronic supplementary information (ESI) available: Synthetic procedures, multivariate modelling procedure, additional tables, catalysis data, R-code. See DOI: 10.1039/c9sc04591k

Inspired by previous reports, which underline the importance of a holistic view on the results obtained,[13,19] we now utilised multivariate analysis[42,43] to further optimise the investigated catalysis. Based on the large amount of experimental data and the dependency of the catalytic system on seven different parameters, we envisioned to increase its performance by modelling and predicting conditions optimally accounting for parameter interaction. For this purpose, we devised a multistep process combining elements from machine learning, optimisation and experimental design (design of experiments, DoE). Fig. 1 gives a schematic overview of the easy-to-use algorithmic workflow, which was developed in this work and is applicable for any catalytic screening. Experimental data (Fig. 1(I)) was modelled using the random forest (RF) algorithm (Fig. 1(II)) to identify promising subspaces with high catalytic performance (Fig. 1(III)). To better understand the origin of the exceptional activity and to extend the amount of data for further modelling, the subspace was augmented (Fig. 1(IV)) by additional experiments (Fig. 1(V)) that were based on experimental design. Starting from these first experiments, an iterative workflow – consisting of DoE (Fig. 1(V) and (VI)), optimisation (relaxation; Fig. 1(VII) and (VIII)) and evaluation (Fig. 1(IX)) – was applied until the final optimum was reached (Fig. 1(X)).

Results and discussion

Catalytic system

The selective transformation of CO_2 to DMM was performed using the ruthenium catalyst [Ru(*N*-triphos^{Ph})(tmm)] (tmm = trimethylenemethane dianion) for hydride transfer and Al(OTf)$_3$ to facilitate the acetalisation with methanol (Scheme 1). Beneficially, the robust catalyst can be obtained on a large scale in a simple three-step procedure, which underlines its suitability for industrial and large scale applications.[27] The catalysis is mainly affected by the reaction temperature (T), partial pressure of H_2 (p_{H_2}) and CO_2 (p_{CO_2}), reaction time (t), the amount of catalyst (n_{cat}) and Lewis acid (n_{add}) as well as the reaction volume (V).

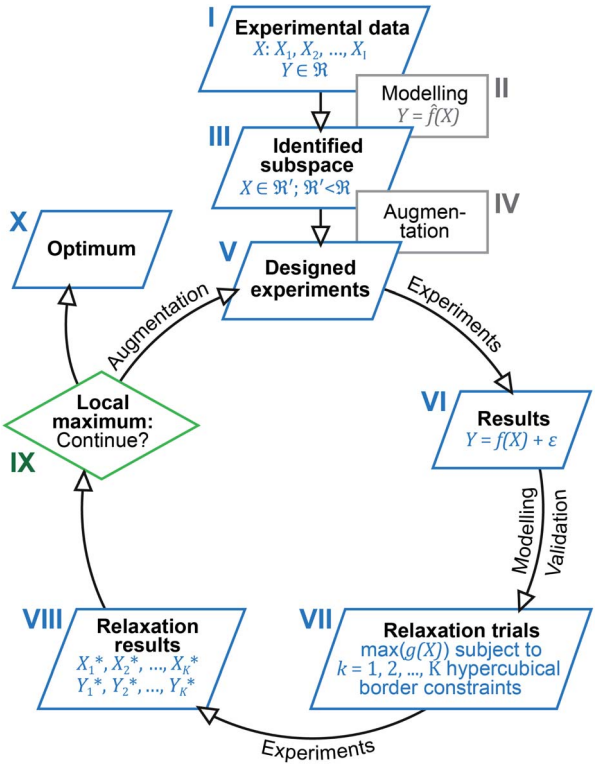

Fig. 1 Outline of the algorithm-based workflow combining experimental data analysis, DoE and optimisation.

Experimental data analysis

Following the rationale outlined in the previous section, the optimisation started with a corpus of 49 unique settings of the seven process factors (X: X_1, X_2, …, $X_7 = T$, p_{H_2}, p_{CO_2}, t, n_{cat}, n_{add}, V), two responses (Y: Y_1, Y_2 = TON$_{DMM}$, TON$_{MF}$) and 144 observations, which are measured values of the responses (Table 1, Fig. 1(I), ESI Table 1†).[27] Each setting was run as a triple replicate, except for three settings that were realised as simple replicates, thus making up the 144 cases of the dataset. Goal of the optimisation was finding reaction conditions X^*: X_1^*, X_2^*, …, X_7^*, that maximise TON$_{DMM}$ (for a theoretical introduction on this approach, see the Methods section). As process factors, six of the previously investigated parameters, namely temperature, partial pressure of H_2 and CO_2, reaction time as well as the amount of catalyst and Lewis acid, proved suitable for the optimisation. The influence of varying the nature of the Lewis acid was neglected here, because statistical analysis of the dataset revealed Al(OTf)$_3$ as the only promising candidate. Instead, the volume of the catalysis solution was considered for the multivariate analysis to account for mass transfer phenomena and gas solubility effects (concentration effects) potentially influencing the performance of the catalyst.

Modelling and analysis of datasets based on empirical optimisation (*e.g.* OFAT) is complex and more difficult than estimating parametric surrogate models from well-designed data. The difficulties arise primarily from non-linearities, which simple parametric models cannot appropriately describe. Furthermore, OFAT variations often and inadvertently lead to co-varying and thereby confounding the effects of process parameters. For instance, in the present dataset the process parameters n_{cat} and n_{add} were found to be highly correlated with a Pearson correlation coefficient $r(n_{cat} - n_{add}) = 0.895$, rendering the data non-informative in terms of the independent effects of n_{cat} and n_{add}.

Table 1 Factors and responses of the dataset[27]

Entry	Variable	Mean	Median	Min	Max
1	T (°C)	89.2	90	20	120
2	p_{H_2} (bar)	82.1	90	40	100
3	p_{CO_2} (bar)	17.9	20	5	40
4	t (h)	26.5	18	1	168
5	n_{cat} (μmol)	1.3	1.5	0	3
6	n_{add} (μmol)	5.4	6.25	0	12.5
7	V (mL)	0.5	0.5	0.25	0.5
8	TON$_{DMM}$	275	263	0	906
9	TON$_{MF}$	145	71	0	1377

Next, the problem for these datasets is finding an appropriate functional representation, $\hat{f}()$, of the target response as a function of the process factors X_i, that is $TON_{DMM} = f(T,p_{H_2},p_{CO_2},t,n_{cat},n_{add},V) + \varepsilon$, without making any prior assumptions about the analytical form of the 'true' function $f()$. Here, we used RF as a powerful non-linear and easy-to-use method for the empirical model building of complex datasets (Fig. 1(II)).[44,45]

The RF models describe 79% of the responses' variance on average ($R^2(TON_{DMM}) = 0.83$; $R^2(TON_{MF}) = 0.74$), which is a good result given the heterogeneous nature of the dataset. Further, tuning the RF hyperparameters using 10-fold cross validation with consecutive blocks (mtry* = 2 with $R^2 = 0.83$) revealed that the default RF hyperparameters describe the data appropriately. The effect structure of the models can be conveniently explored by plotting the RF model predictions $\hat{f}(X)$ against the process factors $X_1, X_2, \ldots, X_7$. Fig. 2 shows the effects of the process parameters T, p_{CO_2}, n_{cat} and n_{add}, given the median values $p_{H_2} = 90$ bar, $t = 18$ h and $V = 0.5$ mL, as a conditional trellis plot.

As a tree-based ensemble method, RF splits and mean-aggregates the experimental space into hyperrectangles, the consequence being that the RF model surface becomes non-smooth (Fig. 2). This property of RF is a particular strength when it comes to identifying promising domains of the experimental space and was another motivation for choosing RF as modelling technique.

Evidently, n_{cat} and n_{add} exert strong non-linear, step like negative effects on the process performance (TON_{DMM}), dividing the $n_{cat} \times n_{add}$ space into domains of different performance. The pressure, p_{CO_2}, reveals a positive and temperature, T, a small convex effect, both, however, negligible compared to the dominant effects of n_{cat} and n_{add}. At this point, the erroneous impression may arise that the heuristic interpretation of the experimental data could lead to a further improvement by a trivial reduction of the amount of catalyst, which is often reduced to minimise catalyst deactivation. However, a closer look at the experimental data shows that a reduction in the amount of catalyst without changing other parameters leads to a decrease in catalytic activity with respect to DMM. This case shows exemplarily how important multivariate analytical methods can be, because they can easily identify complex correlations of process parameters that are not detectable by a univariate analysis of the scientist.

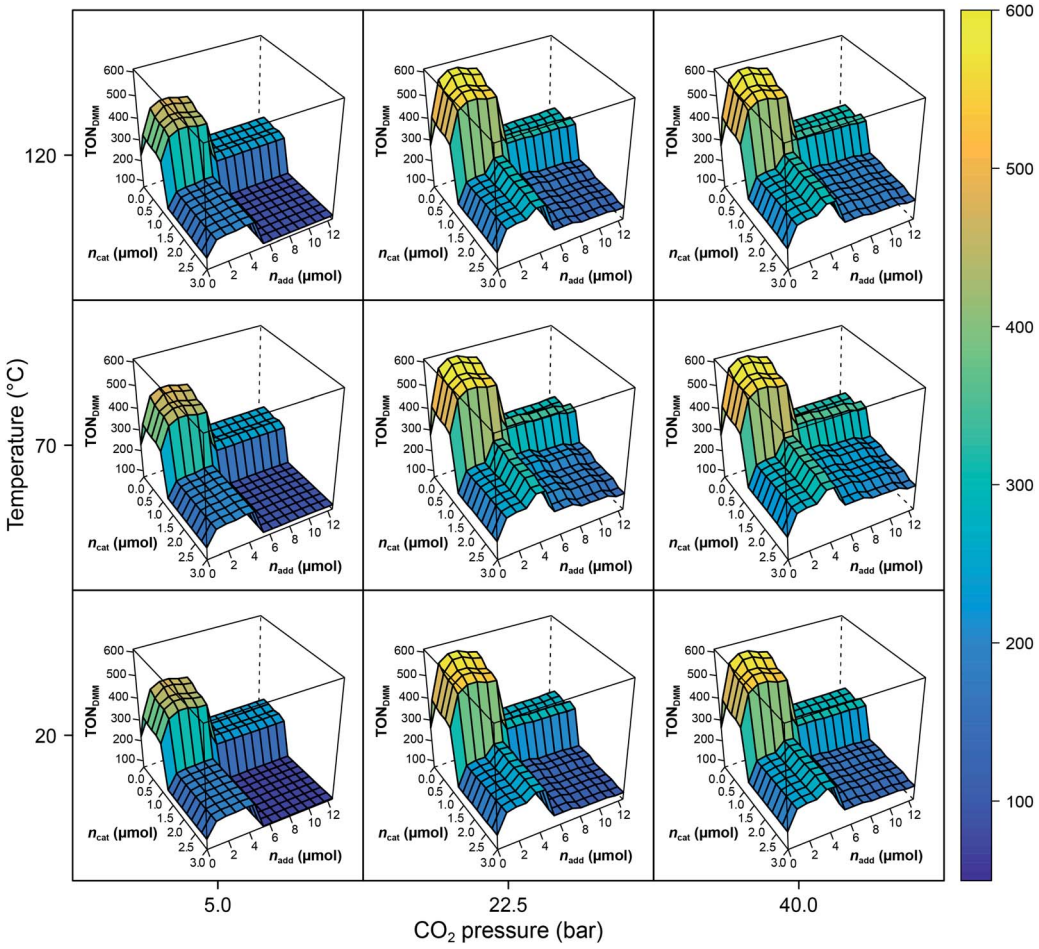

Fig. 2 Trellis plot of the random forest predictions $\hat{f}(T,p_{H_2},p_{CO_2},t,n_{cat},n_{add},V)$ with $p_{H_2} = 90$ bar, $t = 18$ h and $V = 0.5$ mL. Note the difference of max(TON_{DMM}) in the experimental data (Table 1, entry 8) and the model. The RF values are predictions causing the range of the z-axis to be smaller than the range of the empirical data.

With the condition $TON_{DMM} > 400$ deduced from the landscape of TON_{DMM} over $n_{cat} \times n_{add}$ (Fig. 2), a subset of 26 observations with 9 unique settings was selected from the data (Fig. 1(III)). In this subset, the parameters T, p_{H_2}, p_{CO_2} and t were found constant at $T = 90$ °C, $p_{H_2} = 90$ bar, $p_{CO_2} = 20$ bar and $t = 18$ h, thereby suggesting to conditionally optimise n_{cat}, n_{add} and V first, while keeping T, p_{H_2}, p_{CO_2} and t constant for the time being.

First DoE

These 9 candidate points (identified unique settings mentioned above) were subsequently augmented by an additional number of 6 points to fully support all second order effects of n_{cat}, n_{add} and V (Fig. 1(IV)). The intention behind this augmentation was to render the formerly confounded effects of n_{cat} and n_{add} estimable as well as, assuming high complexity, to allow for interactions and non-linearities of the process parameters as a solid basis for further optimisation (Fig. 1(V)).

The 6 augmentation trials were realised as triple replicates in the lab, added to the 9 settings already available and the responses (TON_{DMM}, TON_{MF}) were modelled as a function of the least square parameters with stepwise ordinary least squares (OLS; Fig. 1(VI)). Both models accurately describe the data within the replication error and explain 91% ($R^2(TON_{DMM}) = 0.91$; DF = 37) and 97% ($R^2(TON_{MF}) = 0.97$; DF = 35) of the responses' variance with DF denoting the degrees of freedom (number of data points minus number of estimated model parameters).

The local effects of n_{cat}, n_{add} and V are depicted in Fig. 3A as response surface trellis plot. Again, there is a strong negative effect for n_{cat} along with positive effects for n_{add} and V. Together with the positive, synergistic effect between n_{add} and V, the effect structure suggests to decrease n_{cat} and to increase n_{add} and V to further maximise the catalytic performance beyond the best result of the first DoE (Fig. 4A, entry 4).

First relaxation

To optimise towards the direction of maximal improvement, following the procedure outlined in the Methods section [eqn (5)], the experimental space was relaxed with 10% step size. The triple obtained from relaxing the design space together with the achieved experimental results are listed in Fig. 4B (Fig. 1(VII) and (VIII); see the Methods section).

The joint condition max(TON_{DMM}), max(TON_{MF}) was best met by the 20% relaxation trial (Fig. 4B, entry 2), and the factor setting $n^*_{cat} = 0.075$ μmol, $n^*_{add} = 3.576$ μmol and $V^* = 0.550$ mL thus became the reference point for further optimisation. The 30% relaxation trial was very poor, indicating that a local maximum had been exceeded (Fig. 4B, entry 3). The pronounced drop in activity, resulting most likely from the reduced catalyst loading, indicates a molecular deactivation pathway of the catalytically active species due to potential inhibitors, such as carbon monoxide, moisture and oxygen, which are probably present in low concentrations.

At this point, there were two alternatives to proceed: (1) create an experimental design around n^*_{cat}, n^*_{add} and V^* to fully identify the topology around the relaxation point at the desired resolution (complexity). (2) Consider $n^*_{cat} = 0.075$ μmol, $n^*_{add} = 3.576$ μmol and $V^* = 0.550$ mL as locally optimal and switch to optimising the candidates T, p_{H_2}, p_{CO_2} and t, which had so far been kept constant.

The poor outcome of the third relaxation trial (Fig. 4B, entry 3) showed that not much was to be expected from exploring the three-dimensional environment of the 20% relaxation trial any further. Therefore, option 2 was chosen and the 20% relaxation trial became the reference point for optimising the candidates T, p_{H_2}, p_{CO_2} and t.

Second DoE

A small linear design [eqn (2)] with 5 runs in the ranges listed in Fig. 4C was created with the reference point $n^*_{cat} = 0.075$ μmol, $n^*_{add} = 3.576$ μmol and $V^* = 0.550$ mL, $T^* = 90$ °C, $p^*_{H_2} = 90$ bar, $p^*_{CO_2} = 20$ bar bar, $t^* = 18$ h at the design centre as replicate (Fig. 1(V); see the Methods section). The experiments were realised in the lab as triple replicate to provide a measure of accuracy (Fig. 1(VI)).

The measured responses (TON_{DMM}, TON_{MF}) were linearly modelled as a function of the process parameters with stepwise OLS. The models explain 92% ($R^2(TON_{DMM}) = 0.92$; DF = 16) and 78% ($R^2(TON_{MF}) = 0.78$; DF = 18) variance of the responses thus indicating a large signal-to-noise ratio for TON_{DMM} and to a lesser extent for TON_{MF}.

Fig. 3B shows the linear effects of the process parameters on TON_{DMM} as trellis response surface plot. The factors T and p_{H_2} both have strong positive effects on TON_{DMM}, whereas t reveals only a small positive and p_{CO_2} a moderate negative effect on TON_{DMM}. Optimal conditions were found in the upper left panel and these are the conditions of the top candidate found in the design list with T, p_{H_2}, t at the upper and p_{CO_2} at the lower bound, yielding respective TONs for DMM and MF of 2610 and 2356 (Fig. 4C, entry 4).

Second relaxation

Following eqn (5), the experimental space was relaxed in 25% and 50% steps and the relaxation trials were experimentally realised in the lab (Fig. 4D and 1(VII); see the Methods section).

Again, we saw a small improvement of the 25% relaxation trial (Fig. 4D, entry 1) compared with the best candidate from the second DoE (Fig. 4C, entry 4), whereas the 50% relaxation candidate performed comparatively poorly (Fig. 4D, entry 2; Fig. 1(VIII)). With these relaxation trials, we reached the technical limits of our setup regarding hydrogen gas pressure, and therefore, the conditions of the 25% relaxation experiment can be considered locally optimal given the constraints of technical feasibility (Fig. 1(IX) and (X)). We would like to point out that the catalytic conditions optimised by the here presented strategy may still represent a local maximum. Modification of the catalyst and the additive might also result in further improvement, but as demonstrated in this work the identification of high-performance catalytic conditions should be a prerequisite for a design strategy of new catalysts.

A complete overview of the results obtained at each step of the optimisation project is given in Fig. 4E, overall tripling the

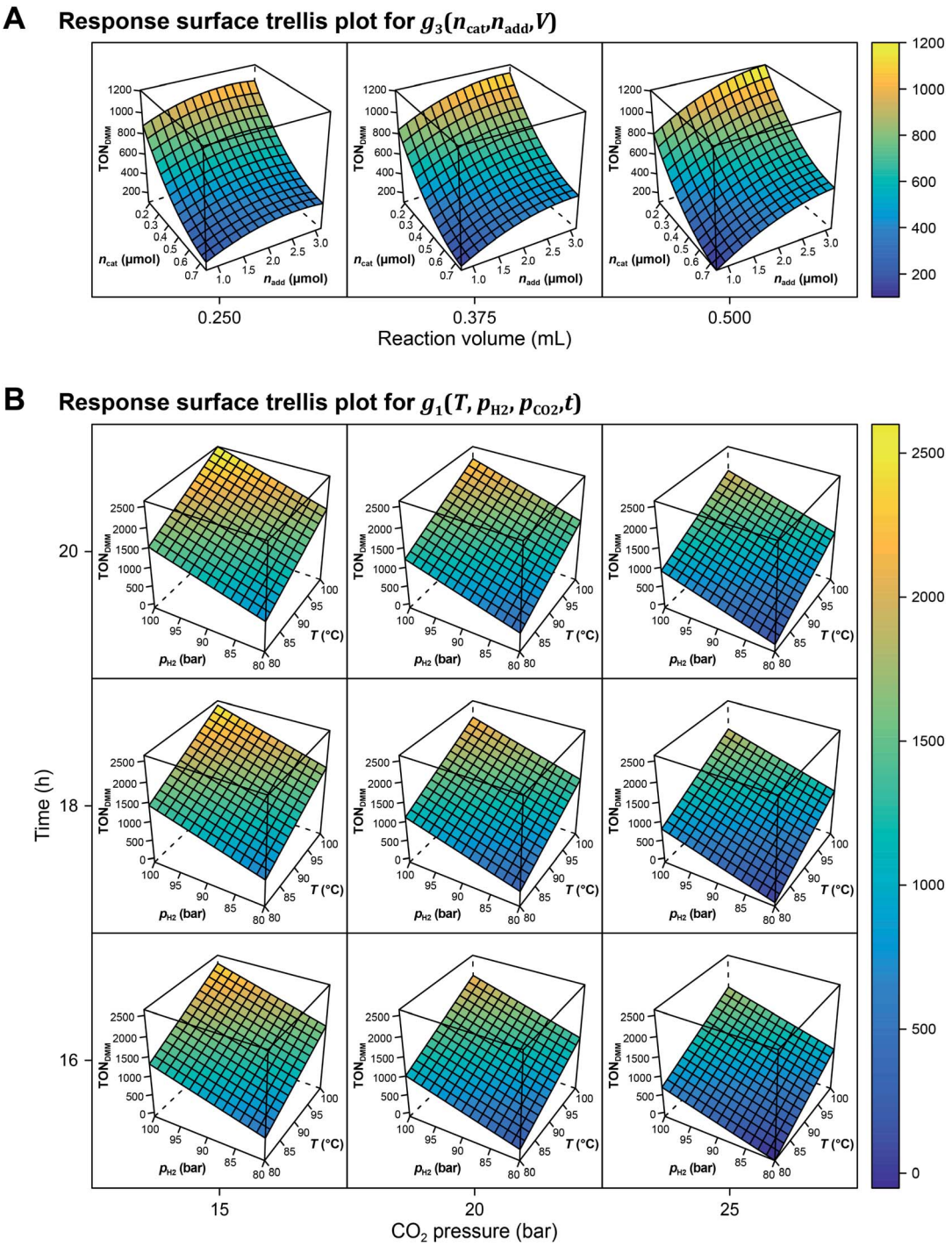

Fig. 3 Calculated response surfaces. (A) Trellis plot of the response surface for $g_3(n_{cat},n_{add},V)$ from OLS modelling with $T = 90$ °C, $p_{H_2} = 90$ bar, $p_{CO_2} = 20$ bar and $t = 18$ h. (B) Response surface trellis plot of the linear OLS model for $g_1(T,p_{H_2},p_{CO_2},t)$ with $n^*_{cat} = 0.075$ μmol, $n^*_{add} = 3.576$ μmol and $V^* = 0.550$ mL. For a mathematical definition of the polynomial parametric surrogates, $g_{1,3}()$, see the Methods section.

initial TON_{DMM} value of 786 to a final value of 2761. As illustrated, the standard deviation (SD) of TON_{DMM} tends to increase with increasing mean value of TON_{DMM} (Fig. 4E), which might be a joint effect from decreasing n_{cat} and increasing both n_{add} and V over the course of the optimisation project. Decreasing n_{cat} and increasing V is equivalent to reducing the concentration of the catalyst, which presumably renders the system more susceptible to random disturbances by catalyst deactivation, thereby providing an explanation for the observed increase of the standard deviation. Simple Spearman rank correlation analysis of the relationship between $SD(TON_{DMM})$, $SD(TON_{MF})$ and the process parameters X_i supports this hypothesis by revealing a negative and a positive association of $SD(TON_{DMM})$ with n_{cat} and V, respectively (ESI Table 26†).

A First DoE

entry	n_{cat} (µmol)	n_{add} (µmol)	V (mL)	TON_{DMM}	TON_{MF}
1	0.750	0.781	0.250	204	90
2	0.750	0.781	0.500	119	205
3	0.750	1.953	0.375	342	116
4	0.188	3.125	0.250	1116	437
5	0.750	3.125	0.250	314	79
6	0.469	3.125	0.375	617	201

B First relaxation

entry	n_{cat} (µmol)	n_{add} (µmol)	V (mL)	TON_{DMM}	TON_{MF}
1	0.131	3.359	0.525	1374	1560
2	0.075	3.576	0.550	1375	2762
3	0.019	3.659	0.575	180	1040

C Second DoE

entry	T (°C)	p_{H2} (bar)	p_{CO2} (bar)	t (h)	TON_{DMM}	TON_{MF}
RS1	90	90	20	18	1310	2858
1	80	100	25	20	889	3281
2	100	80	25	20	1181	2936
3	80	80	15	16	466	1996
4	100	100	15	20	2610	2356
5	100	100	25	16	1788	3189

D Second relaxation

entry	T (°C)	p_{H2} (bar)	p_{CO2} (bar)	t (h)	TON_{DMM}	TON_{MF}
RS2	100	100	15	20	2563	2401
1	105	105	12.5	21	2761	1769
2	110	110	10	22	2209	1276

E Scatter plot TON_{MF} versus TON_{DMM}

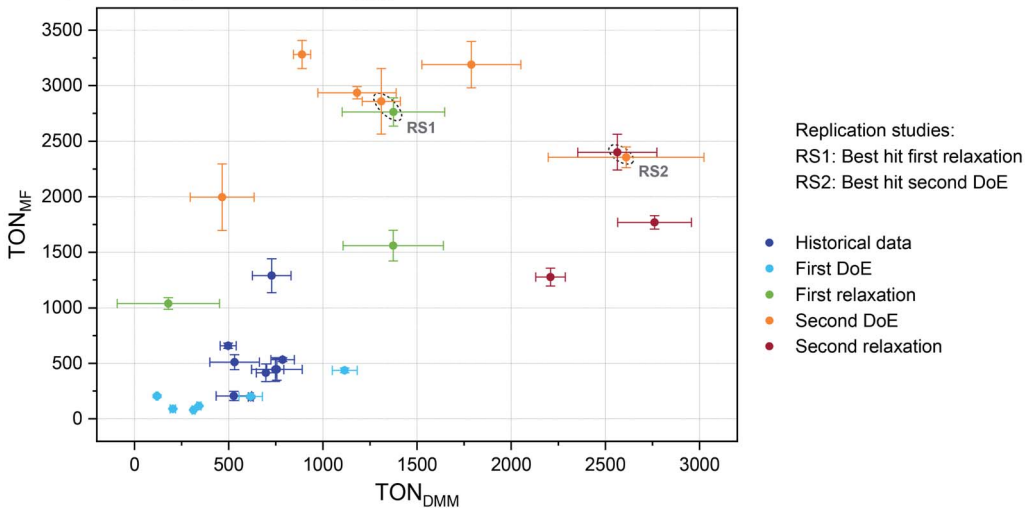

Fig. 4 Optimisation summary. Process parameters and TONs for DMM and MF at different optimisation steps: (A) first DoE. (B) First relaxation (10, 20 and 30%). (C) Second DoE. (D) Second relaxation (25 and 50%). (E) Scatter plot TON_{MF} *versus* TON_{DMM} summarising the outcome of the optimisation project. The results of each optimisation step are marked according to the colour code. Replication studies (RS): the circled data points label the best hit of the first relaxation and the respective replication trials in the second DoE (RS1) as well as the best hit of the second DoE and the respective replication trials in the second relaxation (RS2).

Another interesting result in Fig. 4E refers to the independent replication error. The linear design of the second DoE includes two independent settings of the 20% reference as centre points with each point measured as triple replicate (ESI Tables 11 and 17†). This sextet from the second DoE (Fig. 4C, entry RS1) excellently matches the 20% relaxation triple (Fig. 4B, entry 2) indicating good repeatability and reliability of the system (Fig. 4E, ESI Tables 27 and 28†). In a similar way, the best candidate from the second DoE (Fig. 4C, entry 4) has been independently replicated when running the second relaxation sequence (Fig. 4D, entry RS2) and both replicates turned out identical within the experimental error (Fig. 4E, ESI Tables 29 and 30†).

Technical adaption

The results of the non-biased mathematical modelling approach presented in this study revealed that a better catalytic performance is *inter alia* strongly correlated to a combination of lower catalyst loadings and higher reaction volumes. The heuristic interpretation of this finding indicates that the poor solubility of hydrogen gas in methanol and mass transfer might be limiting factors within our experimental setup. We anticipated that a larger reaction volume, a higher surface to volume

ratio and improved mixing would lead to better mass transfer and thus designed an experimental setup accordingly to enhance the catalytic performance. With this upscale autoclave, the TON for DMM increased to 3874, while the TON for MF reached a value of 1445, resulting in a higher selectivity toward DMM (ESI Table 21†). The result of this technical adaption shows that while the reaction is already optimised to a high degree with respect to reaction parameters, further improvements can be expected by focusing on engineering aspects of the reaction setup.

Conclusion

We demonstrated the power of multivariate optimisation for catalytic processes over the usually applied cumbersome one-factor-at-a-time method. In the homogeneously catalysed transformation of CO_2 to DMM (dimethoxymethane) and MF (methyl formate) using the ruthenium-triphos complex [Ru(*N*-triphos^{Ph})(tmm)], the TON (turnover number) for DMM was drastically increased to 2761 (with it: TON_{MF} 1769) by an easy-to-use algorithmic workflow combined with only a small number of catalytic experiments. Given the complexity of the transformation, which depends on seven parameters, conventional OFAT screening techniques would have been very costly and time-consuming, with uncertain outcome.

Starting from catalytic data using RF (random forest) for empirical model building, an experimental subspace was identified and subsequently augmented to render the effects of a first set of three process factors estimable. Modelling and optimisation, followed by relaxation led to a sequence of relaxation trials with one candidate assumed to be locally optimal. With this candidate as reference, a linear design of the remaining four variables yielded another substantial improvement. Relaxation of the second design further enhanced the catalytic performance, thereby reaching the technical limits of the setup.

The optimised conditions were used in a specifically designed experimental setup and the highest TON for DMM of 3874 (with it: TON_{MF} 1445) was obtained, which is, to the best of our knowledge, the by far highest value reported in the investigated catalysis.

Methods

Theoretical introduction

Experimental design (design of experiments, DoE) methods can be used to study the joint effects of several parameters X: X_1, X_2, …, X_I on response Y.[26,42,43] This can formally be written as:

$$Y = f(X) + \varepsilon \quad (1)$$

$f()$ denotes the true, however unknown function, linking the responses Y with the process conditions X: X_1, X_2, …, X_I, whereas ε is a random element taken from a normal distribution with variance σ^2, $\varepsilon \sim N(0,\sigma^2)$ to account for experimental uncertainties. Conceptually, nature evaluates in an experiment the function $f()$ known to her only at reaction conditions X, then adds some random noise ε and returns the experimental results Y [eqn (1)].

Under the weak assumption that $f()$ is smooth and continuous, $f()$ can be locally approximated as polynomial parametric surrogates, $g_{1,2,3}()$, of increasing complexity, formally:

$$f(X) \cong g_1(X) = a_0 + \sum_i a_i X_i \quad (2)$$

$$f(X) \cong g_2(X) = a_0 + \sum_i a_i X_i + \sum_{j>i} a_{ij} X_i X_j \quad (3)$$

$$f(X) \cong g_3(X) = a_0 + \sum_i a_i X_i + \sum_i a_{ii} X_i^2 + \sum_{j>i} a_{ij} X_i X_j \quad (4)$$

These are linear [eqn (2)], bilinear [eqn (3)] or quadratic [eqn (4)] parametric surrogates of the true function $f()$. With the experimental values Y, X_1, X_2, …, X_I available, the unknown parameters a_i, a_{ii}, a_{ij} can be estimated from the data using ordinary least squares (OLS).[46]

Given process factors X_1, X_2, …, X_I, their ranges $X_i \in \{LB,UB\}$ with LB, UB denoting the lower and upper bounds of the process factors X_i and, depending on the expected complexity, the parametric form of the surrogate model, the design points X (experimental design) optimally supporting the chosen model can be calculated. However, in an early project phase it is often unclear which factors X_i and ranges should be chosen and what levels of complexity must be assumed for the domain under investigation. Therefore, DoE can benefit from experimental data analysis, with the latter helping to answer the questions arising in the former.

After first optimisation by an experimental design, ascending in the direction of maximal improvement can be easily achieved by increasing (relaxing) the experimental space in discrete steps and by solving a maximisation problem subject to a sequence of hypercubical constraints, that is

$$\max(g(X)) \text{ subject to } LB - k\Delta X < X < UB + k\Delta X \quad (5)$$

with ΔX being the step size of the relaxation, here taken to be 10% of the initial factor ranges, that is $\Delta X = 0.1[UB - LB]$, and LB, UB denoting the lower and upper bounds of the process factors X_i. Varying $k = 1, 2, \ldots, K$ leads to a sequence of relaxation trials $X_1^*, X_2^*, \ldots, X_K^*$ to be realised in the lab.

Additional information

The detailed description of all experiments, the performed multivariate analysis, the spectroscopic data of compounds as well as the NMR spectra of compounds and catalysis samples can be found in the ESI.† In order to improve comprehensibility, simplified names were used in some cases rather than using exact IUPAC names.

All calculations were done using the statistical software R.[47] Random forest modelling was performed with the R-package 'randomForest'.[48] Experimental designs were calculated with the D-optimal criterion of the function optFederov() in the R-package 'AlgDesign'.[49] Optimisation was achieved with the

augmented Lagrange method from the R-package 'Rsolnp'.[50] Graphics were produced with the R-package 'lattice'.[51]

All catalyses and the corresponding analyses were performed following a procedure previously reported by our group.[27] The catalysis was also performed in the absence of a catalyst, a co-catalyst or both to demonstrate the need of the catalytic system for the formation of DMM and MF. In all cases, no significant conversions for both of these compounds were observed (ESI†).

Reproduction of modelling results

The R-code used as well as the catalytic data analysed (Excel sheet) are available online. The multivariate analysis can be reproduced by following the instructions in the ESI.†

Author contributions

M. Siebert and G. K. designed the experiments. M. Siebert performed the experiments. G. K. performed computer modelling and analysis of the data. All authors contributed to the interpretation of the data. The manuscript was co-written by M. Siebert and G. K. and all authors contributed to the manuscript. O. T. supervised the project.

Conflicts of interest

There are no conflicts to declare.

Acknowledgements

Generous financial support by the German Federal Ministry of Education and Research (BMBF) within the funding initiative 'CO_2Plus – Stoffliche Nutzung von CO_2 zur Verbreiterung der Rohstoffbasis' is gratefully acknowledged. We thank A. Closs, A. Schreieck and P. Laloire for fruitful discussions.

References

1 P. J. Crutzen, *Nature*, 2002, **415**, 23.
2 J.-L. Martin, V. Maris and D. S. Simberloff, *Proc. Natl. Acad. Sci. U. S. A.*, 2016, **113**, 6105–6112.
3 T. Sterner, E. B. Barbier, I. Bateman, I. van den Bijgaart, A.-S. Crépin, O. Edenhofer, C. Fischer, W. Habla, J. Hassler, O. Johansson-Stenman, A. Lange, S. Polasky, J. Rockström, H. G. Smith, W. Steffen, G. Wagner, J. E. Wilen, F. Alpízar, C. Azar, D. Carless, C. Chávez, J. Coria, G. Engström, S. C. Jagers, G. Köhlin, Å. Löfgren, H. Pleijel and A. Robinson, *Nature Sustainability*, 2019, **2**, 14–21.
4 Y. Geng, J. Sarkis and R. Bleischwitz, *Nature*, 2019, **565**, 153–155.
5 W. Keim, in *Carbon Dioxide as a Source of Carbon: Biochemical and Chemical Uses*, ed. M. Aresta and G. Forti, Springer, Dordrecht, 1st edn, 1987, DOI: 10.1007/978-94-009-3923-3.
6 M. Aresta, in *Carbon Dioxide as Chemical Feedstock*, ed. M. Aresta, Wiley-VCH, Weinheim, 2010.
7 E. J. Beckman, *Nature*, 2016, **531**, 180–181.
8 R. A. Sheldon, *Green Chem.*, 2016, **18**, 3180–3183.
9 J. A. Martens, A. Bogaerts, N. De Kimpe, P. A. Jacobs, G. B. Marin, K. Rabaey, M. Saeys and S. Verhelst, *ChemSusChem*, 2017, **10**, 1039–1055.
10 Y. Gil, M. Greaves, J. Hendler and H. Hirsh, *Science*, 2014, **346**, 171–172.
11 M. I. Jordan and T. M. Mitchell, *Science*, 2015, **349**, 255–260.
12 G. Rothenberg, *Catalysis: Concepts and Green Applications*, Wiley, Weinheim, 2017.
13 M. S. Sigman, K. C. Harper, E. N. Bess and A. Milo, *Acc. Chem. Res.*, 2016, **49**, 1292–1301.
14 M. H. S. Segler, M. Preuss and M. P. Waller, *Nature*, 2018, **555**, 604–610.
15 C. W. Coley, W. H. Green and K. F. Jensen, *Acc. Chem. Res.*, 2018, **51**, 1281–1289.
16 H. Gao, T. J. Struble, C. W. Coley, Y. Wang, W. H. Green and K. F. Jensen, *ACS Cent. Sci.*, 2018, **4**, 1465–1476.
17 D. T. Ahneman, J. G. Estrada, S. Lin, S. D. Dreher and A. G. Doyle, *Science*, 2018, **360**, 186–190.
18 J. M. Granda, L. Donina, V. Dragone, D.-L. Long and L. Cronin, *Nature*, 2018, **559**, 377–381.
19 C. B. Santiago, J.-Y. Guo and M. S. Sigman, *Chem. Sci.*, 2018, **9**, 2398–2412.
20 S. Zhao, T. Gensch, B. Murray, Z. L. Niemeyer, M. S. Sigman and M. R. Biscoe, *Science*, 2018, **362**, 670–674.
21 A. F. Zahrt, J. J. Henle, B. T. Rose, Y. Wang, W. T. Darrow and S. E. Denmark, *Science*, 2019, **363**, eaau5631.
22 J. P. Reid and M. S. Sigman, *Nature*, 2019, **571**, 343–348.
23 A. V. Brethomé, R. S. Paton and S. P. Fletcher, *ACS Catal.*, 2019, **9**, 7179–7187.
24 P. S. Gromski, A. B. Henson, J. M. Granda and L. Cronin, *Nat. Rev. Chem.*, 2019, **3**, 119–128.
25 G. E. P. Box, W. G. Hunter and J. S. Hunter, *Statistics for Experimenters*, John Wiley & Sons, New York, 1st edn, 1978.
26 G. E. P. Box, W. G. Hunter and J. S. Hunter, *Statistics for Experimenters: Design, Innovation, and Discovery*, John Wiley & Sons, Hoboken, 2st edn, 2005.
27 M. Siebert, M. Seibicke, A. F. Siegle, S. Kräh and O. Trapp, *J. Am. Chem. Soc.*, 2019, **141**, 334–341.
28 M. Seibicke, M. Siebert, A. F. Siegle, S. M. Gutenthaler and O. Trapp, *Organometallics*, 2019, **38**, 1809–1814.
29 S. Dabral and T. Schaub, *Adv. Synth. Catal.*, 2019, **361**, 223–246.
30 R. Sun, I. Delidovich and R. Palkovits, *ACS Catal.*, 2019, **9**, 1298–1318.
31 K. Thenert, K. Beydoun, J. Wiesenthal, W. Leitner and J. Klankermayer, *Angew. Chem., Int. Ed.*, 2016, **55**, 12266–12269.
32 B. G. Schieweck and J. Klankermayer, *Angew. Chem., Int. Ed.*, 2017, **56**, 10854–10857.
33 S. Bontemps, L. Vendier and S. Sabo-Etienne, *Angew. Chem., Int. Ed.*, 2012, **51**, 1671–1674.
34 S. Bontemps, L. Vendier and S. Sabo-Etienne, *J. Am. Chem. Soc.*, 2014, **136**, 4419–4425.
35 G. Jin, C. G. Werncke, Y. Escudié, S. Sabo-Etienne and S. Bontemps, *J. Am. Chem. Soc.*, 2015, **137**, 9563–9566.

36 A. Aloisi, J.-C. Berthet, C. Genre, P. Thuéry and T. Cantat, *Dalton Trans.*, 2016, **45**, 14774–14788.
37 M. R. Espinosa, D. J. Charboneau, A. Garcia de Oliveira and N. Hazari, *ACS Catal.*, 2019, **9**, 301–314.
38 T. T. Metsänen and M. Oestreich, *Organometallics*, 2015, **34**, 543–546.
39 P. Ríos, N. Curado, J. López-Serrano and A. Rodríguez, *Chem. Commun.*, 2016, **52**, 2114–2117.
40 Y. Jiang, O. Blacque, T. Fox and H. Berke, *J. Am. Chem. Soc.*, 2013, **135**, 7751–7760.
41 F. A. LeBlanc, W. E. Piers and M. Parvez, *Angew. Chem., Int. Ed.*, 2014, **53**, 789–792.
42 G. E. P. Box and N. R. Draper, *Empirical Model-Building and Response Surfaces*, John Wiley & Sons, New York, 1987.
43 D. C. Montgomery, *Design and Analysis of Experiments*, John Wiley & Sons, New York, 3rd edn, 1991.
44 L. Breiman, *Mach. Learn.*, 2001, **45**, 5–32.
45 T. Hastie, R. Tibshirani and J. Friedman, *The Elements of Statistical Learning*, Springer-Verlag, New York, 2nd edn, 2009.
46 A. Sen and M. Srivastava, *Regression Analysis*, Springer-Verlag, New York, 1990.
47 R Core Team, *R: A Language and Environment for Statistical Computing*, R Foundation for Statistical Computing, Vienna, Austria, 2017, https://www.R-project.org/.
48 A. Liaw and M. Wiener, *R News*, 2002, **2**, 18–22.
49 B. Wheeler, *AlgDesign: Algorithmic Experimental Design*, R package version 1.1-7.3, 2014, https://CRAN.R-project.org/package=AlgDesign.
50 A. Ghalanos and S. Theussl, *Rsolnp: General Non-Linear Optimization*, R package version 1.16, 2015, https://CRAN.R-project.org/package=Rsolnp.
51 D. Sarkar, *Lattice*, Springer-Verlag, New York, 2008.

4.4 A Fast and Reliable Screening Setup for Homogeneous Catalysis with Gaseous Reactants at Extreme Temperatures and Pressures

Max Siebert, Golo Storch, and Oliver Trapp

Prologue

An efficient reaction setup is presented that was designed for screening catalytic reactions involving gaseous reactants under inert conditions at high pressures over a broad temperature range. The setup consists of different types of autoclaves as well as a filling system that makes preparation in the glovebox unnecessary. Different analytic techniques can be coupled to the autoclaves, and their modular design allows further adaption to specific needs. Proof-of-concept examples are discussed to demonstrate the potential of the setup.

Author Contributions

All authors contributed to the design and construction of the setup. M. S. and G. S. designed the experiments. M. S. performed the experiments. All authors contributed to the interpretation of the data. The manuscript was co-written by M. S. and G. S., and all authors contributed to the manuscript. O. T. supervised the project.

License

Supporting Information

The supporting information is available at https://doi.org/10.1021/acs.oprd.0c00192.

ORGANIC PROCESS RESEARCH & DEVELOPMENT
OPR&D

pubs.acs.org/OPRD

Article

A Fast and Reliable Screening Setup for Homogeneous Catalysis with Gaseous Reactants at Extreme Temperatures and Pressures

Max Siebert, Golo Storch, and Oliver Trapp*

Cite This: https://dx.doi.org/10.1021/acs.oprd.0c00192

Read Online

ACCESS | Metrics & More | Article Recommendations | Supporting Information

ABSTRACT: Modern catalysis research strongly focusses on optimizing multiple reaction parameters *en route* to find optimal conditions. However, a very limited number of fundamental parameter combinations, such as inert conditions, gaseous reactants, variable temperature, and elevated pressure, can be screened in a convenient and straightforward manner. We report a ready-to-use reaction setup that is designed for screening reactions with gaseous reactants under inert conditions in standard NMR tubes (0.5 mL) using temperatures between −40 and +100 °C and extreme pressures. Proof-of-concept reaction examples are discussed, and the coupling to modern analytic techniques including in situ IR spectroscopy is possible.

KEYWORDS: *homogeneous catalysis, asymmetric catalysis, high-pressure reactions, catalysis screening setup, reaction mechanism elucidation, IR spectroscopy*

The optimization of catalytic systems includes thorough screening of process parameters. Although great efforts are made to develop algorithms and computational tools to support the screening process and to reduce the number of experiments,[1] ultimate success still relies on obtaining raw data on reactions run under all possible conditions. Several commercial solutions exist for screening of pressurized reactions, but most of them are specialized to a specific application scenario and even small adaptations of the systems are not possible. The scale in these solutions is usually fixed and too large for screening of numerous catalytic reactions involving precious chemicals. In addition, it is still challenging to use the combination of low temperatures and two different gases under pressurized conditions. Reaction setups beyond what is commercially available are rarely described in publications[2] and often consist of custom-made devices hindering their reproduction and improvement. As a consequence, some combinations of fundamental parameters such as inert conditions, gaseous reactants, variable temperature, and elevated pressure, are still screened on a "what is possible" level rather than focusing on "what is best".

The interplay of pressure and temperature serves as an ideal example. For catalytic transformations, there is an optimum in temperature regarding reactivity and selectivity.[3] However, when gaseous reactants are involved at higher pressures and autoclaves have to be used, the screening of temperatures becomes challenging—especially below room temperature. The possibility to quickly and reliably screen several combinations of pressures and extreme temperatures would drastically improve the optimization of such reactions and lead to superior results that would otherwise remain undisclosed.

There are numerous scenarios in which control over the abovementioned parameters is crucial for obtaining new information on a chemical system, and three representative examples from our own experience shall serve as illustration. Low-temperature hydrogenation allowed us to discover significant differences in catalytic activity of two diastereomeric rhodium complexes (Scheme 1A). When applying the equilibrium catalyst with 22% *de*, we were able to obtain the hydrogenation products in up to 74% *ee* simply by lowering the reaction temperature to −40 °C, which would not have been possible using standard reaction setups.[4] Using the same setup, we observed enantiodivergence[5] solely as a function of reaction conditions in a single catalytic system—a rare phenomenon, which in this case is caused by noncovalent catalyst−product interactions (Scheme 1B). Being able to conduct catalytic reactions at −20 °C with hydrogen gas pressures ranging from 5 to 60 bar allowed us to determine the extreme values for both (*R*)- and (*S*)-products.[6] Common to these examples is the question whether they are actually rare or whether similar observations are only not made because of the unavailability of a suitable reaction setup. During a study on catalytic conversion of CO_2 to a formaldehyde derivative (Scheme 1C), the straightforward and time-efficient screening protocol allowed us to perform over 200 catalytic reactions in independent atmospheres. In this unusual setup with two gases, optimized reaction conditions were identified, leading to a 13-fold increase in activity.[7]

Additionally, a vast number of catalytic reactions involving gaseous reactants need inert conditions to avoid catalyst deactivation or decomposition. Therefore, such reactions have to be set up in autoclaves using a glovebox, which makes the screening process tedious and time-consuming. Although these autoclaves can potentially be filled with several glass insets, the

Received: April 16, 2020
Published: June 1, 2020

Scheme 1. Examples for the Use of the Experimental Setup

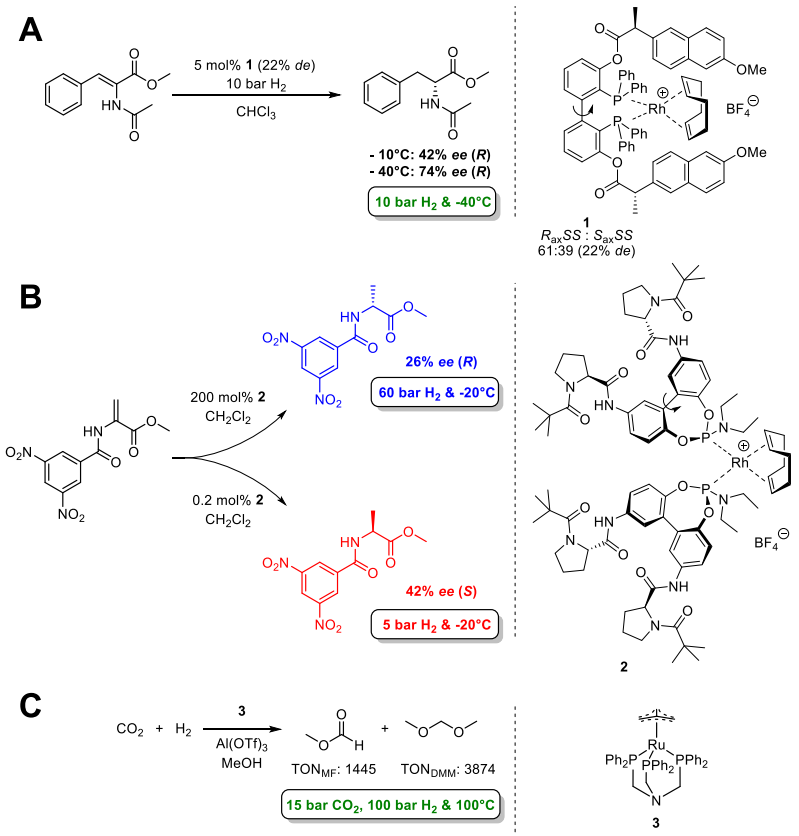

catalytic reactions all share the same parameter set and gas atmosphere. As a consequence, the samples influence each other over the course of the reaction and only one combination of temperature and pressure can be screened simultaneously.

To address these challenges and to overcome the corresponding limitations, we designed an efficient ready-to-use experimental setup for homogeneous catalytic reactions. Herein, the designed autoclaves are set up, run, and analyzed individually, allowing precise yet rapid screening in independent atmospheres. The entire setup is built from standard parts (see the Supporting Information for all details) and allows gas pressures between 5 and 155 bar as well as reaction temperatures from −40 to 100 °C, thereby covering the majority of catalytic transformations. The temperature and pressure ranges refer to the here tested reaction conditions and could even be extended up to the manufacturer's specifications for the individual components.

Depending on the application and the respective requirements, several different types of autoclaves have been designed and built, ranging from 0.5 mL (NMR tube) to 10 mL of reaction solution with gas volumes of 10−35 mL, respectively (Figure 1A). In the smallest type, the catalysis proceeds in an NMR tube inside the autoclave, which allows direct analysis before and after the reaction and thus speeds up catalytic screening (Figure 1A-1; see the Supporting Information). The larger autoclaves allow better mixing, thereby improving mass transfer within the catalytic system if, for instance, gas solubility in the solvent is low (Figure 1A-3; see the Supporting Information).[7a] Although it is challenging to perform catalytic gas reactions at low temperatures of up to −40 °C with commercially available autoclave setups, such reactions were easily performed using our autoclaves and a standard cryostat or cooling mixture. Additionally, high temperatures of up to 100 °C were applied. Each reaction is performed in a fully independent atmosphere, allowing precise adjustment and screening of the reaction parameters.

Fully independent reactions also allow to measure reaction kinetics. For this purpose, we built an autoclave, in which the total pressure is measured via a pressure transducer and by which the reaction kinetics of such catalytic gas reactions can directly be determined (Figure 1A-2; see the Supporting Information). Furthermore, we constructed an autoclave to directly measure in situ IR spectroscopy during high-pressure reactions in a wide temperature range (Figure 1A-4; see the Supporting Information). The flexibility of our modular autoclave system is additionally extended by coupling the two just mentioned tools in a single autoclave (Figure 1A-5; see the Supporting Information). Combined in situ IR spectroscopy analysis and on-line pressure measurements allow for the simultaneous identification of reaction intermediates and the determination of reaction kinetics of complex transformations.

The central element of the setup is an inert gas pressure line connected to a vacuum pump, an inert gas supply as well as two gas cylinders (Figure 1B). It is advantageous of this system that the connected autoclave can be conditioned (vacuum and inert gas) and filled with the desired reaction gases safely without disconnecting in between (see the Supporting Information). The installed three-way valves prevent a short circuit of the pressured parts with the vacuum or inert gas line (Figure 1C). In contrast to commercially available standard

https://dx.doi.org/10.1021/acs.oprd.0c00192
Org. Process Res. Dev. XXXX, XXX, XXX−XXX

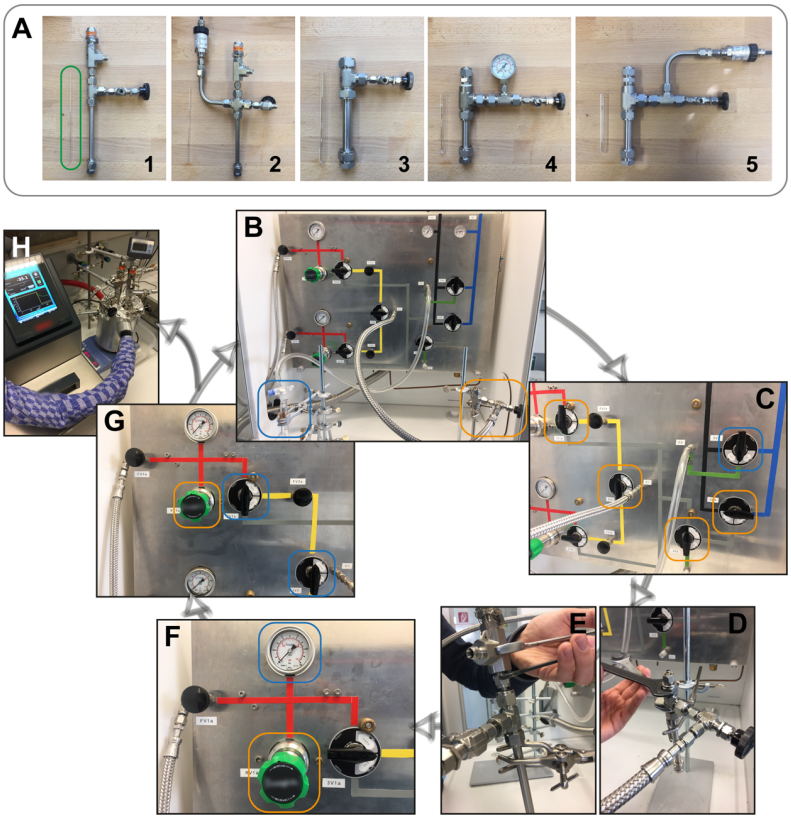

Figure 1. Overview of the designed autoclaves and the workflow. (A) From left to right: NMR tube autoclave with 7 in. NMR tube (green box) (1); NMR tube autoclave for on-line pressure measurements (2); large tube autoclave (3); medium-sized tube autoclave for in situ IR measurements (4); medium-sized tube autoclave for in situ IR and on-line pressure measurements (5). (B) Inert gas pressure line with vacuum (black stripes) and inert gas supply (blue stripes), two high-pressure gas lines (red stripes) as well as a connected Schlenk tube (blue box) and an NMR tube autoclave (orange box). (C) Connecting the Schlenk tube to the inert system by switching a single three-way valve (blue box) and the autoclave by adjusting four three-way valves (orange boxes), whereas only one has to be switched for exchanging the atmospheres. (D + E) After transferring the catalysis solution into the glass inset inside the autoclave, the connector (D) and the proportional relief valve (E) are installed. (F) Purging of the gas line and adjusting the working pressure (blue box) by using the green pressure regulator (orange box). (G) Pressurizing the autoclave using two three-way valves (blue boxes) and releasing the pressure using the green pressure regulator (orange box). (H) Once the autoclave is disconnected from the system, any temperature can be set from a wide range and the catalysis can proceed.

autoclaves, which are normally filled through their "head", the key feature of these designed autoclaves is the connector at its "body" (Figure 1D; see the Supporting Information). As a result, the catalysis mixture can be transferred into the autoclave in counterflow while it is still connected to the inert gas pressure line, which makes preparation in the glovebox unnecessary. Thus, no cumbersome reaction preparation is required and a catalytic reaction can be set up in less than 15 min.

To demonstrate the applicability of our setup, we addressed the asymmetric hydrogenation reaction of prochiral α-substituted acrylic acids catalyzed by a Ru(II)−BINAP complex (Scheme 2).

Scheme 2. Asymmetric Hydrogenation of Prochiral α-Substituted Acrylic Acids

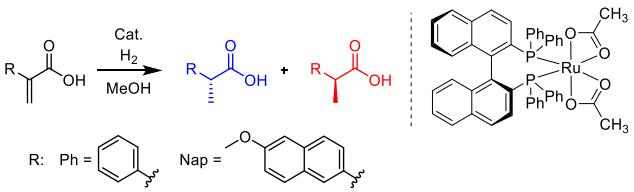

First, we used our autoclaves for screening and determining the kinetics of the reaction by using the asymmetric hydrogenation of 2-phenylacrylic acid as model reaction (Figure 2A−C). The conversion was analyzed directly after the catalysis using NMR spectroscopy without the need for further workup. The products were directly quantified by simply adding an internal standard prior to catalysis (Figure 2A). The change in the total pressure (Figure 2B) as well as the decrease and increase of substrate and product (Figure 2C), respectively, was monitored allowing for the determination of reaction kinetics. Another feature is the temperature measurement by the IR probe within the autoclave, which permits an even more precise determination of rate constants and thermodynamic parameters as the Gibbs free energy (Figure 2C).

For the addressed asymmetric hydrogenation reaction of prochiral α-substituted acrylic acids, which was intensively studied by Noyori (Scheme 2), significant variations of the *ee* have been observed as function of changes in hydrogen gas pressure.[8] However, systematic studies remained tedious and have since been only scarcely performed. For this Ru(II)-catalyzed reaction, the enantioselectivity is strongly dependent on the hydrogen gas pressure and even enantiodivergence is obtained for certain substitution patterns in substrates. For 2-

https://dx.doi.org/10.1021/acs.oprd.0c00192
Org. Process Res. Dev. XXXX, XXX, XXX−XXX

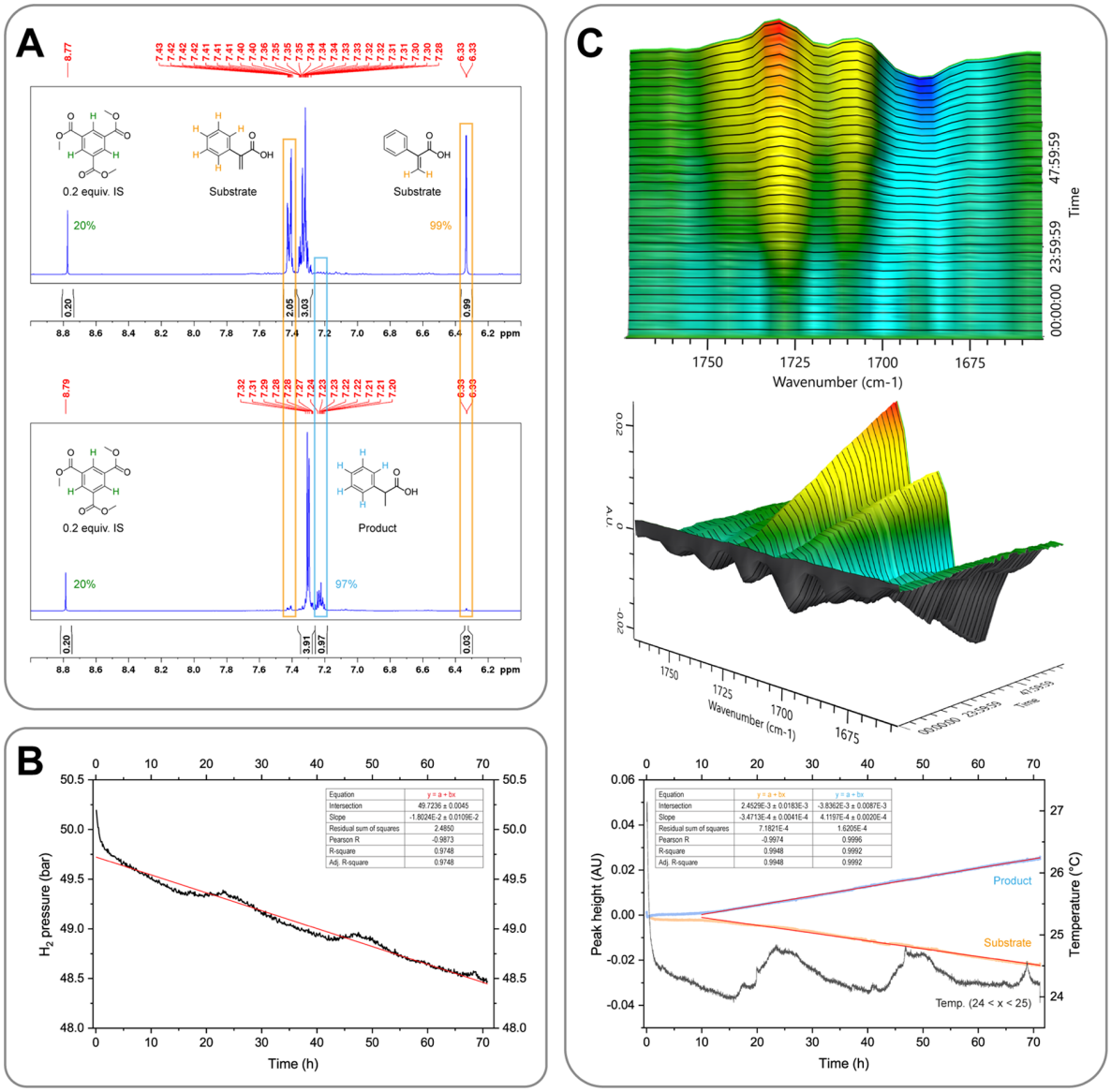

Figure 2. Versatile analysis options in the catalysis workflow. (A) NMR spectra of 2-phenylacrylic acid and its hydrogenation product 2-phenylpropionic acid measured with an internal standard (IS) directly before (top) and after (bottom) asymmetric hydrogenation. (B) Pressure gradient of the asymmetric hydrogenation of 2-phenylacrylic acid. (C) Reaction progress of the asymmetric hydrogenation of 2-phenylacrylic acid monitored with in situ IR spectroscopy. 2-Phenylacrylic acid at 1689 cm^{-1} (orange) and 2-phenylpropionic acid at 1727 cm^{-1} (blue). The temperature at the IR probe is given as black line.

phenylacrylic acid and dehydronaproxen, a higher enantioselectivity for the (*S*)-enantiomer was observed at higher hydrogen gas pressures using the (*S*)-BINAP ligand yet no (*R*)-enantiomer was obtained so far.

We used our setup to perform hydrogenation reactions at five different combinations of hydrogen gas pressure and temperature for both substrates (Figure 3). Increasing the hydrogen gas pressure from 10 to 100 bar led to a higher enantioselectivity in favor of the (*S*)-enantiomer going from 28 to 68% *ee* for 2-phenylacrylic acid and from 14 to 58% *ee* for dehydronaproxen (Figure 3A,B). Both products are now significantly enriched in favor of their (*S*)-enantiomer, but the optical purity obtained is still too low for further useful application.

Besides the pressure dependence, we hypothesized that an additional—and previously unknown—influence of the temperature on the enantioselectivity could be observed under high-pressure conditions. The anticipated extreme reaction conditions can be easily screened with the here-presented setup (Figures 1 and 2). Intriguingly, we observed that the influence of temperature on enantioselectivity is even stronger than the investigated influence of pressure. At 100 bar, the enantioselectivity for the (*S*)-enantiomer decreased drastically upon an increase in temperature to 100 °C, reaching only 2% *ee* for dehydronaproxen (Figure 3B). For 2-phenylacrylic acid, even the (*R*)-enantiomer was obtained with 9% *ee*, thereby revealing an enantiodivergent behavior of the catalytic system (Figure 3A). When the temperature was decreased to 0 °C, the selectivity significantly increased for both substrates, yielding 89% and 90% *ee* of the (*S*)-enantiomer for 2-phenylacrylic acid and dehydronaproxen, respectively (Figure 3A,B).

https://dx.doi.org/10.1021/acs.oprd.0c00192
Org. Process Res. Dev. XXXX, XXX, XXX−XXX

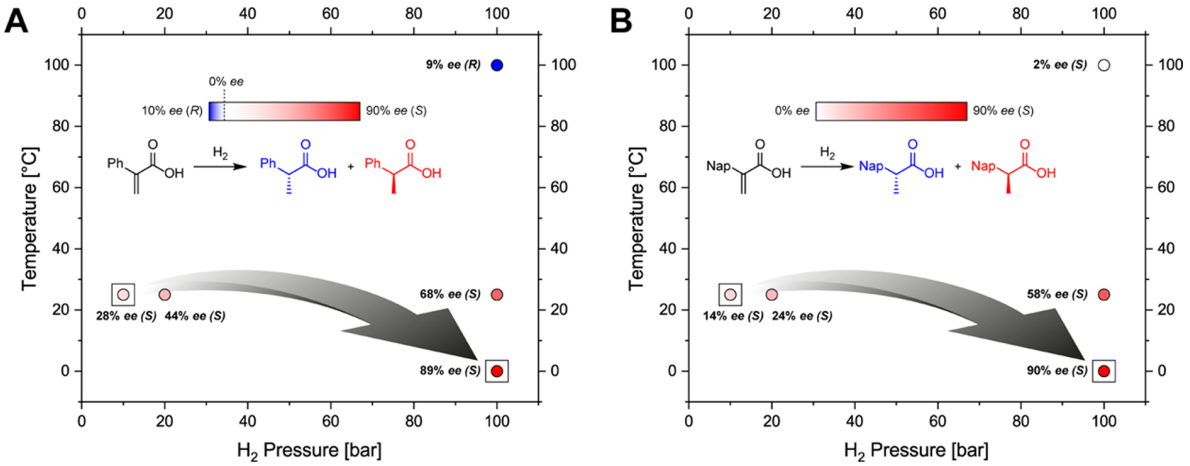

Figure 3. Enantioselectivities in the asymmetric hydrogenation of prochiral α-substituted acrylic acids in dependence of the hydrogen gas pressure and the temperature. The data points in the black boxes represent the first experimental values as well as the obtained optima with regard to the (*S*)-enantiomer. The black arrows indicate the increase of enantioselectivity over the course of optimization. (A) Results obtained for 2-phenylacrylic acid. (B) Results obtained for dehydronaproxen.

In conclusion, the designed ready-to-use experimental setup allows rapid yet precise screening of homogeneous catalytic reactions with gases at 5−155 bar total pressure and reaction temperatures between at least −40 to 100 °C. Catalytic reactions are set up quickly without the need for a glovebox. Qualitative and quantitative analysis by NMR spectroscopy can be performed before and after the catalysis, with no workup in between. The coupling to modern analytic techniques as in situ IR and on-line pressure measurements give access to reaction kinetics and intermediate identification. Because our setup is exclusively built from standard components, it can be easily assembled, and the modular design of the autoclaves allows the user to adapt them to best fit the needs. We demonstrated all features of our fast and reliable screening setup in an important model reaction as well as its potential by revealing a previously unknown temperature dependence of the enantioselectivity in the Ru(II)-catalyzed asymmetric hydrogenation of two prochiral α-substituted acrylic acids.

■ ASSOCIATED CONTENT

Supporting Information

The Supporting Information is available free of charge at https://pubs.acs.org/doi/10.1021/acs.oprd.0c00192.

Pictures, technical drawings, and components of the setup and the autoclaves; information on the application of the setup as well as on the workflow; and experimental details for the investigated catalyses (PDF)

■ AUTHOR INFORMATION

Corresponding Author

Oliver Trapp − *Department Chemie, Ludwig-Maximilians-Universität München, 81377 München, Germany;* orcid.org/0000-0002-3594-5181; Email: oliver.trapp@cup.uni-muenchen.de

Authors

Max Siebert − *Department Chemie, Ludwig-Maximilians-Universität München, 81377 München, Germany;* orcid.org/0000-0002-0151-8886

Golo Storch − *Department Chemie and Catalysis Research Center (CRC), Technische Universität München, 85747 Garching, Germany;* orcid.org/0000-0002-6747-3035

Complete contact information is available at: https://pubs.acs.org/10.1021/acs.oprd.0c00192

Author Contributions

The manuscript was written through contributions of all authors. All authors have given approval to the final version of the manuscript.

Funding

Generous financial support by the European Research Council (ERC) for a Starting grant (no. 258740, AMPCAT) and the German Federal Ministry of Education and Research (BMBF) within the funding initiative "CO2Plus—Stoffliche Nutzung von CO_2 zur Verbreiterung der Rohstoffbasis" is gratefully acknowledged.

Notes

The authors declare no competing financial interest.

■ ACKNOWLEDGMENTS

Technical support through precision mechanics of the Department Chemistry of the LMU Munich is gratefully acknowledged.

■ ABBREVIATIONS

BINAP, 2,2′-bis(diphenylphosphino)-1,1′-binaphthyl; IR, infrared; IS, internal standard; NMR, nuclear magnetic resonance

■ REFERENCES

(1) (a) Neel, A. J.; Hilton, M. J.; Sigman, M. S.; Toste, F. D. Exploiting non-covalent π interactions for catalyst design. *Nature* **2017**, *543*, 637−646. (b) Coley, C. W.; Green, W. H.; Jensen, K. F. Machine Learning in Computer-Aided Synthesis Planning. *Acc. Chem. Res.* **2018**, *51*, 1281−1289. (c) Henson, A. B.; Gromski, P. S.; Cronin, L. Designing Algorithms To Aid Discovery by Chemical Robots. *ACS Cent. Sci.* **2018**, *4*, 793−804. (d) Reid, J. P.; Sigman, M. S. Comparing quantitative prediction methods for the discovery of small-molecule chiral catalysts. *Nat. Rev. Chem.* **2018**, *2*, 290−305. (e) Ahn, S.; Hong, M.; Sundararajan, M.; Ess, D. H.; Baik, M.-H. Design and

Optimization of Catalysts Based on Mechanistic Insights Derived from Quantum Chemical Reaction Modeling. *Chem. Rev.* **2019**, *119*, 6509−6560. (f) Durand, D. J.; Fey, N. Computational Ligand Descriptors for Catalyst Design. *Chem. Rev.* **2019**, *119*, 6561−6594. (g) Gromski, P. S.; Henson, A. B.; Granda, J. M.; Cronin, L. How to explore chemical space using algorithms and automation. *Nat. Rev. Chem.* **2019**, *3*, 119−128. (h) Mater, A. C.; Coote, M. L. Deep Learning in Chemistry. *J. Chem. Inf. Model.* **2019**, *59*, 2545−2559. (i) Zahrt, A. F.; Athavale, S. V.; Denmark, S. E. Quantitative Structure−Selectivity Relationships in Enantioselective Catalysis: Past, Present, and Future. *Chem. Rev.* **2020**, *120*, 1620.

(2) Friis, S. D.; Lindhardt, A. T.; Skrydstrup, T. The Development and Application of Two-Chamber Reactors and Carbon Monoxide Precursors for Safe Carbonylation Reactions. *Acc. Chem. Res.* **2016**, *49*, 594−605.

(3) (a) Behr, A.; Neubert, P. *Applied Homogeneous Catalysis*; Wiley-VCH: Weinheim, 2012. (b) Cornils, B.; Herrmann, W. A.; Beller, M.; Paciello, R. *Applied Homogeneous Catalysis with Organometallic Compounds: A Comprehensive Handbook in Four Volumes*, 3rd ed.; Wiley-VCH: Weinheim, 2017.

(4) Storch, G.; Trapp, O. Temperature-Controlled Bidirectional Enantioselectivity in a Dynamic Catalyst for Asymmetric Hydrogenation. *Angew. Chem., Int. Ed.* **2015**, *54*, 3580−3586.

(5) Beletskaya, I. P.; Nájera, C.; Yus, M. Stereodivergent Catalysis. *Chem. Rev.* **2018**, *118*, 5080−5200.

(6) Storch, G.; Trapp, O. By-design enantioselective self-amplification based on non-covalent product−catalyst interactions. *Nat. Chem.* **2017**, *9*, 179−187.

(7) (a) Siebert, M.; Krennrich, G.; Seibicke, M.; Siegle, A. F.; Trapp, O. Identifying high-performance catalytic conditions for carbon dioxide reduction to dimethoxymethane by multivariate modelling. *Chem. Sci.* **2019**, *10*, 10466−10474. (b) Siebert, M.; Seibicke, M.; Siegle, A. F.; Kräh, S.; Trapp, O. Selective Ruthenium-Catalyzed Transformation of Carbon Dioxide: An Alternative Approach toward Formaldehyde. *J. Am. Chem. Soc.* **2019**, *141*, 334−341.

(8) (a) Ohta, T.; Takaya, H.; Kitamura, M.; Nagai, K.; Noyori, R. Asymmetric hydrogenation of unsaturated carboxylic acids catalyzed by BINAP-ruthenium(II) complexes. *J. Org. Chem.* **1987**, *52*, 3174−3176. (b) Noyori, R. *Asymmetric Catalysis in Organic Synthesis*; John Wiley & Sons: New York, 1994.

https://dx.doi.org/10.1021/acs.oprd.0c00192
Org. Process Res. Dev. XXXX, XXX, XXX−XXX

Part II

Catalytic Isocyanate Trimerization

5 Introduction

Understanding of reaction mechanisms is crucial for process optimization, especially when considering industrial applications in which small improvements scale tremendously with regard to profit. Several catalytic processes applied in industry, however, are still not fully understood at the molecular level, despite the fact that they have been used for production over decades. Among other things, this may be due to the fact that the underlying mechanisms are often complex, and that the investigation of such mechanisms is costly and the knowledge gained does not necessarily lead to improvements.

The formation of isocyanurates from isocyanates dates back to the middle of the 19th century and since then has been widely used in industry. While the net reaction – the reaction of three equivalents of isocyanate followed by cyclization – seems rather simple, the reaction mechanism strongly depends on the catalyst employed and proved to be quite complex for the few examples already investigated. Interestingly, the well-studied systems in academia do not represent the systems used in industrial processes. The latter are mostly still considered to be black box chemistry, with optimization based on empiricism at the macroscopic level. Understanding the underlying mechanisms could, however, drastically improve currently used processes. By identifying limiting steps within the catalysis, the catalyst design can be efficiently adapted, and by revealing undesired catalysis pathways and side-products, their suppression or separation can be optimized, respectively.

6 State of Knowledge

Isocyanates are important chemical compounds, whether in the laboratory or on an industrial scale, and can be used in a variety of reactions. They show high reactivity due to the electrophilic carbon and the relatively nucleophilic nitrogen atom, providing optimal prerequisites for the reaction with nucleophiles carrying active hydrogen atoms. In this context, isocyanates are automatically associated with polyurethane chemistry. Polyurethanes (PUs) are extremely versatile polymers whose properties can be easily controlled and are suitable for a wide range of applications, being applied as foams, coatings, elastomers, fibers, adhesives, and sealants in the automotive, furniture, and mattress industries. Polyurethanes are produced by reacting polyisocyanates with polyols, although other nucleophiles carrying active hydrogen atoms are also partly used while still referring to polyurethane products. In general, isocyanate monomers with two isocyanate functionalities are employed. If water is present in the formulation, amines may be formed during the polymerization process due to isocyanate hydrolysis and CO_2 loss. The gas formation is important for certain applications that require foaming. Additionally, the amines formed react with isocyanates to give ureas (Figure 6.1). Since the urethane and urea bonds still contain active hydrogen atoms themselves, cross-linking reactions may take place to form allophanate and biuret groups. These reactions are often necessary for the application and allow the precise adjustment of desired properties. The high atom efficiency and yield of the reaction of an isocyanate group with nucleophiles containing active hydrogen atoms are of great benefit in industrial applications.[141]

However, isocyanates are often highly toxic and volatile, which makes special safety precautions necessary. One strategy to minimize these negative properties is the polymerization of isocyanates to polyisocyanates if the following application allows, or even favors,

[141]G. Brereton et al. in *Ullmann's Encyclopedia of Industrial Chemistry*, Wiley-VCH, **2019**.

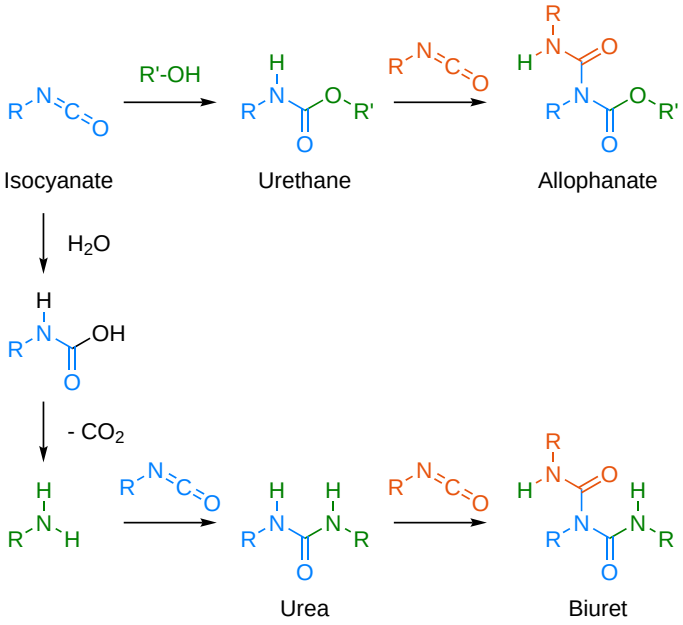

Figure 6.1: Schematic representation of the formation of urethane and allophanate groups from isocyanates and alcohols or of urea and biuret groups from isocyanates and amines. Isocyanates may hydrolyse to carbamic acids, which in turn lose CO_2 and form amines.

these polymerized structures.[142,143] The degree of polymerization as well as the product composition depends on various parameters, such as temperature and reaction time, as well as on the substrate and catalyst used. Beside the previously discussed biurets, the three most prominent polyisocyanates (Figure 6.2) are isocyanurates (symmetrical trimer), iminooxadiazinediones (asymmetrical trimer), and uretdiones (dimer).[142] [14] When using isocyanurates instead of monomeric diisocyanates, the resulting polymers show improved mechanical properties, as for instance dimensional stability and compressive strength, and generally exhibit superior fire retardancy.[141,144,145] To control the cross-linking density, low-functionality polyols are used to avoid increased brittleness.[141] The asymmetric trimer

[142] M. Widemann et al., *ACS Sustain. Chem. Eng.* **2018**, *6*, 9753–9759.

[143] H. J. Laas et al., *J. Prakt. Chem.* **1994**, *336*, 185–200.

[144] U. Meier-Westhues et al., *Polyurethanes: Coatings, Adhesives and Sealants*, 2nd ed., Vincentz Network, Hanover, **2019**.

[145] A. Goldschmidt, H.-J. Streitberger, *BASF Handbook Basics of Coating Technology*, 3rd ed., Vincentz Network, Hanover, **2018**.

[14] The widely used polymeric MDI (methylene diphenyl diisocyanate) does not refer to a polymerized form of MDI but instead describes the MDI homologues with more than one methylene bridge and consequently more than two isocyanate functionalities.

is of high interest to the industry due to its comparatively low viscosity while still providing high functionality.[144] The dimer has an even lower viscosity but also a lower functionality. Furthermore, it is not thermostable, leading to ring opening at elevated temperatures. It is mostly used as blocked isocyanate that enables heat-activated cross-linking.[141,144]

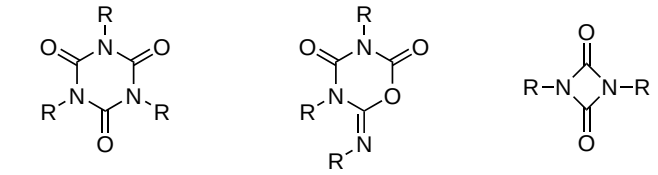

Figure 6.2: Schematic representation of the isocyanurate (symmetrical trimer), iminooxadiazinedione (asymmetrical trimer), and uretdione (dimer) structural element.

6.1 Industrial Relevance of Isocyanates for Polyurethanes

The global polyurethane consumption was about 22.8×10^6 t/a in 2017 (Figure 6.3), with ridged and flexible foams accounting for the largest part of the overall market (73 %). The remaining market shares can be attributed to coatings (8 %), microcellular materials (5 %), elastomers (4 %), fibers (4 %), thermoplastic polyurethane elastomers (TPU, 3 %), or adhesives and sealants (3 %). The global polyurethane consumption can also be related to the individual components used (Figure 6.3). For the isocyanate components (9.2×10^6 t/a), the aromatic diisocyanates methylene diphenyl diisocyanate (MDI, 6.6×10^6 t/a) and toluene diisocyanate (TDI, 2.3×10^6 t/a) cover the largest part, whereas aliphatic and specialty isocyanates (0.3×10^6 t/a) account for a relatively small proportion. For the polyols (10.0×10^6 t/a), the market share is dominated by polyether polyols (7.8×10^6 t/a) and polyester polyols (2.2×10^6 t/a). The remaining market share is represented by additives (3.7×10^6 t/a).[141]

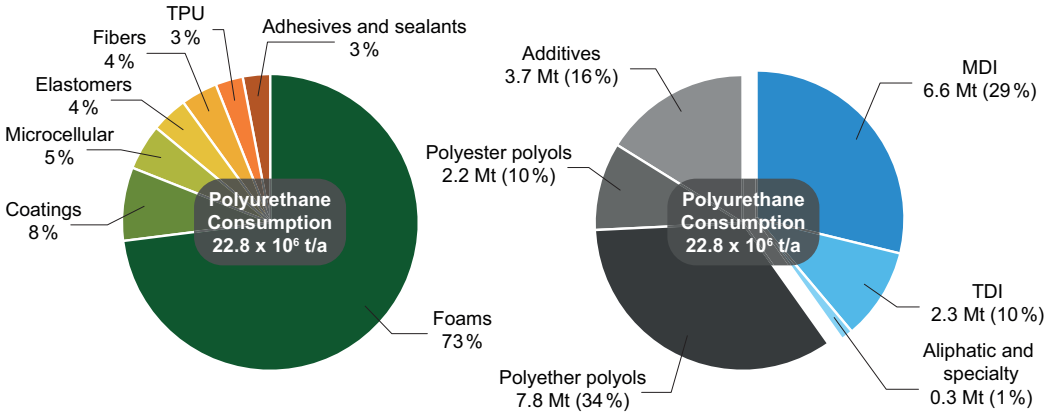

Figure 6.3: Global consumption of polyurethanes in 2017 broken down by technology type (left) and raw materials (right).

The wide range of properties of the polyurethane products are mostly determined by the polyols, especially by their chemical composition and molecular mass. Beside the mostly used polyether and polyester polyols, small quantities of polycarbonate and polycaprolactone polyols are utilized for high-performance coating, adhesive, and elastomer applications. Although isocyanates are as relevant for polyurethane formation, comparatively little innovation with regard to this application is found within the substance class. In this context, isocyanates represent commodity chemicals, and optimization efforts are mostly focused on reducing production costs. Consequently, only a small number of different isocyanates

is used for polyurethanes at all, as can be seen by the market analysis (Figure 6.3). Their production costs are relatively low, and their raw materials are readily available.[146]

Aromatic isocyanates represent the largest part of isocyanates employed for polyurethanes, and almost exclusively MDI and TDI are being used (Figure 6.4). Aromatic isocyanates result in polyurethanes with better mechanical properties, and they are primarily used for foams but also coatings, elastomers, and adhesives. Aliphatic isocyanates account for only a very small proportion, with hexamethylene diisocyanate (HDI) and isophorone diisocyanate (IPDI) being the most relevant representatives (Figure 6.4). These isocyanates yield polyurethanes that are resistant to weathering, *i.e.* they show no undesirable coloration when exposed to heat or light. As a result, the resulting polyurethanes are primarily intended for outdoor applications or as coating materials.[141,146] In case of coating materials, utilization of trimerized aliphatic isocyanates (isocyanurates) as cross-linkers in polyurethane formation increases the coating properties, yielding coatings with outstanding chemical and mechanical resistance.[144,145]

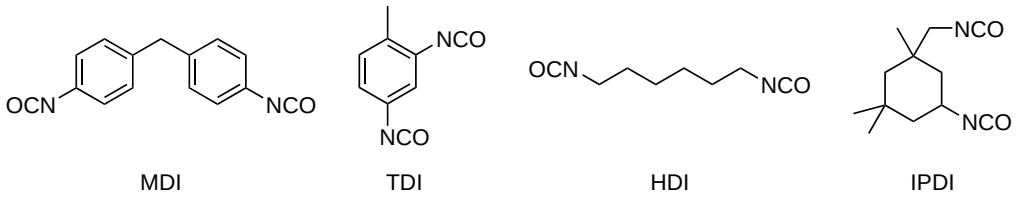

Figure 6.4: Chemical structures of MDI, TDI, HDI, and IPDI.

[146]M. F. Sonnenschein, *Polyurethanes: Science, Technology, Markets, and Trends*, John Wiley & Sons, Hoboken, **2014**.

6.2 Catalytic Studies on the Trimerization of Isocyanates

For the trimerization of isocyanates to isocyanurates, a wide range of catalysts – including organometallic compounds, metal complexes, salts, or neutral Lewis bases – have been employed so far.[15] The generally proposed mechanism differs depending on the catalyst used. For organometallic compounds[199–202] and metal complexes,[203,204] some mechanistic studies were published that mostly describe the characterization of intermediates, and only few of these cover an extended mechanistic investigation. In case of the widely employed nucleophilic bases, the proposed reaction mechanism consists of the successive addition of three equivalents of isocyanate to the catalyst to give linear intermediates, followed by a back-biting reaction and cleavage of the catalyst while generating the cyclic isocyanurate (Figure 6.5).[141,205] However, the catalysis does not always adhere to this pattern, and in some cases unprecedented catalysis pathways are followed, or unexpected catalyst migration or activation takes place.

Some examples of mechanistic studies on nucleophilic bases published in literature shall be discussed in the following to shed light on the undoubtedly large differences between the investigated systems and thus motivate the investigation of industrially used, but so far only little explored systems. The given examples used monoisocyanates in order to avoid higher polymerization products that would further complicate clarification of the underlying mechanisms.

One of the first examples that showed high efficiency in the catalytic trimerization of isocyanates employed proazaphosphatrane catalysts (Figure 6.6A). These catalysts showed high activity in the formation of isocyanurates starting from aromatic isocyanates.[206–208]

[199] W. Yi et al., *Organometallics* **2011**, *30*, 5809–5814.
[200] L. Orzechowski, S. Harder, *Organometallics* **2007**, *26*, 2144–2148.
[201] O. Blacque et al., *J. Organomet. Chem.* **2001**, *634*, 47–54.
[202] L. Mao et al., *Organometallics* **1997**, *16*, 3711–3714.
[203] S. G. Lee et al., *Dalton Trans.* **2015**, *44*, 6537–6545.
[204] F. Paul et al., *J. Am. Chem. Soc.* **2007**, *129*, 7294–7304.
[205] H. E. Reymore et al., *J. Cell. Plast.* **1975**, *11*, 328–344.
[206] S. M. Raders, J. G. Verkade, *J. Org. Chem.* **2010**, *75*, 5308–5311.
[207] J. Tang et al., *J. Org. Chem.* **1994**, *59*, 4931–4938.
[208] J.-S. Tang, J. G. Verkade, *Angew. Chem. Int. Ed.* **1993**, *32*, 896–898.

[15] Examples of catalytic systems for the cyclotrimerization of monoisocyanates based on organometallic compounds,[147–159] metal complexes,[160–172] salts,[173–179] neutral Lewis and Brønsted bases[180–186] or acids,[187] anion radicals,[188,189] or combinations of these[190–198] can be found in literature.

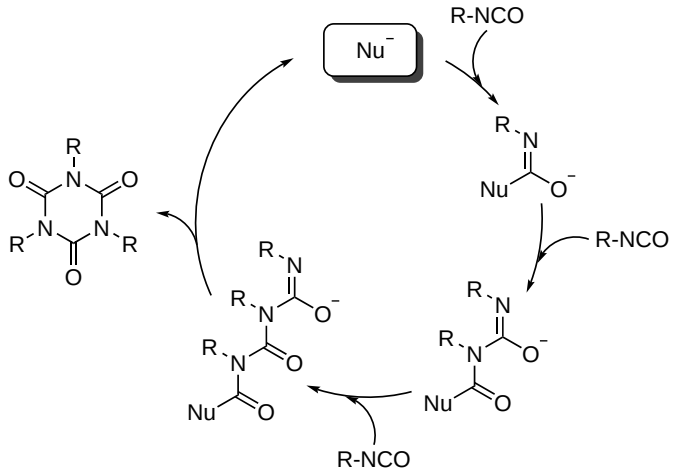

Figure 6.5: General catalysis mechanism for the trimerization of isocyanates to isocyanurates catalyzed by nucleophilic bases. After successive addition of three equivalents of isocyanate, the isocyanurate is formed and the catalyst is released. The catalyst is framed.

The high activity in this catalysis is attributed to the high basicity of the catalyst at the phosphorus atom,[209,210] which can be attributed to the donation of electron density from the neighboring nitrogen atoms and the transannulation of the basal nitrogen to the phosphorus upon protonation.[211–213] For the catalysis, the mechanism stated above was postulated, supported by NMR spectroscopic as well as mass spectrometric results, indicating the formation of the zwitter-ionic mono-adduct.[207,208] A computational study on the catalytic system using methyl isocyanate also predicted the sequential addition of isocyanate and formation of only zwitter-ionic, acyclic intermediates. In these computations, significant transannulation was found for all intermediates, and its presence was correlated to the high basicity and the therefrom resulting potency of the catalyst.[214]

When tri-*n*-butylphosphine was used as catalyst for the trimerization of aliphatic isocyanates, an analogous zwitter-ionic di-adduct intermediate was initially proposed based on NMR experiments, indicating a similar mechanism as in the case of the proazaphosphatrane catalysts (Figure 6.6B, top).[215] However, following NMR spectroscopic experiments

[209]P. B. Kisanga et al., *J. Org. Chem.* **2000**, *65*, 5431–5432.
[210]J. Tang et al., *J. Am. Chem. Soc.* **1993**, *115*, 5015–5020.
[211]J. G. Verkade, P. B. Kisanga, *Tetrahedron* **2003**, *59*, 7819–7858.
[212]J. G. Verkade, *Coord. Chem. Rev.* **1994**, *137*, 233–295.
[213]J. G. Verkade, *Acc. Chem. Res.* **1993**, *26*, 483–489.
[214]J. N. Gibb, J. M. Goodman, *Org. Biomol. Chem.* **2013**, *11*, 90–97.
[215]Z. Pusztai et al., *Angew. Chem. Int. Ed.* **2006**, *45*, 107–110.

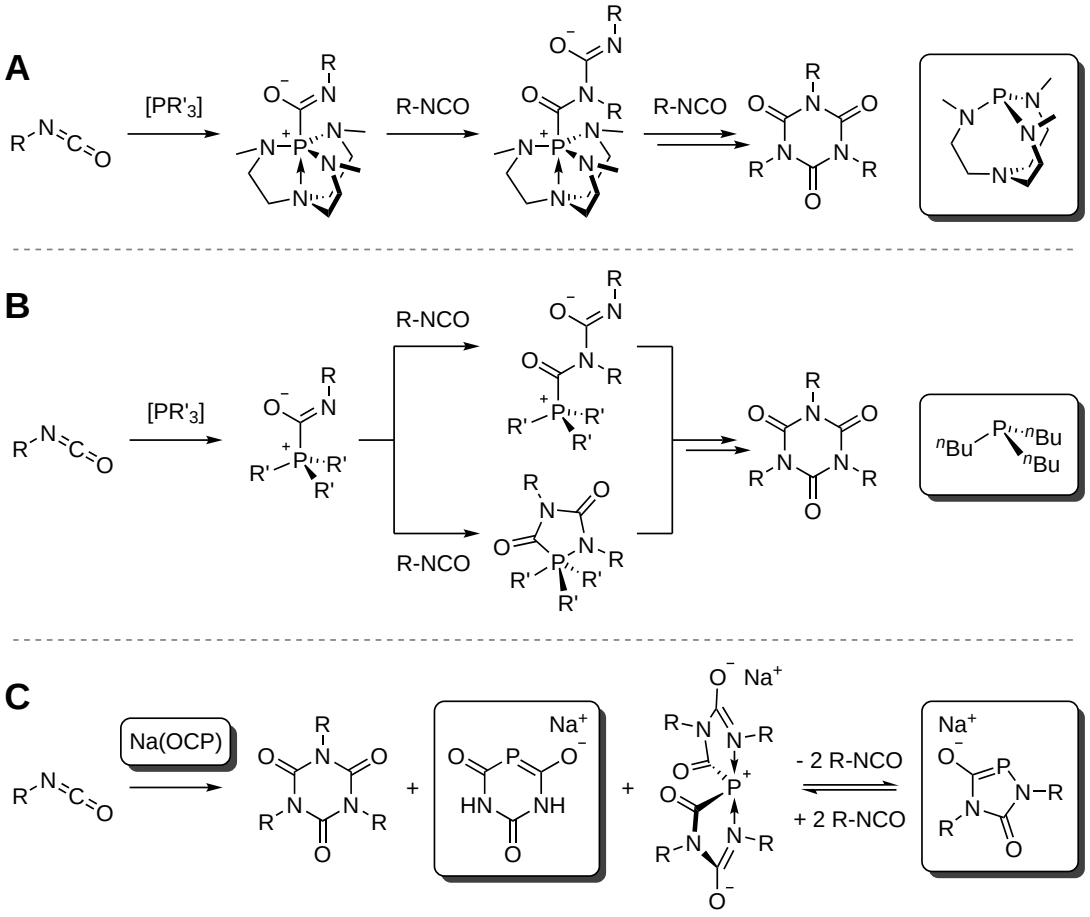

Figure 6.6: Catalytic systems using phosphorus-based catalysts for the trimerization of isocyanates to isocyanurates. The catalysts are framed. **A**: Catalytic system using a proazaphosphatrane for the cyclotrimerization of aromatic isocyanates leading to zwitter-ionic, acyclic intermediates. **B**: Catalytic system using tri-*n*-butylphosphine for the cyclotrimerization of aliphatic isocyanates with only zwitter-ionic, acyclic intermediates proposed (top) or for which a cyclic intermediate is proposed (bottom). **C**: Formation of catalytically active five- and six-membered heterocycles starting from the 2-phosphaethynolate anion and aliphatic as well as aromatic isocyanates.

combined with a computational study revealed different results. Several cyclic pentacoordinated phosphorous intermediates were proposed, and the spectroscopic data of the intermediate previously declared as zwitter-ionic were assigned to a cyclic intermediate with a phosphorus-nitrogen bond (Figure 6.6B, bottom).[216]

For another nucleophilic phosphorous compound, the 2-phosphaethynolate anion, the catalytic trimerization of aromatic isocyanates was stated to proceed via five- or six-membered heterocycles that represent the actual catalysts as it was shown by experimental

[216]J. Helberg et al., *Chem. Eur. J.* **2018**, *24*, 14387–14391.

and computational studies (Figure 6.6C). In addition to the 2-phosphaethynolate anion itself, both these types of heterocycles successively add three equivalents of isocyanate via nucleophilic attacks before isocyanurate is released after cyclization.[217]

In 2018, thorough mechanistic experiments were performed on a catalytic system consisting of an acetate catalyst and an alcohol for the cyclotrimerization of aromatic isocyanates, thereby approaching industrially used systems (Figure 6.7). The latter mostly consist of complex carboxylate catalysts together with functionalized counter-anions and use additives such as alcohols. As acetate was found to be too reactive for the study, trifluoroacetate was used as catalyst. The formation of intermediates was monitored using NMR spectroscopy both in the presence or absence of the alcohol. Without adding an alcohol, the catalysis is proposed to proceed via the generally assumed mechanism (Figure 6.7 black cycle). In the presence of diethyleneglycol monomethyl ether, however, the catalysis proceeds preferentially through the formation of the isocyanate-alcohol carbamate and successive formation of allophanate, which reacts readily with the catalyst-isocyanate mono-adduct species to finally give the isocyanurate product (Figure 6.7 green cycles).[218] Previous kinetic studies on complex systems consisting of carboxylate catalysts and alcohol co-catalysts demonstrated that the alcohol leads to an significant increase in reactivity.[219–221]

These mechanistic findings demonstrate that no general mechanism applies to the different catalytic systems employed for this catalysis and that each system has to be studied individually. But beside these mechanistic investigations on intermediates, pre-catalyst activation might even increase the complexity of the system. It has been shown or proposed for several catalysts, that the mono-adduct is the actual catalyst for the trimerization reaction. This, however, is not considered to be of equal relevance in terms of pre-catalyst activation as in the case discussed in the following. An example of such an activation is known for hexamethyldisilazane (HMDS) in the catalyzed trimerization of aliphatic isocyanates (Figure 6.8). When HMDS is used, a silylated alkyl amine is formed by addition of an equivalent of alkyl isocyanate to HMDS, migration of one trimethylsilyl (TMS) group within the formed

[217]D. Heift et al., *Chem. Sci.* **2015**, *6*, 4017–4024.
[218]A. Al Nabulsi et al., *Polym. Chem.* **2018**, *9*, 4891–4899.
[219]K. Schwetlick, R. Noack, *J. Chem. Soc., Perkin Trans. 2* **1995**, 395–402.
[220]M. Špírková et al., *J. Appl. Polym. Sci.* **1994**, *53*, 1435–1446.
[221]I. S. Bechara, R. L. Mascioli, *J. Cell. Plast.* **1979**, *15*, 321–332.

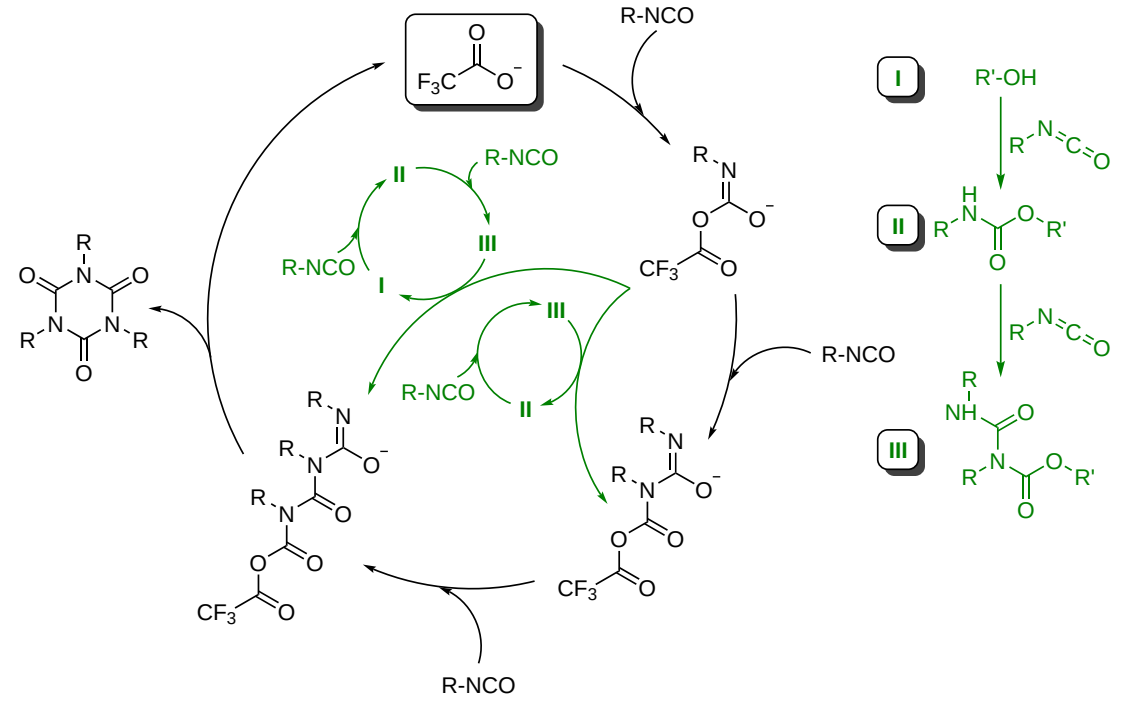

Figure 6.7: Catalytic system based on potassium trifluoroacetate and diethyleneglycol monomethyl ether for the catalytic trimerization of aromatic isocyanates. The successive reaction of the alcohol (I) with isocyanate provides the respective carbamate (II) and then the allophanate (III), which readily reacts with the nucleophilic mono-adduct intermediate in the overall trimerization reaction. The catalyst is framed.

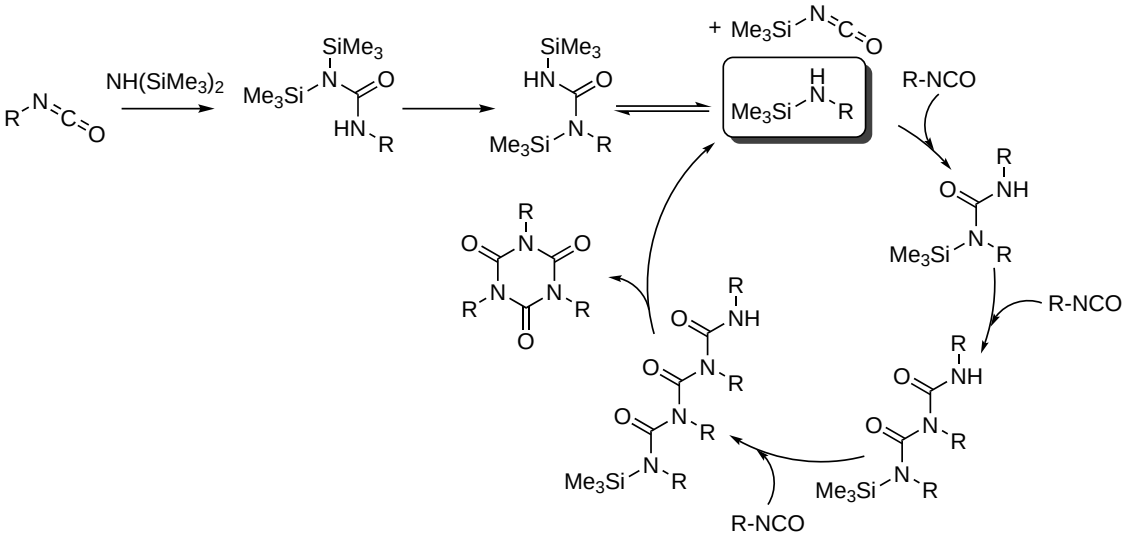

Figure 6.8: Catalytic system based on hexamethyldisilazane (HMDS) for the catalytic trimerization of aliphatic isocyanates. Pre-catalyst activation of HMDS via isocyanate addition and elimination of TMS isocyanate after an intramolecular rearrangement leads to the silylated alkyl amine, representing the actual catalyst for the trimerization. The catalyst is framed.

urea derivative, and elimination of TMS isocyanate. The silylated alkyl amine represents the actual catalyst for the catalytic trimerization.[222]

These results indicate that the catalytic systems need to be studied in great detail. Especially since the resulting isocyanurates must meet extremely high quality standards, and already few impurities can have a major impact on product performance.

[222]M. Roman et al., *Tetrahedron* **2011**, *67*, 1506–1510.

7 Objectives

The trimerization of isocyanates to isocyanurates is of high industrial importance. The few mechanistic studies published so far are not fully representative for the catalytic systems employed in industry, and a better understanding of these is highly needed. Investigating the catalysis on the molecular level could enable process optimization due to the identification of undesired catalysis pathways and side-products or by improved catalyst design adapted to the catalysis mechanism. Industrial systems consist of rather complex carboxylate catalysts together with functionalized counter-anions as well as additives such as alcohols. Initial mechanistic investigations, however, can start at reference systems of reduced complexity and still make important contributions to the overall understanding.

The objective of this part of the dissertation is the investigation into the trimerization reaction of aliphatic isocyanates to isocyanurates using a carboxylate catalyst. To achieve adequate complexity, hexyl isocyanate shall be used instead of diisocyanates together with tetrabutylammonium acetate as catalyst and toluene as non-nucleophilic solvent. Starting from a first mechanistic evaluation based on quantum chemical computations (BASF), the actual catalytic mechanism shall be experimentally determined using several analytic techniques, including NMR spectroscopy and Orbitrap mass spectrometry.

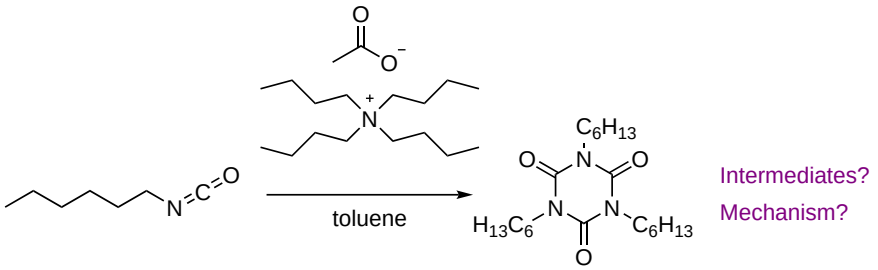

Figure 7.1: Model system for the carboxylate-catalyzed trimerization of aliphatic isocyanates, consisting of hexyl isocyanate and tetrabutylammonium acetate. The mechanism for the product formation shall be investigated, and intermediates shall be identified (purple).

8 Published Work

8.1 Mechanistic Investigation into the Acetate-Initiated Catalytic Trimerization of Aliphatic Isocyanates: A Bicyclic Ride

Max Siebert, Rebecca Sure, Peter Deglmann, Anna C. Closs, Frederic Lucas, and Oliver Trapp

Prologue

The mechanism of the acetate-initiated catalytic trimerization of aliphatic isocyanates to isocyanurates was investigated by experimental and computational methods. Because this model system is of great industrial relevance, a microscopic understanding was highly needed. An unexpected complexity of the system was revealed, in which acetate only acts as pre-catalyst, initiating catalysis with a deprotonated amide. From this cycle, a further catalyst migration takes place to result in the final deprotonated urea catalysis.

Author Contributions

M. S. and A. C. C. designed and performed the experiments. R. S. and P. D. performed the quantum chemical computations. All authors contributed to the interpretation of the data. The manuscript was co-written by M. S., A. C. C., R. S., and F. L., and all authors contributed to the manuscript. F. L. and O. T. supervised the project.

License

Supporting Information

The supporting information is available at https://doi.org/10.1021/acs.joc.0c00944.

JOC The Journal of Organic Chemistry

pubs.acs.org/joc Article

Mechanistic Investigation into the Acetate-Initiated Catalytic Trimerization of Aliphatic Isocyanates: A Bicyclic Ride

Max Siebert, Rebecca Sure, Peter Deglmann, Anna C. Closs, Frederic Lucas,* and Oliver Trapp*

Cite This: https://dx.doi.org/10.1021/acs.joc.0c00944 Read Online

ACCESS | Metrics & More | Article Recommendations | Supporting Information

ABSTRACT: The acetate-initiated aliphatic isocyanate trimerization to isocyanurate was investigated by state-of-the-art analytical and computational methods. Although the common cyclotrimerization mechanism assumes the consecutive addition of three equivalents of isocyanate to acetate prior to product formation, we found that the underlying mechanism is more complex. In this work, we demonstrate that the product, in fact, is formed via the connection of two unexpected catalytic cycles, with acetate being only the precatalyst. The initial discovery of a precatalyst activation by quantum chemical computations and the resulting first catalysis cycle were corroborated by mass spectrometric and NMR experiments, thereby additionally revealing a catalyst migration to the second catalytic cycle. These results were further confirmed by computations, completing the full mechanistic understanding of this catalytic system. Identification of a side product with undesired properties for final coating applications allows for process optimization in the chemical industry.

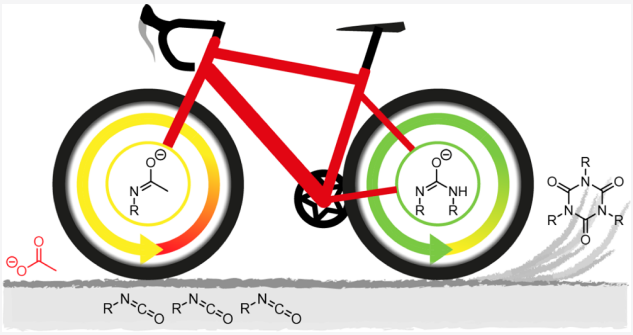

INTRODUCTION

Isocyanurates—formed via the cyclotrimerization of isocyanates—have been widely used in important industrial applications since their first report in 1858.[1−3] Whereas aromatic diisocyanates are often polymerized into polyisocyanurate (PIR) foams with excellent mechanical and insulating properties,[4−6] the controlled trimerization of aliphatic diisocyanates leads to isocyanurate cross-linkers for high-performance polyurethane coatings.[7,8] When considering monomers such as hexamethylene diisocyanate (HDI) or isophorone diisocyanate, the higher molecular weight and functionality of the corresponding aliphatic isocyanurate is advantageous both in terms of health hazard (lower vapor pressure) and coating properties (high cross-linking density). The stable isocyanurate ring coupled with aliphatic hardeners is ideal for the creation of UV-resistant coatings with outstanding chemical and mechanical resistances.[8,9]

In the commonly assumed cyclotrimerization mechanism, a catalyst reacts consecutively with three equivalents of isocyanate via nucleophilic attacks at the electrophilic carbon of the isocyanate. A final back-biting reaction takes place, which leads to the formation of isocyanurate and the regeneration of the catalyst.[10,11] The catalysis, however, does not always follow this generally accepted mechanism and highly depends on the applied catalyst, additives, and solvent. Although alcohols are well known to increase the reactivity via a resulting urethane cocatalyst,[12−14] recent work showed that the formation of aromatic isocyanurates could occur via an allophanate intermediate.[15] When hexamethyldisilazane is used as a catalyst, the catalytic cycle is governed by an intermediate species (silylated amine) generated after the reaction of the silazane with an alkyl isocyanate and the following elimination of trimethylsilyl isocyanate.[16] Furthermore, it was demonstrated that the cyclotrimerization using phosphane could proceed either via zwitterionic[17−20] or cyclic[21] intermediates.

Although in the academic literature a wide variety of organometallic compounds,[22−28] bases,[29−34] and even anion radicals[35] are used as catalysts, patents mostly claim the production of HDI-based isocyanurate cross-linkers via the use of carboxylate catalysts.[36−40] The latter are industrially favored because of their easy synthesis and handling as well as the low color obtained for the products, which is of utmost importance for clear-coat applications. A mechanistic investigation of the cyclotrimerization of aliphatic isocyanates using carboxylate catalysts is not reported yet, which is surprising, as this could enable a better control of the reaction in terms of reactivity and selectivity (uretdione, carbodiimide, or iminooxadiazinedione are well-known side-products[41]). Motivated by the promising benefits as well as the scale of application, we performed quantum chemical calculations on the bulk cyclization of an

Received: April 16, 2020
Published: June 8, 2020

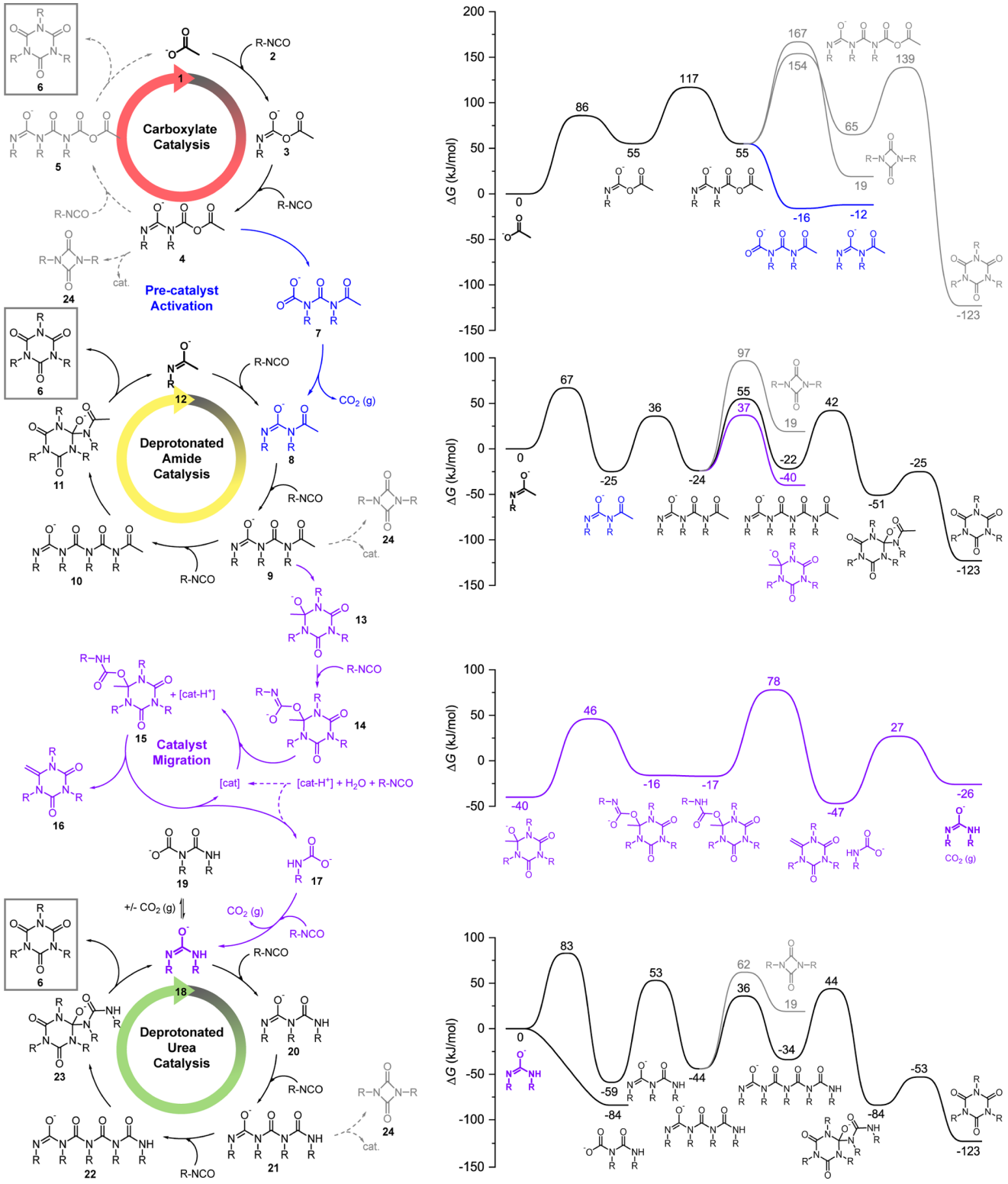

Figure 1. Overview of the different catalytic cycles of the acetate-initiated isocyanate trimerization and their connections as well as the computed activation free energies ($\Delta G^{\ddagger}$) for all TSs and reaction free energies (ΔG) for all intermediates. When calculating energy differences with the rounded values given in the text, there may be deviations from the values shown in the figure by 1 kJ/mol, as the exact values were taken for the latter. The results refer to 80 °C in hexyl isocyanate as reaction conditions and were obtained at the B3LYP-D3/def2-QZVP+COSMO-RS level. All values are given in kJ/mol. *R* is propyl in the computations (note that in the experiments, hexyl isocyanate was used). The color coding (red, yellow, green) refers to the amount of isocyanurate **6** that is formed within the respective catalytic cycle (red = none, yellow = some, green = most).

aliphatic isocyanate using acetate as a catalyst and supported the results with state-of-the-art analytical methods. By combining both approaches, we comprehensively investigated the mechanism that revealed unexpected complexity.

https://dx.doi.org/10.1021/acs.joc.0c00944
J. Org. Chem. XXXX, XXX, XXX−XXX

RESULTS AND DISCUSSION

To gain a first insight into the mechanism of the acetate-catalyzed aliphatic isocyanate trimerization in bulk, a quantum chemical study on the density functional theory (DFT) level with a quadruple-zeta (QZ) basis set (B3LYP[42−45]-D3[46−48]/def2-QZVP[49]+COSMO-RS[50−53]) was carried out (see the Experimental Section). The mechanistic picture with all computed activation and reaction free energies is shown in Figure 1. In the experiments, we used hexyl isocyanate instead of HDI to avoid cross-linking and polymerization to higher oligomers within the analytical tools and tetrabutylammonium acetate as the catalyst (Scheme 1). For the computations, the

Scheme 1. Model Reaction for the Catalyzed Trimerization of Isocyanate to Isocyanurate

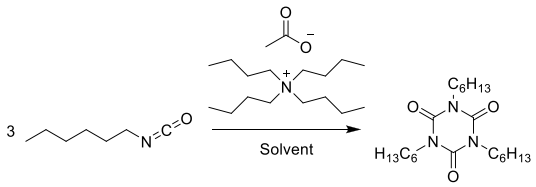

isocyanate was modeled as propyl isocyanate to reduce the system size and save computational time. This is not expected to affect the reactivity of the NCO groups and the occurring intermediate species. So far, the common view of the acetate-catalyzed nucleophilic mechanism was quite simple and limited to the first catalytic cycle shown (Figure 1, red cycle): The acetate catalyst **1** successively undergoes the addition of three isocyanate molecules **2**, the system cyclizes, isocyanurate **6** is formed, and the catalyst **1** is regenerated. However, our DFT computations indicated that the catalysis does not run through this cycle and that acetate is not the actual catalyst for the experimentally observed formation of isocyanurate **6**.

Computational Studies: From Carboxylate to Deprotonated Amide Catalysis. The first addition of isocyanate **2** to the acetate **1** is endergonic because of the loss of delocalization of the negative charge with a reaction free energy (ΔG) of 55 kJ/mol and has an activation free energy ($\Delta G^{\ddagger}$) of 86 kJ/mol. On the first glance, this seems counter-intuitive because the system size increases. The resulting structure, however, is not planar, and the delocalization between two equivalent oxygens in acetate **1** is stronger than that between oxygen and nitrogen in acetylcarbamate **3**. The second addition of isocyanate **2** has a slightly lower free energy of activation (61 kJ/mol) and is thermoneutral ($\Delta G \approx 0$ kJ/mol). Nevertheless, as the first step is endergonic, the relative activation free energy for the second step compared to the starting point is 117 kJ/mol. For a fast catalysis at 80 °C, however, the activation free energy of the rate-limiting step should not exceed 100 kJ/mol. In general, the activation free energies of the addition steps are quite sensitive to the molecular conformation and easily differ by ±10 kJ/mol depending on the conformer used. Further, the choice of the DFT functional has a small influence. B3LYP-D3/def2-QZVP and M06-2X[54]/def2-QZVP usually agree within 5 kJ/mol for the activation free energies and 15 kJ/mol for the reaction free energies (Table S2). Within this error of 10−15 kJ/mol, the second addition step is reasonable for a rapid catalysis at 80 °C.

The third isocyanate addition would have a high activation free energy (100 kJ/mol), but this reaction step will not take place. Instead, the acetylallophanate **4** rearranges and a subsequent decarboxylation occurs (Figure 1, blue pathway). Both reaction steps are barrierless. The rearrangement is exergonic by −70 kJ/mol, and the decarboxylation is thermoneutral. The resulting acetylureate **8** can also be envisioned as a result of the addition of isocyanate **2** to a deprotonated acetamide **12**, thereby representing an intermediate within a new catalytic cycle—the deprotonated amide cycle (Figure 1, yellow cycle). Therefore, the first two isocyanate additions and the subsequent loss of carbon dioxide can be considered as precatalyst activation of acetate **1**, revealing the deprotonated acetamide **12** as the actual catalyst.

Within the deprotonated amide cycle, the activation free energies of the first two isocyanate additions are similar and around 65 kJ/mol. The third one has a higher $\Delta G^{\ddagger}$ of 79 kJ/mol. The first addition is exergonic (ΔG = −25 kJ/mol) because of a higher delocalization of the negative charge in acetylureate **8** compared to the deprotonated acetamide **12**, whereas the second and third additions are thermoneutral. The following cyclization step to form an isocyanurate-catalyst adduct **11** has a $\Delta G^{\ddagger}$ of 64 kJ/mol and is exergonic by −28 kJ/mol. In the final step, the catalyst is regenerated via dissociation and isocyanurate **6** is formed. This step has only a small free energy of activation (26 kJ/mol) and is exergonic by −72 kJ/mol. Already at this point, the calculations revealed new catalytic pathways and a necessary extension of the existing mechanism.

Experimental Studies: From Carboxylate to Deprotonated Urea Catalysis. In order to confirm the results of the calculations indicating a transition to the deprotonated amide cycle, we initially focused our experiments on the detection of carbon dioxide upon precatalyst activation. In a completely inert trimerization reaction in anhydrous dimethyl sulfoxide (DMSO) using 55 and 14 mmol of isocyanate **2** and acetate catalyst **1**, respectively, an intensive gas formation was observed directly after isocyanate addition to the catalyst solution at 80 °C. The gas formed was passed through baryta water, and after the reaction was completed, argon was flushed through the entire system to transfer the remaining gas atmosphere to the wash bottles. The formation of a colorless suspension indicated that carbon dioxide was formed during the catalysis (Figures S1−S4). Nearly one equivalent of barium carbonate with regard to the precatalyst ammonium acetate was obtained, thereby strongly indicating a precatalyst activation including the release of carbon dioxide.

Next, we aimed to identify key intermediates of the deprotonated amide cycle by using high-resolution mass spectrometry (MS). Orbitrap-MS seemed to be the perfect tool for analyzing the catalysis mixtures, as the samples can directly be injected into the ion source without the need for further purification or derivatization. For this purpose, we performed the catalysis at 80 °C in anhydrous and degassed toluene and took samples after certain periods. ESI mass spectra of samples measured after 15 min provided strong evidence for the deprotonated amide cycle as the deprotonated amide **12** (142.1223 m/z) as well as both its mono- and di-isocyanate adducts **8** and **9** (269.2231 and 396.3227 m/z) were observed as characteristic peaks in the negative mode (Figure S62). However, the dominant presence of ureate **18** (227.2122 m/z) and its mono-isocyanate adduct **20** (354.3123 m/z) was not in accordance with our expectations and allowed

https://dx.doi.org/10.1021/acs.joc.0c00944
J. Org. Chem. XXXX, XXX, XXX−XXX

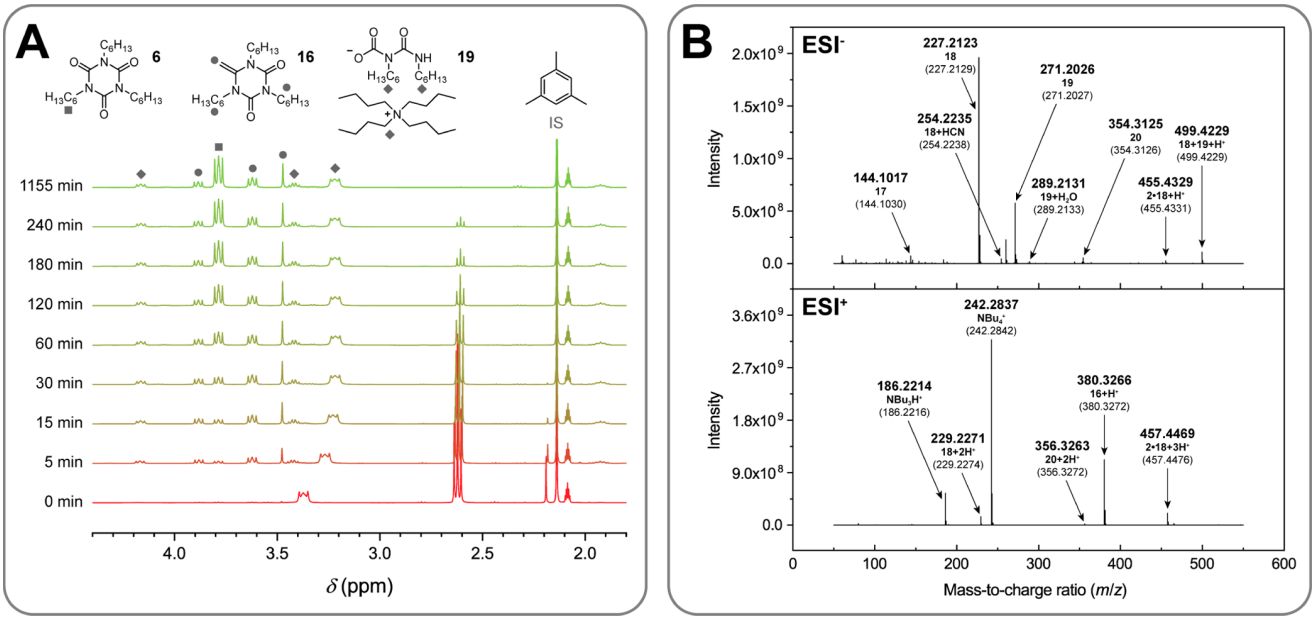

Figure 2. Analysis of the acetate-initiated catalytic trimerization of hexyl isocyanate. (A) Reaction monitoring by ^{1}H NMR spectroscopy in a J. Young NMR tube. The gray shapes are used to assign the signals to the corresponding structures (square: isocyanurate **6**; dots: cyclic olefin **16**; rotated square: amidocarbamate **19**). Mesitylene was used as the internal standard (IS) for quantification. (B) Orbitrap-MS analysis of a reaction mixture after 1155 min without an internal standard in negative (top) and positive (bottom) mode. The bold numbers refer to the experimentally observed masses, whereas the numbers in brackets give the exactly calculated masses.

three potential conclusions: (1) The intermediates of the deprotonated amide cycle are unstable under the conditions of MS analysis and decompose to give ureate fragments in mass spectra. (2) The intermediates of the deprotonated amide cycle can degrade over the course of catalysis by which ureate species are formed. (3) Water is present during the catalysis, leading to carbamic acid formation from isocyanate, which readily loses carbon dioxide and forms ureate species upon loss of a proton and addition of a second equivalent of isocyanate.

In order to rule out certain scenarios, NMR spectroscopy was chosen as additional experimental tool to identify intermediates by characteristic signals. For this purpose, we performed the catalysis at 80 °C in J. Young NMR tubes in a closed atmosphere under inert conditions using anhydrous and degassed toluene-d_8 as the solvent and mesitylene as the internal standard. The catalysis was monitored by ^{1}H and ^{13}C NMR spectroscopy after cooling the J. Young NMR tube to 0 °C at defined reaction times in order to stop the catalysis (Figure 2A). Over time, three different dominant species formed, of which only one had NBu_4^+ as the countercation, as determined by DOSY experiments (Figure S57). The most intense signal in the final ^{1}H NMR spectrum refers to the desired product isocyanurate **6**. Surprisingly, the intensity decrease of the singlet signal of the acetate **1** methyl group at 2.19 ppm did not match with the increase of the only arising singlet at 3.47 ppm. This would have been necessary for any intermediate of the deprotonated amide cycle, as all structures possess a characteristic methyl group. However, the intensity of the initial singlet to the final one was in a ratio of 3:2. Further, multiplicity edited HSQC (HSQC-ME) experiments showed that the new singlet signal refers to a CH_2 group, and with the help of carbon-coupled HSQC-ME experiments, the $^{1}J_{C-H}$ coupling was determined to be approximately 160 Hz, indicating an olefinic character (Figure S59). This was in agreement with the downfield shifts for the ^{1}H and ^{13}C NMR signals at 3.47 and 69.0 ppm, respectively. Its symmetric molecular structure derived from the intensity ratio of 2:4:2 for the signals at 3.47, 3.62, and 3.89 ppm, together with a similar diffusion coefficient as the symmetrical trimer and 2D NMR experiments, concluded that the cyclic olefinic structure **16** is formed. Already after 60 min, this species reached its final concentration under complete consumption of the acetate **1** (Figure 2A).

At this point, we explained the formation of olefin **16** to be as follows: In addition to further running through the catalytic cycle, the deprotonated amide di-isocyanate adduct **9** can undergo cyclization. The thus-formed alkoxide **13** is protonated, most likely by a catalytic amount of protons from ppm traces of water, potentially followed by elimination of water, leading to the olefinic product **16**. The thermodynamic driving force for this reaction could be the formation of water that—under these conditions—should react with isocyanate to carbamate **17**, thereby regenerating the proton and closing the catalytic protonation cycle. Then, carbamate **17** could form the ureate **18** under elimination of carbon dioxide and addition of a second equivalent of isocyanate **2**.

Even though the remaining signals between 3.0 and 4.4 ppm in the ^{1}H NMR spectra do not refer to ureate **18**, they can be assigned to amidocarbamate **19**, which is formed by the reversible addition of carbon dioxide to ureate **18** in an equilibrium reaction (see the Supporting Information for 2D NMR experiments necessary for the assignment). Amidocarbamate **19** is the only remaining negatively charged species with NBu_4^+ as countercation, which can potentially act as a catalyst (Figure S57). Considering the nucleophilicity of ureate **18** compared to amidocarbamate **19**, however, only the former acts as a catalyst for the trimerization reaction, while the latter gives stabilization as the resting state. Thus, the negatively charged amidocarbamate **19** loses CO_2, and the resulting ureate **18** forms isocyanurate **6** by consecutive addition of

https://dx.doi.org/10.1021/acs.joc.0c00944
J. Org. Chem. XXXX, XXX, XXX−XXX

three equivalents of isocyanate **2**, followed by cyclization, and elimination of the product. Ureate **18** is released again and immediately stabilized as the amidocarbamate **19** by the addition of CO_2 (Figure 1, green cycle).

Overall, one equivalent of olefin **16** is formed per equivalent of precatalyst **1**, thereby enabling the formation of one equivalent of ureate **18**. By this, five equivalents of isocyanate **2** are consumed in total, which equals already 50% of isocyanate **2** in case of the 10 mol % catalyst used. The remaining 50% of isocyanate **2** are converted to isocyanurate **6**. This derived ratio and the resulting overall mass balance is confirmed by quantification in the ^{1}H NMR spectrum of our final catalysis mixture (Table S1).

In a further NMR experiment, the catalysis was performed in a standard NMR tube, which was opened during heating to 80 °C, allowing carbon dioxide to gas out of the catalytic system during precatalyst activation and ureate **18** formation. Interestingly, the amidocarbamate **19** is still formed as dominant resting state at the beginning, but over the course of catalysis as isocyanate is consumed, the respective ureate species **18** becomes visible in the NMR spectra. After complete conversion, amidocarbamate **19** is nearly depleted, yielding ureate **18** as the only prominent catalytic species (Figures S53−S56).

Additionally, the first NMR experiment in a closed atmosphere was repeated without an internal standard, demonstrating that mesitylene had no influence on the catalysis (Figures S49−S52). Analysis of the catalysis solution after complete conversion by Orbitrap-MS further confirmed that only the catalytic species of the deprotonated urea cycle (Figure 1, green cycle) are present (Figure 2B). In the negative ESI mode, most dominantly ureate **18** (227.2123 m/z) and amidocarbamate **19** (271.2026 m/z) were present, as well as the ureate-mono-isocyanate adduct **20** (354.3125 m/z) and hexylcarbamate **17** (144.1017 m/z) to a smaller extent. All remaining peaks can also be identified as adduct species of the catalytic cycle, which are formed during mass spectrometric analysis (**18** + **HCN**, **2**·**18** + H^+, **19** + H_2O and **18** + **19** + H^+). In positive mode, the countercation NBu_4^+ (242.2837 m/z) and the cyclic olefinic structure **16** (380.3266 m/z) gave the most intense signals, whereas the positive counterpart of ureate (**18** + $2H^+$, 229.2271 m/z) and the ureate-mono-isocyanate adduct (**20** + $2H^+$, 356.3263 m/z) are present to a low extent. Again, a dimeric adduct formed in the Orbitrap-MS was observed for the ureate (**2**·**18** + $3H^+$). Interestingly, the detection of $NHBu_3^+$ (186.2214 m/z) indicates that at 80 °C, catalyst decomposition takes place, most likely via nucleophilic attack at a butyl group and formation of NBu_3 and the deactivated butylated nucleophile. In conclusion, all dominant signals in the mass spectra were assigned to species of the deprotonated urea cycle indicating the high plausibility of the proposed reaction mechanism.

Computational Studies: Deprotonated Urea Catalysis. For full validation of the experimentally derived catalyst migration to the deprotonated urea cycle (Figure 1, purple and green cycles), we performed further DFT calculations and determined activation and reaction free energies for all relevant steps and intermediates, respectively. This catalyst migration consists of the transformation of the deprotonated amide di-isocyanate adduct **9** to olefin **16** and the formation of carbamate **17** and its subsequent reaction with isocyanate **2** to ureate **18**.

The catalyst migration (Figure 1, purple cycle) starts with the cyclization of the deprotonated amide di-isocyanate adduct **9** to alkoxide **13**, which competes with another addition of isocyanate **2** to form the tri-isocyanate adduct **10**. The former pathway has a slightly lower activation free energy of 62 kJ/mol, compared to 79 kJ/mol for the isocyanate addition. However, the irreversible elimination reaction that concludes the catalyst migration requires a high activation free energy of 118 kJ/mol with respect to alkoxide **13** (see below). Ring opening of alkoxide **13** back to **9** and addition of isocyanate **2** is a competing alternative, as the total activation free energy is only 95 kJ/mol with respect to alkoxide **13**. This is consistent with experimental evidence that both the deprotonated amide and deprotonated urea cycle contribute to the product formation.

Several of the following transformations involve deprotonation and protonation, which is enabled by proton-transfer catalysis. To identify a suitable acid/base catalyst pair, the pK_a values for the conjugated acids of the occurring anionic species in hexyl isocyanate were computed (Table S3). Within the deprotonated amide cycle (Figure 1, yellow cycle), amide **12** + H^+ has the highest computed pK_a value of 22.6, and thus, it is the most probable protonated species. The traces of the proton-transfer catalyst **12** + H^+ are initially formed via the reaction of isocyanate **2** with the deprotonated amide **12** and water (the few ppm of water present even under such inert conditions are sufficient to initiate the catalytic proton transfer cycle). In addition, the tautomer **17*** of carbamate **17** is formed. This transformation is exergonic (ΔG = −40 kJ/mol) with an activation free energy of 75 kJ/mol. The tautomer rearranges to carbamate **17**. The rearrangement is barrierless and exergonic with a ΔG of −56 kJ/mol.

For the subsequent formation of the experimentally observed olefin **16**, different pathways were evaluated: (1) protonation of alkoxide **13** by water and a consecutive deprotonation−elimination reaction (**12**/**12** + H^+ as base/acid) under loss of water, (2) protonation of alkoxide **13** by **12** + H^+, followed by deprotonation (**12** as base) and simultaneous transfer of an intermediary hydroxide anion to isocyanate **2**, or (3) addition of an isocyanate **2** to alkoxide **13**, protonation by **12** + H^+, and a subsequent deprotonation−elimination reaction (**12**/**12** + H^+ as base/acid). The first two possibilities have rate-limiting steps with activation free energies over 150 kJ/mol and can therefore be ruled out. The latter pathway is both kinetically and thermodynamically plausible and consistent with experimental findings.

Isocyanate **2** is added to alkoxide **13** in an endergonic reaction (ΔG = 24 kJ/mol), forming carbamate **14**. This step has an activation free energy of 86 kJ/mol, which is only slightly higher than those for the isocyanate addition reactions in the deprotonated amide cycle. Next, **14** is protonated (**12** + H^+ as acid) to yield **15**. The protonation is barrierless and thermoneutral. The following deprotonation−elimination reaction (**12** as base) results in olefin **16**, additionally releasing carbamate **17**. The activation free energy is 95 kJ/mol, and the reaction step is exergonic (ΔG = −30 kJ/mol). Finally, isocyanate **2** is added to carbamate **17**, CO_2 dissociates simultaneously, and the ureate catalyst **18** is formed. The last step has a $\Delta G^{\ddagger}$ of 74 kJ/mol and is endergonic (ΔG = 21 kJ/mol). As the system is closed, CO_2 cannot escape and associates with the ureate **18** to form the catalyst resting state amidocarbamate **19**. The addition of CO_2 is barrierless and strongly exergonic with a reaction free energy of −84 kJ/mol.

https://dx.doi.org/10.1021/acs.joc.0c00944
J. Org. Chem. XXXX, XXX, XXX−XXX

For the deprotonated urea catalysis, all activation free energies are higher compared to the deprotonated amide catalysis. The first isocyanate addition has a computed $\Delta G^{\ddagger}$ of 83 kJ/mol, the second addition has a $\Delta G^{\ddagger}$ of 112 kJ/mol, and the third addition has a $\Delta G^{\ddagger}$ of 80 kJ/mol. Thus, the second isocyanate addition has the highest activation free energy in the deprotonated urea cycle and is the rate-limiting step. The reason for this is an intramolecular hydrogen bond that stabilizes the ureate-mono-isocyanate adduct **20**. These activation free energies are in agreement with the NMR and MS analyses because species **20** was observed as the only adduct intermediate. The thermochemistry of the first addition is exergonic (ΔG = −59 kJ/mol) and the second and third additions are slightly endergonic. The exergonic cyclization step (ΔG = −50 kJ/mol) follows with an activation free energy of 78 kJ/mol. The isocyanurate **6** formation and catalyst regeneration have a low $\Delta G^{\ddagger}$ of 31 kJ/mol and are also exergonic (ΔG = −39 kJ/mol). Overall, these calculations are in good agreement with the experimental results, thereby proving the deprotonated urea cycle as the actual catalytic cycle.

Further, the formation of uretdione **24**, which is observed as a side-product with several oligomerization catalysts, was computed for all three potential catalysts (**1**, **12**, and **18**), but it always had a high activation free energy, which matches its absence in the experiments. As catalyst deactivation was observed in the NMR and MS analyses, we performed calculations on two different catalyst deactivation pathways: (1) the nucleophilic attack of the catalyst anion at a propyl group of the tetrapropylammonium model countercation to form NPr_3 and the propylated nucleophile and (2) the abstraction of a proton from the propyl group by the catalyst anion and formation of propene and NPr_3. Both pathways are highly exergonic but have high activation free energies of more than 130 kJ/mol for all three catalysts, which is in agreement with the very small amount of the decomposed catalyst formed (Tables S1 and S4).

CONCLUSIONS

We investigated the acetate-initiated aliphatic isocyanate trimerization to isocyanurate by state-of-the-art analytical and computational methods. Astonishingly, we found that acetate is only a precatalyst, which is activated to a first active catalytic species by isocyanate addition, rearrangement, and carbon dioxide cleavage. While only a limited amount of isocyanurate is formed in the resulting deprotonated amide cycle, a catalyst migration pathway leads to the formation of a catalytically inactive olefin and a carbamate species. The latter reacts with isocyanate to form the main ureate catalyst. In this "bicyclic ride", both catalytic cycles contribute to the final product, whereas their contribution to product formation shifts over time because of the irreversible catalyst migration. Besides achieving mechanistic understanding, the knowledge about the formation of the olefinic side-product can lead to improvements in industrial applications. Because such olefinic structures can react further, leading to unwanted by-products and increased color in the final coating, the process and workup can now be optimized to minimize their negative influence.[55−57]

EXPERIMENTAL SECTION

General Procedures. Air- and moisture-sensitive syntheses and catalyses were carried out under an argon atmosphere under exclusion of air and moisture. All glassware were flame-dried prior to use, and standard Schlenk techniques were applied. For reactions at NMR scale, all compounds (substrate, catalyst, internal standard) were added using stock solutions. All reactions that required heating were conducted with a temperature-controlled oil bath. The temperature of the oil bath was stable within ±0.1 °C after the reaction vessel had reached the desired temperature. The given yields refer to isolated and purified products.

Solvents and Reagents. Toluene (Chromasolv for HPLC, 99.9%) was purchased from Honeywell (Honeywell International Inc., USA), dried in a MB SPS-800 system (M. Braun Inertgas-Systeme GmbH, Germany), and stored under nitrogen. Anhydrous DMSO (≥ 99.9%) and anhydrous toluene-d_8 (≥ 99.0%, 99.6 atom % D) were purchased from Sigma-Aldrich (Sigma-Aldrich, Inc., USA) and stored under an argon atmosphere under exclusion of air and moisture. All anhydrous solvents were further degassed by four freeze−pump−thaw cycles. The anhydrous and degassed solvents were stored under an argon atmosphere over molecular sieve (3 Å). Acetonitrile (HiPerSolv CHROMANORM for HPLC, ≥99.9%) for Orbitrap-MS analysis was purchased from VWR (VWR International, LLC., USA). Argon gas (Ar 5.0) was purchased from Air Liquide (Air Liquide Deutschland GmbH, Germany) and dried by silica gel and molecular sieve (4 Å). All other solvents and chemicals were purchased from manufacturing and trading companies (Sigma-Aldrich, Inc., USA and TCI Europe N.V., Belgium) and stored according to the respective instructions.

Commercially purchased *n*-hexyl isocyanate was distilled under inert conditions and stored under an argon atmosphere under exclusion of air and moisture at 5 °C. Commercially purchased tetrabutylammonium acetate was always weighed and stored under an argon atmosphere under exclusion of air and moisture. Isolated compounds were stored under argon and, if needed, at 5 or −20 °C.

Analytical Methods. NMR spectra were recorded on a 400 MHz Bruker AVANCE III HD spectrometer, 400 MHz Bruker AVANCE III HD spectrometer with a CryoProbe Prodigy, or 800 MHz Bruker AVANCE III HD spectrometer with a CryoProbe (Bruker Corporation, USA). The NMR spectra during reaction monitoring were exclusively recorded on the 400 MHz Bruker AVANCE III HD spectrometer with a CryoProbe Prodigy. NMR spectra of air- and moisture-sensitive compounds were measured using J. Young NMR tubes. Reactions at NMR scale (reaction monitoring) were performed in J. Young NMR tubes under an argon atmosphere under exclusion of air and moisture unless otherwise noted. The solvent residual signals were used for internal calibration.[58] Chemical shifts δ are reported in ppm, and coupling constants J are reported in Hz. The different multiplicities are defined by s (singlet), t (triplet), and m (multiplet). The assignments in ^{13}C NMR spectra refer to proton-decoupled experiments. The assignment of signals was realized by two-dimensional NMR spectroscopy (inter alia $^{1}H-^{1}H$-COSY, $^{1}H-^{13}C$-HSQC-ME and $^{1}H-^{13}C$-HMBC experiments) and partly by DOSY experiments. For data processing, the software TopSpin 4 (Bruker Corporation, USA) was used. For visualization of the reaction monitoring, the software OriginPro 2018G (OriginLab Corporation, USA) was used.

For the reaction monitoring in the presence of an internal standard, ^{1}H NMR spectra were obtained with a pulse width of 3.6 μs (30° flip angle), acquisition time of 4.1 s, and delay time of 5.0 s. For qualitative analysis, ^{1}H NMR spectra were obtained with a pulse width of 3.6 μs (30° flip angle), acquisition time of 4.1 s, and delay time of 1.0 s. For the DOSY experiments, a gradient distance (diffusion time) *big delta* Δ of 49.9 ms and a diffusion gradient length *little delta* δ of 4.0 ms were chosen.

Mass spectrometric measurements were performed on a Thermo Scientific Finnigan LTQ Ultra FT-ICR or on a Thermo Scientific Q Exactive Plus mass spectrometer (Thermo Fisher Scientific Inc., USA). The investigations of the catalysis mixtures were carried out exclusively on the last-mentioned mass spectrometer. Electrospray ionization was used as the ionization technique. The mode (positive/negative) of the experiment, solvent used to dissolve the sample, and method of injection together with potential solvents are listed. In case

https://dx.doi.org/10.1021/acs.joc.0c00944
J. Org. Chem. XXXX, XXX, XXX−XXX

of the catalysis mixtures, a syringe pump was used to continuously inject the diluted sample into the ion source. For compound characterization, the m/z value of the most abundant or characteristic peak is given in comparison to the calculated m/z value. For Orbitrap-MS analysis of catalysis mixtures, all relevant m/z values are given in comparison to the calculated m/z values. If isotopic patterns are pronounced, the most intensive peak is indicated. Molecular ions are abbreviated as M. For data processing, the Qual Browser of the Thermo Scientific Xcalibur 4.1 software suite (Thermo Fisher Scientific Inc., USA) was used. For visualization of the mass spectra, the software OriginPro 2018G (OriginLab Corporation, USA) was used.

For the analysis of reaction intermediates with the Thermo Scientific Q Exactive Plus mass spectrometer, *Full MS* (scan type) was performed in a scan range of 50 to 750 m/z. A resolution of 140,000 with an automatic gain control target of 1×10^6 was set, and no additional fragmentation was induced.

Elemental analyses were performed using an Elementar vario MICRO cube instrument (Elementar Analysensysteme GmbH, Germany).

Investigation of Precatalyst Activation. A three-necked Schlenk flask was equipped with a dropping funnel and Dimroth condenser. The upper end of the condenser was connected by a hose to three gas washing bottles connected in series, the two rear ones of which were filled with saturated barium hydroxide solution (baryta water). The inert setup was closed off with a pressure relief valve behind the gas washing bottles.

Tetrabutylammonium acetate **1** (4.15 g, 13.8 mmol, 0.25 equiv) was dissolved in dry DMSO (80 mL) and added to the Schlenk flask. The catalyst solution was heated to 90 °C. A solution of *n*-hexyl isocyanate **2** (7.00 g, 8.01 mL, 55.0 mmol, 1.00 equiv) in anhydrous DMSO (20 mL) was added to the catalyst solution via the dropping funnel over a period of 30 min. The reaction mixture was stirred for 2 h at 90 °C. An intensive gas formation as well as a yellow coloration of the solution was visible upon addition of the isocyanate solution. After no further gas formation could be observed, the gas formed was passed through the gas washing bottles with the help of a gentle argon gas flow, leading to the formation of a milky suspension with high turbidity and a colorless precipitate. After filtration of the suspension solids, washing with water, and drying at 100 °C for 24 h, the solid was weighed. By this, nearly 1 equiv of barium carbonate (2.39 g, 12.1 mmol, 88%) with regard to the precatalyst tetrabutylammonium acetate **1** was obtained, thereby strongly indicating a precatalyst activation including the cleavage of carbon dioxide.

Synthesis of Reference Compounds. Compounds **6** and **24** are literature known and were synthesized according to a reported procedure.[21]

Neat *n*-hexyl isocyanate **2** (5.09 g, 5.83 mL, 40.0 mmol, 1.00 equiv) was heated to 60 °C, and tri-*n*-butylphosphine (405 mg, 500 μL, 2.00 mmol, 0.05 equiv) was added. The reaction mixture was stirred for 4 h at 60 °C and 15 h at room temperature. Dimethyl sulfate (252 mg, 190 μL, 2.0 mmol, 0.05 equiv) was added, and the reaction mixture was stirred for 1 h at 60 °C. The products were purified by distillation (**24**: 0.05 mbar and 170 °C; **6**: 0.05 mbar and 210 °C) followed by flash column chromatography (silica, DCM/*n*-pentane 1:5/1:3/1:0). Both products *n*-hexyl isocyanurate **6** (785 mg, 2.06 mmol, 15%) and *n*-hexyl uretdione **24** (331 mg, 1.30 mmol, 7%) were obtained as colorless oils.

Characterization of Compounds. *Tetrabutylammonium Acetate* ***1***. ^{1}H NMR (toluene-d_8, 400 MHz, 298 K): δ [ppm] = 0.99 (t, $^3J_{H-H}$ = 7.3 Hz, 12H), 1.33−1.44 (m, 8H), 1.52−1.66 (m, 8H), 2.22 (s, 3H), 3.27−3.54 (m, 8H). ^{13}C{^{1}H} NMR (toluene-d_8, 101 MHz, 298 K): δ [ppm] 14.1 (s, 4C), 20.3 (s, 4C), 24.6 (s, 4C), 27.1 (s, 1C), 58.6 (s, 4C), 173.9 (s, 1C).

n-Hexyl Isocyanate ***2***. ^{1}H NMR (toluene-d_8, 400 MHz, 298 K): δ [ppm] 0.82 (t, $^3J_{H-H}$ = 7.3 Hz, 3H), 0.95−1.03 (m, 4H), 1.05−1.18 (m, 4H), 2.62 (t, $^3J_{H-H}$ = 6.6 Hz, 2H). ^{13}C{^{1}H} NMR (toluene-d_8, 101 MHz, 298 K): δ [ppm] 14.1 (s, 1C), 22.8 (s, 1C), 26.4 (s, 1C), 31.4 (s, 1C), 31.5 (s, 1C), 42.8 (s, 1C), 123.1 (s, 1C).

n-Hexyl Isocyanurate ***6***. ^{1}H NMR (toluene-d_8, 400 MHz, 298 K): δ [ppm] 0.77−0.90 (m, 9H), 1.11−1.27 (m, 18H), 1.48−1.69 (m, 6H), 3.71−3.86 (m, 6H). ^{13}C{^{1}H} NMR (toluene-d_8, 101 MHz, 298 K): δ [ppm] 14.2 (s, 3C), 23.0 (s, 3C), 26.8 (s, 3C), 28.3 (s, 3C), 31.8 (s, 3C), 42.9 (s, 3C), 149.0 (s, 3C). HR-MS (ESI$^+$, $CHCl_3$, FIA: ACN/H_2O) m/z: $[M + H]^+$ calcd for $C_{21}H_{40}N_3O_3^+$, 382.3064; found, 382.3066. EA (%): calcd for $C_{21}H_{39}N_3O_3$: C, 66.11; H, 10.30; N, 11.01; found: C, 66.34; H, 10.32; N, 11.98.

n-Hexyl Uretdione ***24***. ^{1}H NMR (toluene-d_8, 400 MHz, 298 K): δ [ppm] 0.79−0.85 (m, 6H), 1.02−1.11 (m, 8H), 1.12−1.20 (m, 4H), 1.31−1.40 (m, 4H), 2.80 (t, $^3J_{H-H}$ = 7.1 Hz, 4H). ^{13}C{^{1}H} NMR (toluene-d_8, 101 MHz, 298 K): δ [ppm] 14.1 (s, 2C), 22.9 (s, 2C), 26.7 (s, 2C), 28.9 (s, 2C), 31.5 (s, 2C), 40.5 (s, 2C), 157.8 (s, 2C). EA (%): calcd for $C_{14}H_{26}N_2O_2$: C, 66.11; H, 10.30; N, 11.01; found: C, 66.23; H, 10.31; N, 12.12.

Cyclic Olefin ***16***. ^{1}H NMR (toluene-d_8, 400 MHz, 298 K): δ [ppm] 3.47 (s, 2H), 3.58−3.66 (m, 4H), 3.86−3.91 (m, 2H). ^{13}C{^{1}H} NMR (toluene-d_8, 101 MHz, 298 K): δ [ppm] 42.5 (s, 1C), 44.7 (s, 2C), 69.0 (s, 1C), 140.1 (s, 1C), 148.9 (s, 2C). The NMR assignments are based on the spectra from the reaction monitoring. Because of the complexity between 0.6 and 1.8 ppm in the ^{1}H NMR spectra and between 12 and 34 ppm in the ^{13}C{^{1}H} NMR spectra, no assignments were possible for several nuclei.

Amidocarbamate ***19***. ^{1}H NMR (toluene-d_8, 400 MHz, 298 K): δ [ppm] 1.87−1.99 (m, 2H), 3.15−3.29 (m, 8H), 3.39−3.45 (m, 2H), 4.12−4.21 (m, 2H), 11.24 (t, $^3J_{H-H}$ = 10.9 Hz, 1H). ^{13}C{^{1}H} NMR (toluene-d_8, 101 MHz, 298 K): δ [ppm] 30.9 (s, 1C), 40.5 (s, 1C), 44.1 (s, 1C), 58.3 (s, 4C), 158.8 (s, 1C), 159.4 (s, 1C). The NMR assignments are based on the spectra from the reaction monitoring. Because of the complexity between 0.6 and 1.8 ppm in the ^{1}H NMR spectra and between 12 and 34 ppm in the ^{13}C{^{1}H} NMR spectra, no assignments were possible for several nuclei.

Reaction Monitoring via NMR with an Internal Standard. Tetrabutylammonium acetate **1** (6.03 mg, 20.0 μmol, 0.10 equiv) and mesitylene (2.16 mg, 2.50 μL, 18.0 μmol, 0.09 equiv) were dissolved in anhydrous toluene-d_8 (0.5 mL) in a J. Young NMR tube, and *n*-hexyl isocyanate **2** (25.4 mg, 29.1 μL, 200 μmol, 1.00 equiv) was added (see Section S3.1). The sealed J. Young NMR tube was heated to 80 °C for 1155 min. After defined time periods, the NMR tube was taken out of the heating bath and cooled to 0 °C, and immediately, a ^{1}H and ^{13}C NMR spectrum was measured.

Reaction Monitoring via NMR without an Internal Standard. Tetrabutylammonium acetate **1** (6.03 mg, 20.0 μmol, 0.10 equiv) was dissolved in anhydrous toluene-d_8 (0.5 mL) in a J. Young NMR tube (see Section S3.2.1) or standard NMR tube (see Section S3.2.2). Next, *n*-hexyl isocyanate **2** (25.4 mg, 29.1 μL, 200 μmol, 1.00 equiv) was added. The sealed J. Young NMR tube or opened standard NMR tube was heated to 80 °C for 1155 min. After defined time periods, the NMR tube was taken out of the heating bath and cooled to 0 °C, and immediately, a ^{1}H and ^{13}C NMR spectrum was measured.

Qualitative comparison of the two sets of NMR spectra demonstrates that in case of the opened NMR tube, the amount of ureate increases while the amount of the stabilized form amidocarbamate decreases over the course of catalysis. This is easily rationalized by the fact that carbon dioxide is released from the catalysis mixture as soon as the ureate is formed from the amidocarbamate, which is necessary for catalysis to proceed. Further, the amount of symmetrical trimer is significantly lower in case of the opened NMR tube as the volatile isocyanate also evaporates during heating.

Analysis of Reaction Mixtures via Orbitrap-MS, Analysis after the Short Reaction Time (15 min). Tetrabutylammonium acetate **1** (60.3 mg, 200 μmol, 0.10 equiv) was dissolved in anhydrous toluene (6.5 mL). The catalyst solution was heated to 80 °C before *n*-hexyl isocyanate **2** (254 mg, 291 μL, 2.00 mmol, 1.00 eq.) was added. The reaction mixture was stirred for 15 min at 80 °C. An aliquot of the reaction mixture was diluted in ACN and directly analyzed via Orbitrap-MS. Both intermediates from the deprotonated amide as well as the deprotonated urea cycle are present in the analyzed sample

https://dx.doi.org/10.1021/acs.joc.0c00944
J. Org. Chem. XXXX, XXX, XXX−XXX

(Figure S62). For an overview of the exact masses of all intermediates, see Figure S65.

Analysis of Reaction Mixtures via Orbitrap-MS, Analysis after the Complete Reaction. The Orbitrap-MS analysis was performed on the reaction mixture of the J. Young NMR tube without an internal standard after complete conversion.

Tetrabutylammonium acetate **1** (6.03 mg, 20.0 μmol, 0.10 equiv) was dissolved in anhydrous toluene-d_8 (0.5 mL) in a J. Young NMR tube, and *n*-hexyl isocyanate **2** (25.4 mg, 29.1 μL, 200 μmol, 1.00 equiv) was added. The sealed J. Young NMR tube was heated to 80 °C for 1155 min. After the reaction was completed, an aliquot of the reaction mixture was diluted in ACN and directly analyzed via Orbitrap-MS. Exclusively, the intermediates of the deprotonated urea cycle are present in the analyzed sample (Figures S63 and S64). For an overview of the exact masses of all intermediates, see Figure S65.

Computational Details. For the mechanistic investigations, hexyl isocyanate was modeled as propyl isocyanate to reduce the system size and save computational time. This should not affect the reactivity of the NCO group and the occurring intermediate species. The tetrabutylammonium countercation was reduced to a tetrapropylammonium cation. The countercation was omitted for the investigation of the catalytic cycles and taken into account only for the computations regarding the catalyst decomposition pathways.

All quantum chemical computations were performed on the DFT level using the TURBOMOLE 7.3 program package.[59,60] The structures of all species and transition states (TSs) were optimized on the BP86 level[61−63] employing the triple-zeta basis set def2-TZVP,[49] the cosmo continuum solvation model[50] with epsilon equals infinity, and the D3 dispersion correction[48] with Becke−Johnson damping.[46,47] For all structural optimizations as well as all single-point energy computations, the resolution-of-identity approximation for the Coulomb integrals was applied using matching default auxiliary basis sets.[64−66] Conformational searches were carried out with an in-house tool that rotates around specified bonds in an iterative fashion to find the nearest local minimum structure and subsequently submits the necessary structural optimizations on the BP86-D3-cosmo/def2-TZVP level. Here, the propyl chains were kept frozen in a straight arrangement and all other single bonds were rotated by 120°. Only the energetically lowest conformers were used further, for example, to compute single-point energies.

Initial guess structures for the TSs were either built manually or obtained via scans of the potential energy surface along certain bonds. These structures were then optimized using eigenvector following as implemented in TURBOMOLE. The resulting TS geometries were subjected to a conformational search (as described above) with a frozen TS region. The energetically lowest conformer was again optimized using eigenvector following. All minimum and TS geometries were confirmed as such by the vibrational frequencies.

The activation and reaction free energies were obtained as a sum of three contributions: (1) the gas-phase activation/reaction energy on the B3LYP-D3/def2-QZVP or M06-2X/def2-QZVP level, (2) the difference in zero-point vibrational energies and thermostatistical contributions for products and reactants on the BP86-D3-cosmo/def2-TZVP level, and (3) the difference in solvation free energies for products and reactants computed with the COSMO-RS solvation model:

ad (1) Single-point energies in the gas phase were computed for the optimized structures on the B3LYP[42−45]-D3 and M06-2X[54] level using the QZ basis set def2-QZVP.[49] For such a large basis set, the basis set superposition error almost vanishes and no special treatment, for example, a computationally demanding counter-poise correction, is required.

ad (2) Computations of the harmonic vibrational frequencies on the BP86-D3-cosmo/def2-TZVP level were performed numerically and used to calculate the zero-point vibrational energy and the thermostatistical corrections to obtain a free energy at finite temperature (80 °C).

ad (3) The COSMO-RS solvation model[51,52] was used as implemented in COSMOtherm 2015[53] employing the 2015 BP86/def-TZVP parametrization. To obtain the solvation free energies in hexyl isocyanate at 80 °C, the standard procedure with two single-point calculations, one in the gas phase and one in an ideal conductor (cosmo with epsilon equals infinity) on the default BP86/def-TZVP level of theory, was performed and the results were used as the input for COSMOtherm. The thermodynamic reference state for computing the solvation free energies is 1 mol L^{-1}.

For the computation of pK_a values (in isocyanate), 2,6-dimethylpyridine/2,6-dimethylpyridinium was used as a reference system, and free energies for the protonation reaction of 2,6-dimethylpyridine to 2,6-dimethylpyridinium and the corresponding base of the acid used were computed according to the workflow described above. The resulting free energy was transferred to pK_a units, and the experimental pK_a value of the reference system (4.46 in DMSO) was subtracted to obtain the desired pK_a value of the acid.

■ ASSOCIATED CONTENT

Supporting Information

The Supporting Information is available free of charge at https://pubs.acs.org/doi/10.1021/acs.joc.0c00944.

Pictures of investigation of precatalyst activation; NMR spectra of reference compounds; NMR spectra of reaction monitoring; mass spectra of reaction mixtures; and inputs for quantum chemical computations (PDF)

Cartesian coordinate catalytic cycles (ZIP)

■ AUTHOR INFORMATION

Corresponding Authors

Frederic Lucas − *Advanced Materials & Systems Research, BASF SE, 67056 Ludwigshafen, Germany*; Email: frederic.lucas@basf.com

Oliver Trapp − *Department Chemie, Ludwig-Maximilians-Universität München, 81377 München, Germany*; orcid.org/0000-0002-3594-5181; Email: oliver.trapp@cup.uni-muenchen.de

Authors

Max Siebert − *Department Chemie, Ludwig-Maximilians-Universität München, 81377 München, Germany*; orcid.org/0000-0002-0151-8886

Rebecca Sure − *Advanced Materials & Systems Research, BASF SE, 67056 Ludwigshafen, Germany*

Peter Deglmann − *Advanced Materials & Systems Research, BASF SE, 67056 Ludwigshafen, Germany*

Anna C. Closs − *Department Chemie, Ludwig-Maximilians-Universität München, 81377 München, Germany*

Complete contact information is available at: https://pubs.acs.org/10.1021/acs.joc.0c00944

Author Contributions

The manuscript was written through contributions of all authors. All authors have given approval to the final version of the manuscript.

Notes

The authors declare no competing financial interest.

■ ACKNOWLEDGMENTS

We acknowledge the financial support from BASF SE, the Ludwig-Maximilians-University Munich, and the Deutsche Forschungsgemeinschaft DFG (INST 86/1807-1 FUGG).

REFERENCES

(1) Hofmann, A. W. *Jahresber. Fortschr. Gesamtgeb. Agrikulturchem.* **1858**, *1*, 349.
(2) Sandler, S. R.; Karo, W. *Polymer Syntheses*, 1st ed.; Academic Press: New York, 1980.
(3) Ulrich, H. *Chemistry and Technology of Isocyanates*; John Wiley & Sons: New York, 1996.
(4) Ball, G. W.; Haggis, G. A.; Hurd, R.; Wood, J. F. A New Heat Resistant Rigid Foam. *J. Cell. Plast.* **1968**, *4*, 248−261.
(5) Hoffman, D. K. Model System for a Urethane-Modified Isocyanurate Foam. *J. Cell. Plast.* **1984**, *20*, 129−137.
(6) Landrock, A. H. *Handbook of Plastic Foams*; Noyes Publications: New Jersey, 1995.
(7) Laas, H. J.; Halpaap, R.; Pedain, J. Zur Synthese aliphatischer Polyisocyanate − Lackpolyisocyanate mit Biuret-, Isocyanurat- oder Uretdionstruktur. *J. Prakt. Chem.* **1994**, *336*, 185−200.
(8) Meier-Westhues, U.; Danielmeier, K.; Kruppa, P.; Squiller, E. P. *Polyurethanes: Coatings, Adhesives and Sealants*, 2nd ed.; Vincentz Network: Hanover, 2019.
(9) Goldschmidt, A.; Streitberger, H.-J. *BASF Handbook Basics of Coating Technology*, 3rd ed.; Vincentz Network: Hanover, 2018.
(10) Shashoua, V. E.; Sweeny, W.; Tietz, R. F. The Homopolymerization of Monoisocyanates. *J. Am. Chem. Soc.* **1960**, *82*, 866−873.
(11) Iwakura, Y.; Uno, K.; Kobayashi, N. Polymerization of Isocyanates. III. Chemical Behavior and Structure of Polyisocyanates. *J. Polym. Sci., Part A-1* **1968**, *6*, 1087−1096.
(12) Bechara, I. S.; Mascioli, R. L. The Mechanism of the Hydroxyalkyl Quaternary Ammonium Carboxylate Catalyzed Reactions of Phenyl Isocyanate. *J. Cell. Plast.* **1979**, *15*, 321−332.
(13) Špírková, M.; Kubín, M.; Špaček, P.; Krakovský, I.; Dušek, K. Cyclotrimerization of Isocyanate Groups. II. Catalyzed Reactions of Phenyl Isocyanate in the Presence of 1-Butanol or Butyl-N-Phenylurethane. *J. Appl. Polym. Sci.* **1994**, *53*, 1435−1446.
(14) Schwetlick, K.; Noack, R. Kinetics and Catalysis of Consecutive Isocyanate Reactions. Formation of Carbamates, Allophanates and Isocyanurates. *J. Chem. Soc., Perkin Trans. 2* **1995**, 395−402.
(15) Al Nabulsi, A.; Cozzula, D.; Hagen, T.; Leitner, W.; Müller, T. E. Isocyanurate formation during rigid polyurethane foam assembly: a mechanistic study based on in situ IR and NMR spectroscopy. *Polym. Chem.* **2018**, *9*, 4891−4899.
(16) Roman, M.; Andrioletti, B.; Lemaire, M.; Bernard, J.-M.; Schwartz, J.; Barbeau, P. Investigations providing a plausible mechanism in the hexamethyldisilazane-catalyzed trimerization of alkyl isocyanates. *Tetrahedron* **2011**, *67*, 1506−1510.
(17) Tang, J.-S.; Verkade, J. G. $[P(MeNCH_2CH_2)_3N]$ as a Superior Catalyst for the Conversion of Isocyanates to Isocyanurates. *Angew. Chem., Int. Ed.* **1993**, *32*, 896−898.
(18) Tang, J.; Mohan, T.; Verkade, J. G. Selective and Efficient Syntheses of Perhydro-1,3,5-triazine-2,4,6-triones and Carbodiimides from Isocyanates Using $ZP(MeNCH_2CH_2)_3N$ Catalysts. *J. Org. Chem.* **1994**, *59*, 4931−4938.
(19) Pusztai, Z.; Vlád, G.; Bodor, A.; Horváth, I. T.; Laas, H. J.; Halpaap, R.; Richter, F. U. In Situ NMR Spectroscopic Observation of a Catalytic Intermediate in Phosphine-Catalyzed Cyclo-Oligomerization of Isocyanates. *Angew. Chem., Int. Ed.* **2006**, *45*, 107−110.
(20) Gibb, J. N.; Goodman, J. M. The formation of high-purity isocyanurate through proazaphosphatrane-catalysed isocyanate cyclotrimerisation: computational insights. *Org. Biomol. Chem.* **2013**, *11*, 90−97.
(21) Helberg, J.; Oe, Y.; Zipse, H. Mechanistic Analysis and Characterization of Intermediates in the Phosphane-Catalyzed Oligomerization of Isocyanates. *Chem. Eur. J.* **2018**, *24*, 14387−14391.
(22) Montilla, F.; Clara, E.; Avilés, T.; Casimiro, T.; Aguiar Ricardo, A.; Nunes da Ponte, M. Transition-metal-mediated activation of arylisocyanates in supercritical carbon dioxide. *J. Organomet. Chem.* **2001**, *626*, 227−232.
(23) Orzechowski, L.; Harder, S. Isolation of an Intermediate in the Catalytic Trimerization of Isocyanates by a Monomeric Calcium Carbene with Chelating Iminophosphorane Substituents. *Organometallics* **2007**, *26*, 2144−2148.
(24) Paul, F.; Moulin, S.; Piechaczyk, O.; Le Floch, P.; Osborn, J. A. Palladium(0)-Catalyzed Trimerization of Arylisocyanates into 1,3,5-Triarylisocyanurates in the Presence of Diimines: A Nonintuitive Mechanism. *J. Am. Chem. Soc.* **2007**, *129*, 7294−7304.
(25) Zhu, X.; Fan, J.; Wu, Y.; Wang, S.; Zhang, L.; Yang, G.; Wei, Y.; Yin, C.; Zhu, H.; Wu, S.; Zhang, H. Synthesis, Characterization, Selective Catalytic Activity, and Reactivity of Rare Earth Metal Amides with Different Metal−Nitrogen Bonds. *Organometallics* **2009**, *28*, 3882−3888.
(26) Wang, H.-M.; Li, H.-X.; Yu, X.-Y.; Ren, Z.-G.; Lang, J.-P. Cyclodimerization and cyclotrimerization of isocyanates promoted by one praseodymium benzenethiolate complex $[Pr(SPh)_3(THF)_3]$. *Tetrahedron* **2011**, *67*, 1530−1535.
(27) Hernán-Gómez, A.; Bradley, T. D.; Kennedy, A. R.; Livingstone, Z.; Robertson, S. D.; Hevia, E. Developing catalytic applications of cooperative bimetallics: competitive hydroamination/trimerization reactions of isocyanates catalysed by sodium magnesiates. *Chem. Commun.* **2013**, *49*, 8659−8661.
(28) Barman, M. K.; Baishya, A.; Peddarao, T.; Nembenna, S. Guanidinate stabilized germanium(II) and tin(II) amide complexes and their catalytic activity for aryl isocyanate cyclization. *J. Organomet. Chem.* **2014**, *772*−*773*, 265−270.
(29) Taguchi, Y.; Shibuya, I.; Yasumoto, M.; Tsuchiya, T.; Yonemoto, K. The Synthesis of Isocyanurates on the Trimerization of Isocyanates under High Pressure. *Bull. Chem. Soc. Jpn.* **1990**, *63*, 3486−3489.
(30) Nambu, Y.; Endo, T. Synthesis of Novel Aromatic Isocyanurates by the Fluoride-Catalyzed Selective Trimerization of Isocyanates. *J. Org. Chem.* **1993**, *58*, 1932−1934.
(31) Duong, H. A.; Cross, M. J.; Louie, J. N-Heterocyclic Carbenes as Highly Efficient Catalysts for the Cyclotrimerization of Isocyanates. *Org. Lett.* **2004**, *6*, 4679−4681.
(32) Dekamin, M. G.; Varmira, K.; Farahmand, M.; Sagheb-Asl, S.; Karimi, Z. Organocatalytic, rapid and facile cyclotrimerization of isocyanates using tetrabutylammonium phthalimide-N-oxyl and tetraethylammonium 2-(carbamoyl)benzoate under solvent-free conditions. *Catal. Commun.* **2010**, *12*, 226−230.
(33) Giuglio-Tonolo, A. G.; Spitz, C.; Terme, T.; Vanelle, P. An expeditious method for the selective cyclotrimerization of isocyanates initiated by TDAE. *Tetrahedron Lett.* **2014**, *55*, 2700−2702.
(34) Li, C.; Zhao, W.; He, J.; Zhang, Y. Highly efficient cyclotrimerization of isocyanates using N-heterocyclic olefins under bulk conditions. *Chem. Commun.* **2019**, *55*, 12563−12566.
(35) Servos, M. A.; Smart, N. C.; Kassabaum, M. E.; Scholtens, C. A.; Peters, S. J. Phenyl Isocyanate Anion Radicals and Their Cyclotrimerization to Triphenyl Isocyanurate Anion Radicals. *J. Org. Chem.* **2013**, *78*, 3908−3917.
(36) Bechara, I. S.; Holland, D. G. Delayed Polyurethane Action Catalysts. U.S. Patent 3,862,150A, Air Products and Chemicals, Inc., 1972.
(37) Disteldorf, J.; Hübel, W.; Wolf, E. Verfahren zur Trimerisierung von Diisocyanaten. German Patent DE 2916201 A1, Chemische Werke Hüls AG, 1979.
(38) Kirchmeyer, S.; Wolfrum, C.; Müller, H. P. Isocyanate-Trimerization Catalyst. International Patent WO1993012153A1, Bayer AG, 1991.
(39) Kohlstruk, S.; Kreczinski, M.; Lomölder, R. Verfahren zur Herstellung von geruchsarmen und lagerstabilen monomerhaltigen Polyisocyanuraten auf Basis von Isophorondiisocyanat. European Patent EP1273603A1, Degussa GmbH, 2001.
(40) Binder, H.; Graf, H.; Braun, F.; Spies, B.; Kieslich, H. Verfahren zur Herstellung von Isocyanuratgruppen aufweisenden Polyisocyanaten und ihre Verwendung. European Patent EP 1727842 B1, BASF SE, 2005.
(41) Widemann, M.; Driest, P. J.; Orecchia, P.; Naline, F.; Golling, F. E.; Hecking, A.; Eggert, C.; Pires, R.; Danielmeier, K.; Richter, F. U.

https://dx.doi.org/10.1021/acs.joc.0c00944
J. Org. Chem. XXXX, XXX, XXX−XXX

Structure−Property Relations in Oligomers of Linear Aliphatic Diisocyanates. *ACS Sustainable Chem. Eng.* **2018**, *6*, 9753−9759.
(42) Vosko, S. H.; Wilk, L.; Nusair, M. Accurate spin-dependent electron liquid correlation energies for local spin density calculations: a critical analysis. *Can. J. Phys.* **1980**, *58*, 1200−1211.
(43) Lee, C.; Yang, W.; Parr, R. G. Development of the Colle-Salvetti correlation-energy formula into a functional of the electron density. *Phys. Rev. B: Condens. Matter Mater. Phys.* **1988**, *37*, 785−789.
(44) Becke, A. D. Density-functional thermochemistry. III. The role of exact exchange. *J. Chem. Phys.* **1993**, *98*, 5648−5652.
(45) Stephens, P. J.; Devlin, F. J.; Chabalowski, C. F.; Frisch, M. J. Ab Initio Calculation of Vibrational Absorption and Circular Dichroism Spectra Using Density Functional Force Fields. *J. Phys. Chem.* **1994**, *98*, 11623−11627.
(46) Johnson, E. R.; Becke, A. D. A post-Hartree−Fock model of intermolecular interactions. *J. Chem. Phys.* **2005**, *123*, 024101.
(47) Becke, A. D.; Johnson, E. R. A density-functional model of the dispersion interaction. *J. Chem. Phys.* **2005**, *123*, 154101.
(48) Grimme, S.; Antony, J.; Ehrlich, S.; Krieg, H. A consistent and accurate ab initio parametrization of density functional dispersion correction (DFT-D) for the 94 elements H-Pu. *J. Chem. Phys.* **2010**, *132*, 154104.
(49) Weigend, F.; Ahlrichs, R. Balanced basis sets of split valence, triple zeta valence and quadruple zeta valence quality for H to Rn: Design and assessment of accuracy. *Phys. Chem. Chem. Phys.* **2005**, *7*, 3297−3305.
(50) Klamt, A.; Schüürmann, G. COSMO: a new approach to dielectric screening in solvents with explicit expressions for the screening energy and its gradient. *J. Chem. Soc., Perkin Trans.* **1993**, *2*, 799−805.
(51) Klamt, A. Conductor-like Screening Model for Real Solvents: A New Approach to the Quantitative Calculation of Solvation Phenomena. *J. Phys. Chem.* **1995**, *99*, 2224−2235.
(52) Eckert, F.; Klamt, A. Fast solvent screening via quantum chemistry: COSMO-RS approach. *AIChE J.* **2002**, *48*, 369−385.
(53) Eckert, F.; Klamt, A. *COSMOtherm*, Version C3.0, Release 15.01; COSMOlogic GmbH & Co. KG: Leverkusen, Germany, 2015.
(54) Zhao, Y.; Truhlar, D. G. The M06 suite of density functionals for main group thermochemistry, thermochemical kinetics, noncovalent interactions, excited states, and transition elements: two new functionals and systematic testing of four M06-class functionals and 12 other functionals. *Theor. Chem. Acc.* **2008**, *120*, 215−241.
(55) Étienne, A.; Lonchambon, G.; Giraudeau, P.; Durand, G. La réaction des organomagnésiens sur les trimères de l'isocyanate de méthyle. *C. R. Acad. Sc. Paris, Série C* **1973**, *277*, 795−798.
(56) Étienne, A.; Lonchambon, G.; Giraudeau, P. Dérivés méthyléniques-2 des perhydrotriazines-1.3.5 N-substituées. Acylation, sulfonylation et carbamoylation de la méthylène-2 triméthyl-1.3.5 dioxo-4.6 perhydrotriazine-1.3.5. *C. R. Acad. Sc. Paris, Série C* **1974**, *279*, 659−662.
(57) Étienne, A.; Lonchambon, G.; Giraudeau, P. Méthylène-2 triméthyl-1.3.5 dioxo-4.6 perhydrotriazine-1.3.5 et quelques dérivés de substitution méthylénique. *C. R. Acad. Sc. Paris, Série C* **1977**, *285*, 321−324.
(58) Fulmer, G. R.; Miller, A. J. M.; Sherden, N. H.; Gottlieb, H. E.; Nudelman, A.; Stoltz, B. M.; Bercaw, J. E.; Goldberg, K. I. NMR Chemical Shifts of Trace Impurities: Common Laboratory Solvents, Organics, and Gases in Deuterated Solvents Relevant to the Organometallic Chemist. *Organometallics* **2010**, *29*, 2176−2179.
(59) Furche, F.; Ahlrichs, R.; Hättig, C.; Klopper, W.; Sierka, M.; Weigend, F. Turbomole. *Wiley Interdiscip. Rev.: Comput. Mol. Sci.* **2014**, *4*, 91−100.
(60) Ahlrichs, R.; Armbruster, M. K.; Bär, M.; Baron, H.-P.; Bauernschmitt, R.; Crawford, N.; Deglmann, P.; Ehrig, M.; Eichkorn, K.; Elliott, S.; Furche, F.; Haase, F.; Häser, M.; Hättig, C.; Hellweg, A.; Horn, H.; Huber, C.; Huniar, U.; Kattannek, M.; Kölmel, C.; Kollwitz, M.; May, K.; Nava, P.; Ochsenfeld, C.; Öhm, H.; Patzelt, H.; Rappoport, D.; Rubner, O.; Schäfer, A.; Schneider, U.; Sierka, M.; Treutler, O.; Unterreiner, B.; von Arnim, M.; Weigend, F.; Weis, P.; Weiss, H. *TURBOMOLE 7.3*; Universität Karlsruhe, 2018.
(61) Perdew, J. P. Density-functional approximation for the correlation energy of the inhomogeneous electron gas. *Phys. Rev. B: Condens. Matter Mater. Phys.* **1986**, *33*, 8822−8824.
(62) Perdew, J. P. Erratum: Density-functional approximation for the correlation energy of the inhomogeneous electron gas. *Phys. Rev. B: Condens. Matter Mater. Phys.* **1986**, *34*, 7406.
(63) Becke, A. D. Density-functional exchange-energy approximation with correct asymptotic behavior. *Phys. Rev. A: At., Mol., Opt. Phys.* **1988**, *38*, 3098−3100.
(64) Eichkorn, K.; Treutler, O.; Öhm, H.; Häser, M.; Ahlrichs, R. Auxiliary basis sets to approximate Coulomb potentials. *Chem. Phys. Lett.* **1995**, *240*, 283−290.
(65) Eichkorn, K.; Treutler, O.; Öhm, H.; Häser, M.; Ahlrichs, R. Auxiliary basis sets to approximate Coulomb potentials (Chem. Phys. Letters 240(1995)283-290). *Chem. Phys. Lett.* **1995**, *242*, 652−660.
(66) Weigend, F. Accurate Coulomb-fitting basis sets for H to Rn. *Phys. Chem. Chem. Phys.* **2006**, *8*, 1057−1065.

https://dx.doi.org/10.1021/acs.joc.0c00944
J. Org. Chem. XXXX, XXX, XXX−XXX

List of Abbreviations

Abbreviation	Full Name
a	annum
ACN	acetonitrile
Add.	additive
AF	alkyl formate
BINAP	2,2′-bis(diphenylphosphino)-1,1′-binaphthyl
BP	Becke-Perdew (functional)
Bu	butyl
B3LYP	Becke, 3-parameter, Lee–Yang–Parr (functional)
CA	cyclic acetal
Cat.	catalyst
CCDC	Cambridge Crystallographic Data Centre
COD	cyclooctadiene
cosmo	conductor-like screening model
COSMO-RS	conductor-like screening model for real solvents
COSY	correlation spectroscopy
Cy	cyclohexyl
DAM	dialkoxymethane
DCM	dichloromethane
DF	degrees of freedom
DFT	density functional theory
DMF	dimethylformamide
DMM	dimethoxymethane
DMSO	dimethyl sulfoxide
DoE	design of experiments

Abbreviation	Full Name
DOI	digital object identifier
DOSY	diffusion-ordered spectroscopy
D3	atom-pair wise (atom-triple wise) dispersion correction
EA	elemental analysis
EDTA	ethylenediaminetetraacetic acid
ESI	electronic supplementary information
ESI (MS)	electrospray ionization
Et	ethyl
FT-ICR	fourier transform ion cyclotron resonance
Gt	gigatonne
HDI	hexamethylene diisocyanate
HMBC	heteronuclear multiple-bond correlation
HMDS	hexamethyldisilazane
HPLC	high-performance liquid chromatography
HR	high-resolution
HSQC	heteronuclear single-quantum correlation
HSQC-ME	heteronuclear single-quantum correlation multiplicity-edited
IPDI	isophorone diisocyanate
IR	infrared
IS	internal standard
IUPAC	International Union of Pure and Applied Chemistry
LB	lower bound
LTQ	linear ion trap quadrupole
m	multiplet
MDI	methylene diphenyl diisocyanate
Me	methyl
Mes	mesityl
MF	methyl formate
MM	methoxymethanol
MS	mass spectrometry
M06	Minnesota 06 (functional)

Abbreviation	Full Name
n	*normal*
NMR	nuclear magnetic resonance
o	*ortho*
OFAT	one-factor-at-a-time
OLS	ordinary least squares
OME	oxymethylene ethers
p	*para*
Ph	phenyl
ppm	parts per millions
Pr	propyl
PU	polyurethane
py	pyridyl
RF	random forest
RS	replication study
rt	room temperature
s	singlet
SD	standard deviation
SI	supporting information
SPS	solvent purification system
t	triplet
TDI	toluene diisocyanate
Tf	triflyl
THF	tetrahydrofuran
TMEDA	tetramethylethylenediamine
tmm	trimethylenemethane dianion
TMS	trimethylsilyl
Tol	tolyl
TON	turnover number
TPU	thermoplastic polyurethane elastomer
triphos	1,1,1-tris(diphenylphosphinomethyl)ethane
Ts	tosyl

Abbreviation	Full Name
TS	transition state
TZVP	valence triple-zeta polarization
UB	upper bound
UV	ultraviolet
QZ	quadruple-zeta
QZVP	valence quadruple-zeta polarization

Bibliography

[1] *IPCC, 2019: IPCC Special Report on Climate Change and Land*, (Eds.: P. R. Shukla, J. Skea, E. Calvo Buendia, V. Masson-Delmotte, H.-O. Pörtner, D. Roberts, P. Zhai, R. Slade, S. Connors, R. van Diemen, M. Ferrat, E. Haughey, S. Luz, S. Neogi, M. Pathak, J. Petzold, J. Portugal Pereira, P. Vyas, E. Huntley, K. Kissick, M. Belkacemi, J. Malley), in press, **2019**.

[2] *IPCC, 2019: IPCC Special Report on the Ocean and Cryosphere in a Changing Climate*, (Eds.: H.-O. Pörtner, D. C. Roberts, V. Masson-Delmotte, P. Zhai, M. Tignor, E. Poloczanska, K. Mintenbeck, A. Alegría, M. Nicolai, A. Okem, J. Petzold, B. Rama, N. M. Weyer), in press, **2019**.

[3] *IPCC, 2018: Global Warming of 1.5°C*, (Eds.: V. Masson-Delmotte, P. Zhai, H.-O. Pörtner, D. Roberts, J. Skea, P. R. Shukla, A. Pirani, W. Moufouma-Okia, C. Péan, R. Pidcock, S. Connors, J. B. R. Matthews, Y. Chen, X. Zhou, M. I. Gomis, E. Lonnoy, T. Maycock, M. Tignor, T. Waterfield), in press, **2018**.

[4] R. Neukom, N. Steiger, J. J. Gómez-Navarro, J. Wang, J. P. Werner, No evidence for globally coherent warm and cold periods over the preindustrial Common Era, *Nature* **2019**, *571*, 550–554.

[5] *IPCC, 2014: Climate Change 2014 (Synthesis Report)*, (Eds.: Core Writing Team, R. K. Pachauri, L. Meyer), IPCC, Geneva, Switzerland, **2014**.

[6] T. Eggleton, *A Short Introduction to Climate Change*, Cambridge University Press, New York, **2013**.

[7] P. J. Crutzen, Geology of mankind, *Nature* **2002**, *415*, 23–23.

[8] J. A. Martens, A. Bogaerts, N. De Kimpe, P. A. Jacobs, G. B. Marin, K. Rabaey, M. Saeys, S. Verhelst, The Chemical Route to a Carbon Dioxide Neutral World, *ChemSusChem* **2017**, *10*, 1039–1055.

[9] P. Falkowski, R. J. Scholes, E. Boyle, J. Canadell, D. Canfield, J. Elser, N. Gruber, K. Hibbard, P. Högberg, S. Linder, F. T. Mackenzie, B. Moore III, T. Pedersen, Y. Rosenthal, S. Seitzinger, V. Smetacek, W. Steffen, The Global Carbon Cycle: A Test of Our Knowledge of Earth as a System, *Science* **2000**, *290*, 291–296.

[10] T. Sterner, E. B. Barbier, I. Bateman, I. van den Bijgaart, A.-S. Crépin, O. Edenhofer, C. Fischer, W. Habla, J. Hassler, O. Johansson-Stenman, A. Lange, S. Polasky, J. Rockström, H. G. Smith, W. Steffen, G. Wagner, J. E. Wilen, F. Alpízar, C. Azar, D. Carless, C. Chávez, J. Coria, G. Engström, S. C. Jagers, G. Köhlin, Å. Löfgren, H. Pleijel, A. Robinson, Policy design for the Anthropocene, *Nat. Sustain.* **2019**, *2*, 14–21.

[11] Y. Geng, J. Sarkis, R. Bleischwitz, How to globalize the circular economy, *Nature* **2019**, *565*, 153–155.

[12] R. Schlögl, The Revolution Continues: Energiewende 2.0, *Angew. Chem. Int. Ed.* **2015**, *54*, 4436–4439.

[13] B. Rego de Vasconcelos, J.-M. Lavoie, Recent Advances in Power-to-X Technology for the Production of Fuels and Chemicals, *Front. Chem.* **2019**, *7*, 392.

[14] M. D. Burkart, N. Hazari, C. L. Tway, E. L. Zeitler, Opportunities and Challenges for Catalysis in Carbon Dioxide Utilization, *ACS Catal.* **2019**, *9*, 7937–7956.

[15] J. Artz, T. E. Müller, K. Thenert, J. Kleinekorte, R. Meys, A. Sternberg, A. Bardow, W. Leitner, Sustainable Conversion of Carbon Dioxide: An Integrated Review of Catalysis and Life Cycle Assessment, *Chem. Rev.* **2018**, *118*, 434–504.

[16] M. Aresta, A. Dibenedetto, A. Angelini, Catalysis for the Valorization of Exhaust Carbon: from CO_2 to Chemicals, Materials, and Fuels. Technological Use of CO_2, *Chem. Rev.* **2014**, *114*, 1709–1742.

[17] P. Markewitz, W. Kuckshinrichs, W. Leitner, J. Linssen, P. Zapp, R. Bongartz, A. Schreiber, T. E. Müller, Worldwide innovations in the development of carbon capture technologies and the utilization of CO_2, *Energy Environ. Sci.* **2012**, *5*, 7281–7305.

[18] M. Aresta, Carbon Dioxide: Utilization Options to Reduce its Accumulation in the Atmosphere in *Carbon Dioxide as Chemical Feedstock*, (Ed.: M. Aresta), Wiley-VCH, Weinheim, **2010**.

[19] W. Keim, Industrial Uses of Carbon Dioxide in *Carbon Dioxide as a Source of Carbon: Biochemical and Chemical Uses*, (Eds.: M. Aresta, G. Forti), Springer, Dordrecht, **1987**.

[20] M. Muntean, D. Guizzardi, E. Schaaf, M. Crippa, E. Solazzo, J. G. J. Olivier, E. Vignati, *Fossil CO_2 emissions of all world countries - 2018 Report*, Publications Office of the European Union, Luxembourg, **2018**.

[21] X. Shi, H. Xiao, H. Azarabadi, J. Song, X. Wu, X. Chen, K. S. Lackner, Sorbents for the Direct Capture of CO_2 from Ambient Air, *Angew. Chem. Int. Ed.* **2020**, *59*, 6984–7006.

[22] M. Ding, R. W. Flaig, H.-L. Jiang, O. M. Yaghi, Carbon capture and conversion using metal–organic frameworks and MOF-based materials, *Chem. Soc. Rev.* **2019**, *48*, 2783–2828.

[23] S. Zeng, X. Zhang, L. Bai, X. Zhang, H. Wang, J. Wang, D. Bao, M. Li, X. Liu, S. Zhang, Ionic-Liquid-Based CO_2 Capture Systems: Structure, Interaction and Process, *Chem. Rev.* **2017**, *117*, 9625–9673.

[24] J. Yu, L.-H. Xie, J.-R. Li, Y. Ma, J. M. Seminario, P. B. Balbuena, CO_2 Capture and Separations Using MOFs: Computational and Experimental Studies, *Chem. Rev.* **2017**, *117*, 9674–9754.

[25] D. J. Heldebrant, P. K. Koech, V.-A. Glezakou, R. Rousseau, D. Malhotra, D. C. Cantu, Water-Lean Solvents for Post-Combustion CO2 Capture: Fundamentals, Uncertainties, Opportunities, and Outlook, *Chem. Rev.* **2017**, *117*, 9594–9624.

[26] L. C. Tomé, I. M. Marrucho, Ionic liquid-based materials: a platform to design engineered CO_2 separation membranes, *Chem. Soc. Rev.* **2016**, *45*, 2785–2824.

[27] E. S. Sanz-Pérez, C. R. Murdock, S. A. Didas, C. W. Jones, Direct Capture of CO_2 from Ambient Air, *Chem. Rev.* **2016**, *116*, 11840–11876.

[28] G. Cui, J. Wang, S. Zhang, Active chemisorption sites in functionalized ionic liquids for carbon capture, *Chem. Soc. Rev.* **2016**, *45*, 4307–4339.

[29] S. Wang, C. Xi, Recent advances in nucleophile-triggered CO_2-incorporated cyclization leading to heterocycles, *Chem. Soc. Rev.* **2019**, *48*, 382–404.

[30] B. Grignard, S. Gennen, C. Jérôme, A. W. Kleij, C. Detrembleur, Advances in the use of CO_2 as a renewable feedstock for the synthesis of polymers, *Chem. Soc. Rev.* **2019**, *48*, 4466–4514.

[31] A. Tortajada, F. Juliá-Hernández, M. Börjesson, T. Moragas, R. Martin, Transition-Metal-Catalyzed Carboxylation Reactions with Carbon Dioxide, *Angew. Chem. Int. Ed.* **2018**, *57*, 15948–15982.

[32] R. R. Shaikh, S. Pornpraprom, V. D'Elia, Catalytic Strategies for the Cycloaddition of Pure, Diluted, and Waste CO_2 to Epoxides under Ambient Conditions, *ACS Catal.* **2018**, *8*, 419–450.

[33] J. Vaitla, Y. Guttormsen, J. K. Mannisto, A. Nova, T. Repo, A. Bayer, K. H. Hopmann, Enantioselective Incorporation of CO_2: Status and Potential, *ACS Catal.* **2017**, *7*, 7231–7244.

[34] Y. Li, X. Cui, K. Dong, K. Junge, M. Beller, Utilization of CO_2 as a C1 Building Block for Catalytic Methylation Reactions, *ACS Catal.* **2017**, *7*, 1077–1086.

[35] C. Martín, G. Fiorani, A. W. Kleij, Recent Advances in the Catalytic Preparation of Cyclic Organic Carbonates, *ACS Catal.* **2015**, *5*, 1353–1370.

[36] Q. Liu, L. Wu, R. Jackstell, M. Beller, Using carbon dioxide as a building block in organic synthesis, *Nat. Commun.* **2015**, *6*, 5933.

[37] F. Marques Mota, D. H. Kim, From CO_2 methanation to ambitious long-chain hydrocarbons: alternative fuels paving the path to sustainability, *Chem. Soc. Rev.* **2019**, *48*, 205–259.

[38] W. Li, H. Wang, X. Jiang, J. Zhu, Z. Liu, X. Guo, C. Song, A short review of recent advances in CO_2 hydrogenation to hydrocarbons over heterogeneous catalysts, *RSC Adv.* **2018**, *8*, 7651–7669.

[39] R. Francke, B. Schille, M. Roemelt, Homogeneously Catalyzed Electroreduction of Carbon Dioxide–Methods, Mechanisms, and Catalysts, *Chem. Rev.* **2018**, *118*, 4631–4701.

[40] L. Zhang, Z.-J. Zhao, J. Gong, Nanostructured Materials for Heterogeneous Electrocatalytic CO_2 Reduction and their Related Reaction Mechanisms, *Angew. Chem. Int. Ed.* **2017**, *56*, 11326–11353.

[41] H. Takeda, C. Cometto, O. Ishitani, M. Robert, Electrons, Photons, Protons and Earth-Abundant Metal Complexes for Molecular Catalysis of CO_2 Reduction, *ACS Catal.* **2017**, *7*, 70–88.

[42] J. Qiao, Y. Liu, F. Hong, J. Zhang, A review of catalysts for the electroreduction of carbon dioxide to produce low-carbon fuels, *Chem. Soc. Rev.* **2014**, *43*, 631–675.

[43] A. Goeppert, M. Czaun, J.-P. Jones, G. K. Surya Prakash, G. A. Olah, Recycling of carbon dioxide to methanol and derived products – closing the loop, *Chem. Soc. Rev.* **2014**, *43*, 7995–8048.

[44] X. Li, J. Yu, M. Jaroniec, X. Chen, Cocatalysts for Selective Photoreduction of CO_2 into Solar Fuels, *Chem. Rev.* **2019**, *119*, 3962–4179.

[45] Z. Sun, N. Talreja, H. Tao, J. Texter, M. Muhler, J. Strunk, J. Chen, Catalysis of Carbon Dioxide Photoreduction on Nanosheets: Fundamentals and Challenges, *Angew. Chem. Int. Ed.* **2018**, *57*, 7610–7627.

[46] J. K. Stolarczyk, S. Bhattacharyya, L. Polavarapu, J. Feldmann, Challenges and Prospects in Solar Water Splitting and CO_2 Reduction with Inorganic and Hybrid Nanostructures, *ACS Catal.* **2018**, *8*, 3602–3635.

[47] X. Liu, S. Inagaki, J. Gong, Heterogeneous Molecular Systems for Photocatalytic CO_2 Reduction with Water Oxidation, *Angew. Chem. Int. Ed.* **2016**, *55*, 14924–14950.

[48] K. Li, B. Peng, T. Peng, Recent Advances in Heterogeneous Photocatalytic CO_2 Conversion to Solar Fuels, *ACS Catal.* **2016**, *6*, 7485–7527.

[49] J. L. White, M. F. Baruch, J. E. Pander III, Y. Hu, I. C. Fortmeyer, J. E. Park, T. Zhang, K. Liao, J. Gu, Y. Yan, T. W. Shaw, E. Abelev, A. B. Bocarsly, Light-Driven Heterogeneous Reduction of Carbon Dioxide: Photocatalysts and Photoelectrodes, *Chem. Rev.* **2015**, *115*, 12888–12935.

[50] J. Klankermayer, S. Wesselbaum, K. Beydoun, W. Leitner, Selective Catalytic Synthesis Using the Combination of Carbon Dioxide and Hydrogen: Catalytic Chess at the Interface of Energy and Chemistry, *Angew. Chem. Int. Ed.* **2016**, *55*, 7296–7343.

[51] J. Klankermayer, W. Leitner, Love at second sight for CO_2 and H_2 in organic synthesis, *Science* **2015**, *350*, 629–630.

[52] K. Sordakis, C. Tang, L. K. Vogt, H. Junge, P. J. Dyson, M. Beller, G. Laurenczy, Homogeneous Catalysis for Sustainable Hydrogen Storage in Formic Acid and Alcohols, *Chem. Rev.* **2018**, *118*, 372–433.

[53] A. Álvarez, A. Bansode, A. Urakawa, A. V. Bavykina, T. A. Wezendonk, M. Makkee, J. Gascon, F. Kapteijn, Challenges in the Greener Production of Formates/Formic Acid, Methanol, and DME by Heterogeneously Catalyzed CO_2 Hydrogenation Processes, *Chem. Rev.* **2017**, *117*, 9804–9838.

[54] D. Mellmann, P. Sponholz, H. Junge, M. Beller, Formic acid as a hydrogen storage material – development of homogeneous catalysts for selective hydrogen release, *Chem. Soc. Rev.* **2016**, *45*, 3954–3988.

[55] W.-H. Wang, Y. Himeda, J. T. Muckerman, G. F. Manbeck, E. Fujita, CO_2 Hydrogenation to Formate and Methanol as an Alternative to Photo- and Electrochemical CO_2 Reduction, *Chem. Rev.* **2015**, *115*, 12936–12973.

[56] J. Zhong, X. Yang, Z. Wu, B. Liang, Y. Huang, T. Zhang, State of the art and perspectives in heterogeneous catalysis of CO_2 hydrogenation to methanol, *Chem. Soc. Rev.* **2020**, *49*, 1385–1413.

[57] T. Schaub, CO_2-based hydrogen storage: CO_2 hydrogenation to formic acid, formaldehyde and methanol, *Phys. Sci. Rev.* **2018**, *3*, 20170015.

[58] T. Schaub, CO2-based hydrogen storage: CO2 hydrogenation to formic acid, formaldehyde and methanol in *Hydrogen Storage*, (Eds.: T. Zell, R. Langer), De Gruyter, Berlin, **2018**.

[59] M. Trincado, H. Grützmacher, M. H. G. Prechtl, CO_2-based hydrogen storage – Hydrogen generation from formaldehyde/water, *Phys. Sci. Rev.* **2018**, *3*, 20170013.

[60] M. Trincado, H. Grützmacher, M. H. G. Prechtl, CO_2-based hydrogen storage – Hydrogen generation from formaldehyde/water in *Hydrogen Storage*, (Eds.: T. Zell, R. Langer), De Gruyter, Berlin, **2018**.

[61] L. E. Heim, H. Konnerth, M. H. G. Prechtl, Future perspectives for formaldehyde: pathways for reductive synthesis and energy storage, *Green Chem.* **2017**, *19*, 2347–2355.

[62] A. W. Franz, H. Kronemayer, D. Pfeiffer, R. D. Pilz, G. Reuss, W. Disteldorf, A. O. Gamer, A. Hilt, Formaldehyde in *Ullmann's Encyclopedia of Industrial Chemistry*, Wiley-VCH, **2016**.

[63] J. Ott, V. Gronemann, F. Pontzen, E. Fiedler, G. Grossmann, D. B. Kersebohm, G. Weiss, C. Witte, Methanol in *Ullmann's Encyclopedia of Industrial Chemistry*, Wiley-VCH, **2012**.

[64] S. Dabral, T. Schaub, The Use of Carbon Dioxide (CO_2) as a Building Block in Organic Synthesis from an Industrial Perspective, *Adv. Synth. Catal.* **2019**, *361*, 223–246.

[65] N. Armaroli, V. Balzani, The Hydrogen Issue, *ChemSusChem* **2011**, *4*, 21–36.

[66] S. Dunn, History of Hydrogen in *Concise Encyclopedia of the History of Energy*, (Ed.: C. J. Cleveland), Elsevier, Boston, **2009**.

[67] *IRENA, 2020: Global Renewables Outlook: Energy transformation 2050*, International Renewable Energy Agency, Abu Dhabi, **2020**.

[68] *REN21: Renewables 2019 Global Status Report*, REN21 Secretariat, Paris, **2019**.

[69] *Renewable Hydrogen Technologies*, (Eds.: L. M. Gandía, G. Arzamendi, P. M. Diéguez), Elsevier, Amsterdam, **2013**.

[70] M. Ball, W. Weindorf, U. Bünger, Hydrogen production in *The Hydrogen Economy: Opportunities and Challenges*, (Eds.: M. Ball, M. Wietschel), Cambridge University Press, New York, **2009**.

[71] W. McDowall, M. Eames, Forecasts, scenarios, visions, backcasts and roadmaps to the hydrogen economy: A review of the hydrogen futures literature, *Energy Policy* **2006**, *34*, 1236–1250.

[72] J. R. Bartels, M. B. Pate, N. K. Olson, An economic survey of hydrogen production from conventional and alternative energy sources, *Int. J. Hydrog. Energy* **2010**, *35*, 8371–8384.

[73] *IRENA, 2018: Hydrogen from renewable power: Technology outlook for the energy transition*, International Renewable Energy Agency, Abu Dhabi, **2018**.

[74] S. R. Tamang, M. Findlater, Cobalt catalysed reduction of CO_2 *via* hydroboration, *Dalton Trans.* **2018**, *47*, 8199–8203.

[75] A. Ramos, A. Antiñolo, F. Carrillo-Hermosilla, R. Fernández-Galán, A. Rodríguez-Diéguez, D. García-Vivó, Carbodiimides as catalysts for the reduction of CO_2 with boranes, *Chem. Commun.* **2018**, *54*, 4700–4703.

[76] Y. Yang, L. Yan, Q. Xie, Q. Liang, D. Song, Zwitterionic indenylammonium with carbon-centred reactivity towards reversible CO_2 binding and catalytic reduction, *Org. Biomol. Chem.* **2017**, *15*, 2240–2245.

[77] S. C. Sau, R. Bhattacharjee, P. K. Vardhanapu, G. Vijaykumar, A. Datta, S. K. Mandal, Metal-Free Reduction of CO_2 to Methoxyborane under Ambient Conditions through Borondiformate Formation, *Angew. Chem. Int. Ed.* **2016**, *55*, 15147–15151.

[78] T. Janes, K. M. Osten, A. Pantaleo, E. Yan, Y. Yang, D. Song, Insertion of CO_2 into the carbon–boron bond of a boronic ester ligand, *Chem. Commun.* **2016**, *52*, 4148–4151.

[79] Y. Yang, M. Xu, D. Song, Organocatalysts with carbon-centered activity for CO_2 reduction with boranes, *Chem. Commun.* **2015**, *51*, 11293–11296.

[80] M.-A. Courtemanche, A. P. Pulis, É. Rochette, M.-A. Légaré, D. W. Stephan, F.-G. Fontaine, Intramolecular B/N frustrated Lewis pairs and the hydrogenation of carbon dioxide, *Chem. Commun.* **2015**, *51*, 9797–9800.

[81] T. Wang, D. W. Stephan, Phosphine catalyzed reduction of CO_2 with boranes, *Chem. Commun.* **2014**, *50*, 7007–7010.

[82] T. Wang, D. W. Stephan, Carbene-9-BBN Ring Expansions as a Route to Intramolecular Frustrated Lewis Pairs for CO_2 Reduction, *Chem. Eur. J.* **2014**, *20*, 3036–3039.

[83] H.-W. Suh, L. M. Guard, N. Hazari, A mechanistic study of allene carboxylation with CO_2 resulting in the development of a Pd(II) pincer complex for the catalytic hydroboration of CO_2, *Chem. Sci.* **2014**, *5*, 3859–3872.

[84] H.-W. Suh, L. M. Guard, N. Hazari, Synthesis and reactivity of a masked PSiP pincer supported nickel hydride, *Polyhedron* **2014**, *84*, 37–43.

[85] C. Das Neves Gomes, E. Blondiaux, P. Thuéry, T. Cantat, Metal-Free Reduction of CO_2 with Hydroboranes: Two Efficient Pathways at Play for the Reduction of CO_2 to Methanol, *Chem. Eur. J.* **2014**, *20*, 7098–7106.

[86] M. D. Anker, M. Arrowsmith, P. Bellham, M. S. Hill, G. Kociok-Köhn, D. J. Liptrot, M. F. Mahon, C. Weetman, Selective reduction of CO_2 to a methanol equivalent by $B(C_6F_5)_3$-activated alkaline earth catalysis, *Chem. Sci.* **2014**, *5*, 2826–2830.

[87] M. R. Espinosa, D. J. Charboneau, A. Garcia de Oliveira, N. Hazari, Controlling Selectivity in the Hydroboration of Carbon Dioxide to the Formic Acid, Formaldehyde, and Methanol Oxidation Levels, *ACS Catal.* **2019**, *9*, 301–314.

[88] L. J. Murphy, H. Hollenhorst, R. McDonald, M. Ferguson, M. D. Lumsden, L. Turculet, Selective Ni-Catalyzed Hydroboration of CO_2 to the Formaldehyde Level Enabled by New PSiP Ligation, *Organometallics* **2017**, *36*, 3709–3720.

[89] A. Aloisi, J.-C. Berthet, C. Genre, P. Thuéry, T. Cantat, Complexes of the tripodal phosphine ligands $PhSi(XPPh_2)_3$ (X = CH_2, O): synthesis, structure and catalytic activity in the hydroboration of CO_2, *Dalton Trans.* **2016**, *45*, 14774–14788.

[90] G. Jin, C. G. Werncke, Y. Escudié, S. Sabo-Etienne, S. Bontemps, Iron-Catalyzed Reduction of CO_2 into Methylene: Formation of C–N, C–O, and C–C Bonds, *J. Am. Chem. Soc.* **2015**, *137*, 9563–9566.

[91] S. Bontemps, L. Vendier, S. Sabo-Etienne, Ruthenium-Catalyzed Reduction of Carbon Dioxide to Formaldehyde, *J. Am. Chem. Soc.* **2014**, *136*, 4419–4425.

[92] S. Bontemps, S. Sabo-Etienne, Trapping Formaldehyde in the Homogeneous Catalytic Reduction of Carbon Dioxide, *Angew. Chem. Int. Ed.* **2013**, *52*, 10253–10255.

[93] S. Bontemps, L. Vendier, S. Sabo-Etienne, Borane-Mediated Carbon Dioxide Reduction at Ruthenium: Formation of C_1 and C_2 Compounds, *Angew. Chem. Int. Ed.* **2012**, *51*, 1671–1674.

[94] X. Zhang, J. Sun, G. Wei, Z. Liu, H. Yang, K. Wang, H. Fei, In Situ Generation of an N-Heterocyclic Carbene Functionalized Metal–Organic Framework by Postsynthetic Ligand Exchange: Efficient and Selective Hydrosilylation of CO_2, *Angew. Chem. Int. Ed.* **2019**, *58*, 2844–2849.

[95] D. Specklin, F. Hild, C. Fliedel, C. Gourlaouen, L. F. Veiros, S. Dagorne, Accessing Two-Coordinate Zn^{II} Organocations by NHC Coordination: Synthesis, Structure, and Use as π-Lewis Acids in Alkene, Alkyne, and CO_2 Hydrosilylation, *Chem. Eur. J.* **2017**, *23*, 15908–15912.

[96] J. Chen, L. Falivene, L. Caporaso, L. Cavallo, E. Y.-X. Chen, Selective Reduction of CO_2 to CH_4 by Tandem Hydrosilylation with Mixed Al/B Catalysts, *J. Am. Chem. Soc.* **2016**, *138*, 5321–5333.

[97] Z. Lu, H. Hausmann, S. Becker, H. A. Wegner, Aromaticity as Stabilizing Element in the Bidentate Activation for the Catalytic Reduction of Carbon Dioxide, *J. Am. Chem. Soc.* **2015**, *137*, 5332–5335.

[98] M. L. Scheuermann, S. P. Semproni, I. Pappas, P. J. Chirik, Carbon Dioxide Hydrosilylation Promoted by Cobalt Pincer Complexes, *Inorg. Chem.* **2014**, *53*, 9463–9465.

[99] A. Berkefeld, W. E. Piers, M. Parvez, L. Castro, L. Maron, O. Eisenstein, Decamethylscandocinium-hydrido-(perfluorophenyl)borate: fixation and tandem tris(perfluorophenyl)borane catalysed deoxygenative hydrosilation of carbon dioxide, *Chem. Sci.* **2013**, *4*, 2152–2162.

[100] S. Park, D. Bézier, M. Brookhart, An Efficient Iridium Catalyst for Reduction of Carbon Dioxide to Methane with Trialkylsilanes, *J. Am. Chem. Soc.* **2012**, *134*, 11404–11407.

[101] S. J. Mitton, L. Turculet, Mild Reduction of Carbon Dioxide to Methane with Tertiary Silanes Catalyzed by Platinum and Palladium Silyl Pincer Complexes, *Chem. Eur. J.* **2012**, *18*, 15258–15262.

[102] A. Berkefeld, W. E. Piers, M. Parvez, Tandem Frustrated Lewis Pair/Tris(pentafluorophenyl)borane-Catalyzed Deoxygenative Hydrosilylation of Carbon Dioxide, *J. Am. Chem. Soc.* **2010**, *132*, 10660–10661.

[103] S. N. Riduan, Y. Zhang, J. Y. Ying, Conversion of Carbon Dioxide into Methanol with Silanes over N-Heterocyclic Carbene Catalysts, *Angew. Chem. Int. Ed.* **2009**, *48*, 3322–3325.

[104] T. Matsuo, H. Kawaguchi, From Carbon Dioxide to Methane: Homogeneous Reduction of Carbon Dioxide with Hydrosilanes Catalyzed by Zirconium–Borane Complexes, *J. Am. Chem. Soc.* **2006**, *128*, 12362–12363.

[105] T. C. Eisenschmid, R. Eisenberg, The iridium complex catalyzed reduction of carbon dioxide to methoxide by alkylsilanes, *Organometallics* **1989**, *8*, 1822–1824.

[106] M. Rauch, Z. Strater, G. Parkin, Selective Conversion of Carbon Dioxide to Formaldehyde via a Bis(silyl)acetal: Incorporation of Isotopically Labeled C_1 Moieties Derived from Carbon Dioxide into Organic Molecules, *J. Am. Chem. Soc.* **2019**, *141*, 17754–17762.

[107] N. Del Rio, M. Lopez-Reyes, A. Baceiredo, N. Saffon-Merceron, D. Lutters, T. Müller, T. Kato, N,P-Heterocyclic Germylene/$B(C_6F_5)_3$ Adducts: A Lewis Pair with Multireactive Sites, *Angew. Chem. Int. Ed.* **2017**, *56*, 1365–1370.

[108] P. Ríos, A. Rodríguez, J. López-Serrano, Mechanistic Studies on the Selective Reduction of CO_2 to the Aldehyde Level by a Bis(phosphino)boryl (PBP)-Supported Nickel Complex, *ACS Catal.* **2016**, *6*, 5715–5723.

[109] P. Ríos, N. Curado, J. López-Serrano, A. Rodríguez, Selective reduction of carbon dioxide to bis(silyl)acetal catalyzed by a PBP-supported nickel complex, *Chem. Commun.* **2016**, *52*, 2114–2117.

[110] T. T. Metsänen, M. Oestreich, Temperature-Dependent Chemoselective Hydrosilylation of Carbon Dioxide to Formaldehyde or Methanol Oxidation State, *Organometallics* **2015**, *34*, 543–546.

[111] F. A. LeBlanc, W. E. Piers, M. Parvez, Selective Hydrosilation of CO_2 to a Bis(silylacetal) Using an Anilido Bipyridyl-Ligated Organoscandium Catalyst, *Angew. Chem. Int. Ed.* **2014**, *53*, 789–792.

[112] Y. Jiang, O. Blacque, T. Fox, H. Berke, Catalytic CO_2 Activation Assisted by Rhenium Hydride/$B(C_6F_5)_3$ Frustrated Lewis Pairs–Metal Hydrides Functioning as FLP Bases, *J. Am. Chem. Soc.* **2013**, *135*, 7751–7760.

[113] P. Arya, J. Boyer, R. J. P. Corriu, G. F. Lanneau, M. Perrot, Reactivity of hypervalent species of silicon: reduction of CO_2 to formaldehyde with formation of silanone, *J. Organomet. Chem.* **1988**, *346*, C11–C14.

[114] N. E. Schlörer, E. J. Cabrita, S. Berger, Characterization of Reactive Intermediates by Diffusion-Ordered NMR Spectroscopy: A Snapshot of the Reaction of $^{13}CO_2$ with $[Cp_2Zr(Cl)H]$, *Angew. Chem. Int. Ed.* **2002**, *41*, 107–109.

[115] N. E. Schlörer, S. Berger, First Spectroscopical Evidence of a Dioxomethylene Intermediate in the Reaction of CO_2 with $Cp_2Zr(H)Cl$: A ^{13}C NMR Study, *Organometallics* **2001**, *20*, 1703–1704.

[116] S. Gambarotta, S. Strologo, C. Floriani, A. Chiesi-Villa, C. Guastini, Stepwise reduction of carbon dioxide to formaldehyde and methanol: reactions of carbon dioxide and carbon dioxide like molecules with hydridochlorobis(cyclopentadienyl)zirconium(IV), *J. Am. Chem. Soc.* **1985**, *107*, 6278–6282.

[117] G. Fachinetti, C. Floriani, S. Pucci, Stoicheiometric reduction of CO and CO_2 to methanol: evidence for carbon monoxide insertion into zirconium–hydrogen bond, *J. Chem. Soc., Chem. Commun.* **1978**, 269–270.

[118] P. Etievant, G. Tainturier, B. Gautheron, Quelques aspects de la réactivité de l'hydrurochlorure de zirconocène, *C. R. Acad. Sc. Paris, Série C* **1976**, *283*, 233–236.

[119] M. A. Rankin, C. C. Cummins, Carbon Dioxide Reduction by Terminal Tantalum Hydrides: Formation and Isolation of Bridging Methylene Diolate Complexes, *J. Am. Chem. Soc.* **2010**, *132*, 10021–10023.

[120] O. Tardif, D. Hashizume, Z. Hou, Hydrogenation of Carbon Dioxide and Aryl Isocyanates by a Tetranuclear Tetrahydrido Yttrium Complex. Isolation, Structures, and CO_2 Insertion Reactions of Methylene Diolate and μ_3-Oxo Yttrium Complexes, *J. Am. Chem. Soc.* **2004**, *126*, 8080–8081.

[121] J. Rajpurohit, A. Upadhyay, C. Das, R. Dubey, S. Vaidya, V. Krishnan, A. Kumar, M. Shanmugam, Unusual Methylenediolate Bridged Hexanuclear Ruthenium(III) Complexes: Syntheses and Their Application, *Inorg. Chem.* **2018**, *57*, 14967–14982.

[122] E. Y. Fursova, G. V. Romanenko, V. I. Ovcharenko, Hexanuclear methanediolate bridged iron(III) complex, *Russ. Chem. Bull.* **2005**, *54*, 811–813.

[123] N. E. Chakov, L. N. Zakharov, A. L. Rheingold, K. A. Abboud, G. Christou, New Polynuclear Manganese Clusters from the Use of the Hydrophobic Carboxylate Ligand 2,2-Dimethylbutyrate, *Inorg. Chem.* **2005**, *44*, 4555–4567.

[124] M. Murugesu, K. A. Abboud, G. Christou, New hexanuclear and dodecanuclear Fe(III) clusters with carboxylate and alkoxide-based ligands from cluster aggregation reactions, *Polyhedron* **2004**, *23*, 2779–2788.

[125] V. W. Day, M. F. Fredrich, W. G. Klemperer, R. S. Liu, Polyoxomolybdate-hydrocarbon interactions. Synthesis and structure of the $CH_2Mo_4O_{15}H^{3-}$ anion and related methylenedioxymolybdates, *J. Am. Chem. Soc.* **1979**, *101*, 491–492.

[126] D.-K. Lee, D.-S. Kim, S.-W. Kim, Selective formation of formaldehyde from carbon dioxide and hydrogen over $PtCu/SiO_2$, *Appl. Organomet. Chem.* **2001**, *15*, 148–150.

[127] S. Carenco, C.-H. Wu, A. Shavorskiy, S. Alayoglu, G. A. Somorjai, H. Bluhm, M. Salmeron, Synthesis and Structural Evolution of Nickel–Cobalt Nanoparticles Under H_2 and CO_2, *Small* **2015**, *11*, 3045–3053.

[128] F. L. Chan, G. Altinkaya, N. Fung, A. Tanksale, Low temperature hydrogenation of carbon dioxide into formaldehyde in liquid media, *Catal. Today* **2018**, *309*, 242–247.

[129] W. Ahmad, F. L. Chan, A. Hoadley, H. Wang, A. Tanksale, Synthesis of oxymethylene dimethyl ethers (OME_n) via methanol mediated CO_x hydrogenation over Ru/BEA catalysts, *Appl. Catal. B* **2020**, *269*, 118765.

[130] M. M. T. Khan, S. B. Halligudi, S. Shukla, Reduction of CO_2 by molecular hydrogen to formic acid and formaldehyde and their decomposition to CO and H_2O, *J. Mol. Catal.* **1989**, *57*, 47–60.

[131] K. Thenert, K. Beydoun, J. Wiesenthal, W. Leitner, J. Klankermayer, Ruthenium-Catalyzed Synthesis of Dialkoxymethane Ethers Utilizing Carbon Dioxide and Molecular Hydrogen, *Angew. Chem. Int. Ed.* **2016**, *55*, 12266–12269.

[132] C. H. Gierlich, K. Beydoun, J. Klankermayer, R. Palkovits, Challenges and Opportunities in the Production of Oxymethylene Dimethylether, *Chem. Ing. Tech.* **2020**, *92*, 116–124.

[133] R. Sun, I. Delidovich, R. Palkovits, Dimethoxymethane as a Cleaner Synthetic Fuel: Synthetic Methods, Catalysts, and Reaction Mechanism, *ACS Catal.* **2019**, *9*, 1298–1318.

[134] S. Deutz, D. Bongartz, B. Heuser, A. Kätelhön, L. Schulze Langenhorst, A. Omari, M. Walters, J. Klankermayer, W. Leitner, A. Mitsos, S. Pischinger, A. Bardow, Cleaner production of cleaner fuels: wind-to-wheel – environmental assessment of CO_2-based oxymethylene ether as a drop-in fuel, *Energy Environ. Sci.* **2018**, *11*, 331–343.

[135] S. Wesselbaum, V. Moha, M. Meuresch, S. Brosinski, K. M. Thenert, J. Kothe, T. vom Stein, U. Englert, M. Hölscher, J. Klankermayer, W. Leitner, Hydrogenation of carbon dioxide to methanol using a homogeneous ruthenium–Triphos catalyst: from mechanistic investigations to multiphase catalysis, *Chem. Sci.* **2015**, *6*, 693–704.

[136] T. vom Stein, M. Meuresch, D. Limper, M. Schmitz, M. Hölscher, J. Coetzee, D. J. Cole-Hamilton, J. Klankermayer, W. Leitner, Highly Versatile Catalytic Hydrogenation of Carboxylic and Carbonic Acid Derivatives using a Ru-Triphos Complex: Molecular Control over Selectivity and Substrate Scope, *J. Am. Chem. Soc.* **2014**, *136*, 13217–13225.

[137] J. Coetzee, D. L. Dodds, J. Klankermayer, S. Brosinski, W. Leitner, A. M. Z. Slawin, D. J. Cole-Hamilton, Homogeneous Catalytic Hydrogenation of Amides to Amines, *Chem. Eur. J.* **2013**, *19*, 11039–11050.

[138] B. G. Schieweck, J. Klankermayer, Tailor-made Molecular Cobalt Catalyst System for the Selective Transformation of Carbon Dioxide to Dialkoxymethane Ethers, *Angew. Chem. Int. Ed.* **2017**, *56*, 10854–10857.

[139] M. Meuresch, S. Westhues, W. Leitner, J. Klankermayer, Tailor-Made Ruthenium-Triphos Catalysts for the Selective Homogeneous Hydrogenation of Lactams, *Angew. Chem. Int. Ed.* **2016**, *55*, 1392–1395.

[140] K. Beydoun, J. Klankermayer, Ruthenium-Catalyzed Synthesis of Cyclic and Linear Acetals by the Combined Utilization of CO_2, H_2, and Biomass Derived Diols, *Chem. Eur. J.* **2019**, *25*, 11412–11415.

[141] G. Brereton, R. M. Emanuel Jr, R. Lomax, K. Pennington, T. Ryan, H. Tebbe, M. Timm, P. Ware, K. Winkler, T. Yuan, Z. Zhu, N. Adam, G. Avar, H. Blankenheim, W. Friederichs, M. Giersig, E. Weigand, M. Halfmann, F.-W. Wittbecker, D.-R. Larimer, U. Maier, S. Meyer-Ahrens, K.-L. Noble, H.-G. Wussow, Polyurethanes in *Ullmann's Encyclopedia of Industrial Chemistry*, Wiley-VCH, **2019**.

[142] M. Widemann, P. J. Driest, P. Orecchia, F. Naline, F. E. Golling, A. Hecking, C. Eggert, R. Pires, K. Danielmeier, F. U. Richter, Structure–Property Relations in Oligomers of Linear Aliphatic Diisocyanates, *ACS Sustain. Chem. Eng.* **2018**, *6*, 9753–9759.

[143] H. J. Laas, R. Halpaap, J. Pedain, Zur Synthese aliphatischer Polyisocyanate – Lackpolyisocyanate mit Biuret-, Isocyanurat- oder Uretdionstruktur, *J. Prakt. Chem.* **1994**, *336*, 185–200.

[144] U. Meier-Westhues, K. Danielmeier, P. Kruppa, E. P. Squiller, *Polyurethanes: Coatings, Adhesives and Sealants*, 2nd ed., Vincentz Network, Hanover, **2019**.

[145] A. Goldschmidt, H.-J. Streitberger, *BASF Handbook Basics of Coating Technology*, 3rd ed., Vincentz Network, Hanover, **2018**.

[146] M. F. Sonnenschein, *Polyurethanes: Science, Technology, Markets, and Trends*, John Wiley & Sons, Hoboken, **2014**.

[147] H. R. Sharpe, A. M. Geer, H. E. L. Williams, T. J. Blundell, W. Lewis, A. J. Blake, D. L. Kays, Cyclotrimerisation of isocyanates catalysed by low-coordinate Mn(II) and Fe(II) *m*-terphenyl complexes, *Chem. Commun.* **2017**, *53*, 937–940.

[148] Z. Guo, X. Wei, H. Tong, D. Liu, Tridentate pyrrolylzinc compounds: Synthesis, structures, reactivities and catalytic cyclotrimerization reaction of isocyanate, *J. Organomet. Chem.* **2015**, *776*, 136–142.

[149] A. Hernán-Gómez, T. D. Bradley, A. R. Kennedy, Z. Livingstone, S. D. Robertson, E. Hevia, Developing catalytic applications of cooperative bimetallics: competitive hydroamination/trimerization reactions of isocyanates catalysed by sodium magnesiates, *Chem. Commun.* **2013**, *49*, 8659–8661.

[150] Y. Li, H. Matsumura, M. Yamanaka, T. Takahashi, Haloamidation of alkynes and related reactions using zirconacycles and isocyanates, *Tetrahedron* **2004**, *60*, 1393–1400.

[151] J. Zhang, R. Ruan, Z. Shao, R. Cai, L. Weng, X. Zhou, Insertion of Carbodiimide into the Ln–C σ-Bond of Organolanthanide Complexes. Synthesis, Reaction, and Characterization of Organolanthanide Amidinates $(C_5H_5)_2Ln[^tBuN{=}C(^nBu){=}N^tBu]$ (Ln = Er, Gd, Y), *Organometallics* **2002**, *21*, 1420–1424.

[152] F. Montilla, E. Clara, T. Avilés, T. Casimiro, A. Aguiar Ricardo, M. Nunes da Ponte, Transition-metal-mediated activation of arylisocyanates in supercritical carbon dioxide, *J. Organomet. Chem.* **2001**, *626*, 227–232.

[153] W. Uhl, U. Schütz, S. Pohl, W. Saak, Umsetzungen des Tetrakis[bis(trimethylsilyl)-methyl]dialans(4) mit Methylisothiocyanat und Phenylisocyanat – Insertion in die Al–Al-Bindung bzw. Fragmentierung, *Z. Anorg. Allg. Chem.* **1996**, *622*, 373–379.

[154] R. J. P. Corriu, G. F. Lanneau, V. D. Mehta, Catalytic Trimerization of Isocyanates by Neutral Pentacoordinated Silicon Hydrides, *Heteroat. Chem* **1991**, *2*, 461–463.

[155] E. Martelli, C. Pelizzi, G. Predieri, Cyclotrimerization of Aryl Isocyanates Photocatalyzed by a Metal Carbonyl Complex, *J. Mol. Catal.* **1983**, *22*, 89–91.

[156] T. Kashiwagi, M. Hidai, Y. Uchida, A. Misono, Polymerization and trimerization of isocyanates catalyzed by nickel complexes, *J. Polym. Sci., Part B: Polym. Lett.* **1970**, *8*, 173–175.

[157] J. G. Noltes, J. Boersma, Trimerization of isocyanates by organozinc amines and alkoxides: an example of homogeneous coordination catalysis involving a template effect, *J. Organomet. Chem.* **1967**, *7*, P6–P8.

[158] S. Herbstman, Trimerization of Isocyanates by Trialkylantimony and -arsenic Oxides, *J. Org. Chem.* **1965**, *30*, 1259–1260.

[159] A. J. Bloodworth, A. G. Davies, Organometallic Reactions. Part III. Trimerisation of Isocyanates by Organotin Alkoxides and Oxides, *J. Chem. Soc.* **1965**, 6858–6863.

[160] K. Naktode, S. Das, J. Bhattacharjee, H. P. Nayek, T. K. Panda, Imidazolin-2-iminato Ligand-Supported Titanium Complexes as Catalysts for the Synthesis of Urea Derivatives, *Inorg. Chem.* **2016**, *55*, 1142–1153.

[161] M. K. Barman, A. Baishya, T. Peddarao, S. Nembenna, Guanidinate stabilized germanium(II) and tin(II) amide complexes and their catalytic activity for aryl isocyanate cyclization, *J. Organomet. Chem.* **2014**, *772-773*, 265–270.

[162] Z. Guo, S. Wang, H. Tong, J. Chao, X. Wei, Bidentate pyrrolyl lithium complexes: Synthesis, crystal structure and catalytic activity for the cyclotrimerization of isocyanates, *Inorg. Chem. Commun.* **2013**, *33*, 68–72.

[163] H.-M. Wang, H.-X. Li, X.-Y. Yu, Z.-G. Ren, J.-P. Lang, Cyclodimerization and cyclotrimerization of isocyanates promoted by one praseodymium benzenethiolate complex $[Pr(SPh)_3(THF)_3]$, *Tetrahedron* **2011**, *67*, 1530–1535.

[164] X. Zhu, J. Fan, Y. Wu, S. Wang, L. Zhang, G. Yang, Y. Wei, C. Yin, H. Zhu, S. Wu, H. Zhang, Synthesis, Characterization, Selective Catalytic Activity, and Reactivity of Rare Earth Metal Amides with Different Metal–Nitrogen Bonds, *Organometallics* **2009**, *28*, 3882–3888.

[165] H. Peng, Y. Yao, M. Deng, Y. Zhang, Q. Shen, Synthesis and Characterization of A Polynuclear Yttrium Trifluoroethoxide and Its Activity for Oligomerization of Phenyl Isocyanate, *J. Rare Earths* **2006**, *24*, 509–512.

[166] S. R. Foley, Y. Zhou, G. P. A. Yap, D. S. Richeson, Synthesis of $M^{II}[N(SiMe_3)_2][Me_3SiNC(^tBu)NSiMe_3]$ (M = Sn, Ge) from Amidinate Precursors: Active Catalysts for Phenyl Isocyanate Cyclization, *Inorg. Chem.* **2000**, *39*, 924–929.

[167] S. R. Foley, G. P. A. Yap, D. S. Richeson, Formation of Novel Tetrasulfido Tin Complexes and Their Ability To Catalyze the Cyclotrimerization of Aryl Isocyanates, *Organometallics* **1999**, *18*, 4700–4705.

[168] B. Srinivas, C.-C. Chang, C.-H. Chen, M. Y. Chiang, I.-T. Chen, Y. Wang, G.-H. Lee, Synthesis, characterization and crystal structures of isothiocyanate and carbodiimide complexes derived from organomagnesium reagents: insertion into Mg–X (X = C or N) bonds, *J. Chem. Soc., Dalton Trans.* **1997**, 957–964.

[169] O. Yilmaz, A. Usanmaz, K. Alyürük, Polymerization of Monoisocyanates by the Pruitt–Baggett Adduct, *J. Polym. Sci., Part A: Polym. Chem.* **1993**, *31*, 3205–3211.

[170] J. C. Graham, X. Xu, M. Orticochea, Bis(ethyl-3-oxo-butanolato-O^1, O^3)-bis(2-propanolato) titanium (tyzor DC^R) as a reactant and catalyst in the trimerization of 2-isocyanatoethyl methacrylate (IEM), *Catal. Lett.* **1989**, *3*, 413–420.

[171] A. Flamini, A. M. Giuliani, N. Poli, Catalytic activation of phenylisocyanate by $Ti(bpy)_3$, *Tetrahedron Lett.* **1987**, *28*, 2169–2170.

[172] W. Ikuko, S. Hiroshi, K. Ichiro, The Cyclic Trimerization of Isocyanates by Organic Tin(II) Compounds Containing Sn–O–C Bonds, *Bull. Chem. Soc. Jpn.* **1975**, *48*, 1069–1070.

[173] J. Shi, Z. Guo, X. Wei, D. Liu, M. F. Lappert, Lithium Dibenzylamide, a Simple, Selective and Highly Efficient Catalyst for Isocyanate Cyclotrimerization to Isocyanurate, *Synlett* **2011**, *2011*, 1937–1939.

[174] M. G. Dekamin, K. Varmira, M. Farahmand, S. Sagheb-Asl, Z. Karimi, Organocatalytic, rapid and facile cyclotrimerization of isocyanates using tetrabutylammonium phthalimide-*N*-oxyl and tetraethylammonium 2-(carbamoyl)benzoate under solvent-free conditions, *Catal. Commun.* **2010**, *12*, 226–230.

[175] I. M. Davletbaeva, V. F. Shkodich, E. O. Ekimova, A. M. Gumerov, Study of Isocyanate Group Opening Initiated by Potassium Polyoxyethylene Glycolate, *Polym. Sci., Ser. A* **2007**, *49*, 896–902.

[176] F. M. Moghaddam, M. G. Dekamin, G. R. Koozehgari, A Simple and Efficient Method for Synthesis of Isocyanurates Catalyzed by Potassium Phthalimide Under Solvent-Free Conditions, *Lett. Org. Chem.* **2005**, *2*, 734–738.

[177] M. S. Khajavi, M. G. Dakamin, H. Hazarkhani, Solvent-free cyclotrimerization of isocyanates catalysed by sodium or potassium piperidinedithiocarbamate or nitrite under conventional or microwave heating: preparation of aryl or alkyl isocyanurates, *J. Chem. Res.* **2000**, *2000*, 145–148.

[178] Y. Nambu, T. Endo, Synthesis of Novel Aromatic Isocyanurates by the Fluoride-Catalyzed Selective Trimerization of Isocyanates, *J. Org. Chem.* **1993**, *58*, 1932–1934.

[179] P. A. Argabright, B. L. Phillips, C. H. DePuy, Chemistry of Isocyanurates. I. Synthesis of Disubstituted Isocyanuric Acids from the Reaction of Alkali Metal Cyanates with Organic Isocyanates, *J. Org. Chem.* **1970**, *35*, 2253–2257.

[180] A. G. Giuglio-Tonolo, C. Spitz, T. Terme, P. Vanelle, An expeditious method for the selective cyclotrimerization of isocyanates initiated by TDAE, *Tetrahedron Lett.* **2014**, *55*, 2700–2702.

[181] K. Uehara, K. Fukaya, N. Mizuno, Reactive N-Protonated Isocyanate Species Stabilized by Bis(μ-hydroxo)divanadium(IV)-Substituted Polyoxometalate, *Angew. Chem. Int. Ed.* **2012**, *51*, 7715–7718.

[182] B. C. Norris, D. G. Sheppard, G. Henkelman, C. W. Bielawski, Kinetic and Thermodynamic Evaluation of the Reversible N-Heterocyclic Carbene–Isothiocyanate Coupling Reaction: Applications in Latent Catalysis, *J. Org. Chem.* **2011**, *76*, 301–304.

[183] G. M. Pawar, M. R. Buchmeiser, Polymer-Supported, Carbon Dioxide-Protected N-Heterocyclic Carbenes: Synthesis and Application in Organo- and Organometallic Catalysis, *Adv. Synth. Catal.* **2010**, *352*, 917–928.

[184] H. A. Duong, M. J. Cross, J. Louie, N-Heterocyclic Carbenes as Highly Efficient Catalysts for the Cyclotrimerization of Isocyanates, *Org. Lett.* **2004**, *6*, 4679–4681.

[185] Y. Taguchi, I. Shibuya, M. Yasumoto, T. Tsuchiya, K. Yonemoto, The Synthesis of Isocyanurates on the Trimerization of Isocyanates under High Pressure, *Bull. Chem. Soc. Jpn.* **1990**, *63*, 3486–3489.

[186] I. C. Kogon, New Reactions of Phenyl Isocyanate and Ethyl Alcohol, *J. Am. Chem. Soc.* **1956**, *78*, 4911–4914.

[187] J. F. Villa, H. B. Powell, The Reaction of Some Inorganic Lewis Bases and Acids with Organic Isocyanates, *Synth. React. Inorg. Met.-Org. Chem.* **1976**, *6*, 59–63.

[188] M. A. Servos, N. C. Smart, M. E. Kassabaum, C. A. Scholtens, S. J. Peters, Phenyl Isocyanate Anion Radicals and Their Cyclotrimerization to Triphenyl Isocyanurate Anion Radicals, *J. Org. Chem.* **2013**, *78*, 3908–3917.

[189] S. J. Peters, J. R. Klen, N. C. Smart, Isocyanurate Anion Radicals via Electron-Initiated Cycloaddition of Isocyanates, *Org. Lett.* **2008**, *10*, 4521–4524.

[190] M. Ozaki, Y. Obora, Y. Tada, Y. Ishii, Generation of low-valent alkoxy niobium from $Nb(OEt)_5$ and Grignard reagents and their use as catalysts in the cyclotrimerization of isocyanates, *J. Organomet. Chem.* **2013**, *741-742*, 109–113.

[191] M. Moritsugu, A. Sudo, T. Endo, Development of High-Performance Networked Polymers Consisting of Isocyanurate Structures Based on Selective Cyclotrimerization of Isocyanates, *J. Polym. Sci., Part A: Polym. Chem.* **2011**, *49*, 5186–5191.

[192] M. G. Dekamin, S. Mallakpour, M. Ghassemi, Sulfate catalysed multicomponent cyclisation reaction of aryl isocyanates under green conditions, *J. Chem. Res.* **2005**, *2005*, 177–179.

[193] M. G. Dekamin, S. Mallakpour, M. Ghassemi, Combination of Sulfite Anion and Phase Transfer Catalysts for Green Cyclotrimerization of Aryl Isocyanates, *Synth. Commun.* **2005**, *35*, 427–434.

[194] F. M. Moghaddam, G. R. Koozehgiri, M. G. Dekamin, Solvent-free Efficient Synthesis of Symmetrical Isocyanurates by a Combination Catalyst: Sodium Saccharin and Tetrabutylammonium Iodide, *Monatsh. Chem.* **2004**, *135*, 849–851.

[195] F. M. Moghaddam, M. G. Dekamin, M. S. Khajavi, S. Jalili, Efficient and Selective Trimerization of Aryl and Alkyl Isocyanates Catalyzed by Sodium *p*-Toluenesulfinate in the Presence of TBAI in a Solvent-Free Condition, *Bull. Chem. Soc. Jpn.* **2002**, *75*, 851–852.

[196] M. Špírková, M. Kubín, P. Špaček, I. Krakovský, K. Dušek, Cyclotrimerization of Isocyanate Groups. I. Catalyzed Reactions of Phenyl Isocyanate, *J. Appl. Polym. Sci.* **1994**, *52*, 895–904.

[197] F. Marc, A. Saux, M. Ratier, J. G. Duboudin, G. Daudé, Quaternary ammonium halides/2-tributylstannylpropanol: an efficient cyclotrimerization catalyst system for aromatic isocyanurate synthesis, *Polymer* **1994**, *35*, 5146–5147.

[198] S.-W. Wong, K. C. Frisch, Catalysis in Competing Isocyanate Reactions. I. Effect of Organotin–Tertiary Amine Catalysts on Phenyl Isocyanate and *N*-Butanol Reaction, *J. Polym. Sci., Part A: Polym. Chem.* **1986**, *24*, 2867–2875.

[199] W. Yi, J. Zhang, L. Hong, Z. Chen, X. Zhou, Insertion of Isocyanate and Isothiocyanate into the Ln–P σ-Bond of Organolanthanide Phosphides, *Organometallics* **2011**, *30*, 5809–5814.

[200] L. Orzechowski, S. Harder, Isolation of an Intermediate in the Catalytic Trimerization of Isocyanates by a Monomeric Calcium Carbene with Chelating Iminophosphorane Substituents, *Organometallics* **2007**, *26*, 2144–2148.

[201] O. Blacque, H. Brunner, M. M. Kubicki, J.-C. Leblanc, W. Meier, C. Moise, Y. Mugnier, A. Sadorge, J. Wachter, M. Zabel, Investigation into the reactivity of oxoniobocene complexes [Cp*$_2$Nb(=O)R] (Cp* = η^5-C_5Me_5; R = H, OH, OMe) towards heterocumulenes: formation of carbamato and thiocarbamato complexes and catalytic cyclization of PhNCO, *J. Organomet. Chem.* **2001**, *634*, 47–54.

[202] L. Mao, Q. Shen, M. Xue, J. Sun, Syntheses of {(MeC_5H_4)$_2$Ln(THF)[O=CN(i-Pr)$_2$=NPh]} (Ln = Y, Er, Yb) and the X-ray Crystal Structure of the Yttrium Complex: The Active Species for Polymerization of Phenyl Isocyanate by (Diisopropylamido)bis(methylcyclopentadienyl)lanthanides, *Organometallics* **1997**, *16*, 3711–3714.

[203] S. G. Lee, K.-Y. Choi, Y.-J. Kim, S. Park, S. W. Lee, Cyclic tetramers of a five-membered palladacycle based on a head-to-tail-linked isocyanate dimer and their reactivity in cyclotrimerization of isocyanates, *Dalton Trans.* **2015**, *44*, 6537–6545.

[204] F. Paul, S. Moulin, O. Piechaczyk, P. Le Floch, J. A. Osborn, Palladium(0)-Catalyzed Trimerization of Arylisocyanates into 1,3,5-Triarylisocyanurates in the Presence of Diimines: A Nonintuitive Mechanism, *J. Am. Chem. Soc.* **2007**, *129*, 7294–7304.

[205] H. E. Reymore, P. S. Carleton, R. A. Kolakowski, A. A. R. Sayigh, Isocyanurate Foams: Chemistry, Properties and Processing, *J. Cell. Plast.* **1975**, *11*, 328–344.

[206] S. M. Raders, J. G. Verkade, An Electron-Rich Proazaphosphatrane for Isocyanate Trimerization to Isocyanurates, *J. Org. Chem.* **2010**, *75*, 5308–5311.

[207] J. Tang, T. Mohan, J. G. Verkade, Selective and Efficient Syntheses of Perhydro-1,3,5-triazine-2,4,6-triones and Carbodiimides from Isocyanates Using ZP(MeNCH_2-CH_2)$_3$N Catalysts, *J. Org. Chem.* **1994**, *59*, 4931–4938.

[208] J.-S. Tang, J. G. Verkade, [P(MeNCH_2CH_2)$_3$N] as a Superior Catalyst for the Conversion of Isocyanates to Isocyanurates, *Angew. Chem. Int. Ed.* **1993**, *32*, 896–898.

[209] P. B. Kisanga, J. G. Verkade, R. Schwesinger, pK_a Measurements of P(RNCH_2CH_3)$_3$N, *J. Org. Chem.* **2000**, *65*, 5431–5432.

[210] J. Tang, J. Dopke, J. G. Verkade, Synthesis of New Exceedingly Strong Non-Ionic Bases: RN=P(MeNCH_2CH_2)$_3$N, *J. Am. Chem. Soc.* **1993**, *115*, 5015–5020.

[211] J. G. Verkade, P. B. Kisanga, Proazaphosphatranes: a synthesis methodology trip from their discovery to vitamin A, *Tetrahedron* **2003**, *59*, 7819–7858.

[212] J. G. Verkade, Main group atranes: chemical and structural features, *Coord. Chem. Rev.* **1994**, *137*, 233–295.

[213] J. G. Verkade, Atranes: New Examples with Unexpected Properties, *Acc. Chem. Res.* **1993**, *26*, 483–489.

[214] J. N. Gibb, J. M. Goodman, The formation of high-purity isocyanurate through proazaphosphatrane-catalysed isocyanate cyclo-trimerisation: computational insights, *Org. Biomol. Chem.* **2013**, *11*, 90–97.

[215] Z. Pusztai, G. Vlád, A. Bodor, I. T. Horváth, H. J. Laas, R. Halpaap, F. U. Richter, In Situ NMR Spectroscopic Observation of a Catalytic Intermediate in Phosphine-Catalyzed Cyclo-Oligomerization of Isocyanates, *Angew. Chem. Int. Ed.* **2006**, *45*, 107–110.

[216] J. Helberg, Y. Oe, H. Zipse, Mechanistic Analysis and Characterization of Intermediates in the Phosphane-Catalyzed Oligomerization of Isocyanates, *Chem. Eur. J.* **2018**, *24*, 14387–14391.

[217] D. Heift, Z. Benkő, H. Grützmacher, A. R. Jupp, J. M. Goicoechea, Cyclo-oligomerization of isocyanates with $Na(PH_2)$ or Na(OCP) as "P^-" anion sources, *Chem. Sci.* **2015**, *6*, 4017–4024.

[218] A. Al Nabulsi, D. Cozzula, T. Hagen, W. Leitner, T. E. Müller, Isocyanurate formation during rigid polyurethane foam assembly: a mechanistic study based on *in situ* IR and NMR spectroscopy, *Polym. Chem.* **2018**, *9*, 4891–4899.

[219] K. Schwetlick, R. Noack, Kinetics and Catalysis of Consecutive Isocyanate Reactions. Formation of Carbamates, Allophanates and Isocyanurates, *J. Chem. Soc., Perkin Trans. 2* **1995**, 395–402.

[220] M. Špírková, M. Kubín, P. Špaček, I. Krakovský, K. Dušek, Cyclotrimerization of Isocyanate Groups. II. Catalyzed Reactions of Phenyl Isocyanate in the Presence of 1-Butanol or Butyl-*N*-Phenylurethane, *J. Appl. Polym. Sci.* **1994**, *53*, 1435–1446.

[221] I. S. Bechara, R. L. Mascioli, The Mechanism of the Hydroxyalkyl Quaternary Ammonium Carboxylate Catalyzed Reactions of Phenyl Isocyanate, *J. Cell. Plast.* **1979**, *15*, 321–332.

[222] M. Roman, B. Andrioletti, M. Lemaire, J.-M. Bernard, J. Schwartz, P. Barbeau, Investigations providing a plausible mechanism in the hexamethyldisilazane-catalyzed trimerization of alkyl isocyanates, *Tetrahedron* **2011**, *67*, 1506–1510.

Danksagung

An dieser Stelle möchte ich einer Vielzahl an Menschen danken, die mich in den letzten Jahren unterstützt und begleitet haben:

Zuallererst möchte ich mich bei meinem Doktorvater Prof. Dr. *Oliver Trapp* für die Möglichkeit bedanken, diese Arbeit in seinem Arbeitskreis anzufertigen, aber vielmehr noch für seine professionelle Betreuung, das Vertrauen bei der Umsetzung eigener Ideen, unsere kreative Zusammenarbeit sowie seine immer positive und inspirierende Persönlichkeit.

Prof. Dr. *Paul Knochel* möchte ich herzlich für die Übernahme des Zweitgutachtens danken. Den weiteren Mitgliedern der Prüfungskommission – Prof. Dr. *Konstantin Karaghiosoff*, Prof. Dr. *Franz Bracher*, Prof. Dr. *Manfred Heuschmann* und Dr. *Oliver Thorn-Seshold* – möchte ich ebenfalls danken.

Frederic Lucas möchte ich sehr für die konstruktive, freundschaftliche Zusammenarbeit sowie für die zahlreichen kreativen Ideen und unsere produktiven Telefonate danken. Darüber hinaus möchte ich mich bei *Rebecca Sure* und *Peter Deglmann* für unsere erfolgreiche Kooperation bedanken.

Gerhard Krennrich gilt mein ausgesprochener Dank für die unzähligen Stunden an Einführung in die mathematische Modellierung, unsere produktiven sowie persönlichen bis hin zu philosophischen Gespräche und seine persönliche Unterstützung über die Doktorarbeit hinaus.

Der Ludwig-Maximilians-Universität München und allen Angestellten der Fakultät, die den täglichen Forschungsbetrieb überhaupt erst ermöglichen, möchte ich ebenfalls danken. Dabei möchte ich an dieser Stelle besonders der Feinmechanik danken, die im Laufe meiner Doktorarbeit unzählige Meisterwerke für mich angefertigt hat.

Meinen Forschungspraktikanten – *Milica*, *Sabrina*, *Simone*, *Felix*, *Sophie* und *Marian* – möchte ich für ihren Einsatz während ihres Praktikums danken.

Dem gesamten Arbeitskreis möchte ich für die kurzweiligen und lustigen Jahre in München danken. Dabei möchte ich ein paar Freunden meinen besonderen Dank aussprechen: An *Max*, da wir seit 2011 unzertrennlich durch das Studium in Heidelberg gegangen sind und schlussendlich als Laborpartner hier in München mit viel Spaß und Erfolg zusammengearbeitet haben. An *Fabi*, für die vielen lustigen Abende sowie sportlichen Aktivitäten und unsere ehrlichen, hitzigen, aber freundschaftlichen Diskussionen. An *Jan Felix*, für unsere unzähligen stundenlangen Gespräche über Chemie, den inspierienden Input, die wirklich bewunderswerte ausgleichende Art und vor allem unsere gemeinsamen nächtlichen Arbeitsschichten im Labor mit super Musik. An *Basti*, für unsere witzigen, philosophischen und tiefgründigen Gespräche. An *Golo*, für die jahrelange freundschaftliche Zusammenarbeit und die Hilfsbereitschaft bei jeglichen Problemen. An *Alex*, für unsere zahlreichen lustigen Boulder-Abende. An *Sassi*, für die lustigen gemeinsamen (Spiel-)Abende.

Dabei möchte ich unserer Whisky-Runde – *Fabi*, *Jan Felix* und *Max* – besonders dafür danken, dass durch sie auch die schlimmsten Tage im Labor doch noch ein schönes Ende finden konnten.

Der montaglichen AoE-Runde – *Alex*, *Bechtel*, *Golo* und *Jan* – möchte ich für die konstante Erhöhung meiner Work-Life-Balance während Corona und der Zeit des Schreibens danken.

Ich danke allen meinen Freunden, die mich die letzten Jahre über begleitet haben.

Mein größter und herzlichster Dank gilt *Anna*. Du hast mich immer unterstützt und aufgebaut, warst immer für mich da und hast mir jeden Tag ein Lächeln ins Gesicht gezaubert – danke für all die schönen Momente.

Zuletzt möchte ich von Herzen meiner Familie – *Mama*, *Papa*, *Jan* und *Nils* – danken, die mir nicht nur im Studium und während der Doktorarbeit, sondern in jeder Lebenssituation immer zur Seite stand und mich unterstützt hat.